2012

The Road Not Taken: Applications of Fluorescence Spectroscopy and Electronic Structure Theory to Systems of Materials and Biological Relevance

Philip Carlson
Iowa State University

The road not taken: applications of fluorescence spectroscopy and electronic structure theory to systems of materials and biological relevance

by

Philip Joseph Carlson

A dissertation submitted to the graduate faculty

In partial fulfillment of the requirements for the degree of

DOCTOR OF PHILOSOPHY

Major: Physical Chemistry

Program of Study Committee:
Mark S. Gordon, Major Professor
Jacob W. Petrich, Major Professor
Theresa Windus
Emily Smith
Tom Holme

Iowa State University

Ames, Iowa

2012

This dissertation is dedicated to my wife and children who have supported and sacrificed for me throughout this entire endeavor.

TABLE OF CONTENTS

Acknowledgments

There are many people to thank when one realizes an accomplishment of this magnitude. First, I am indebted to my major professors Dr. Mark Gordon and Dr. Jake Petrich. Without their guidance, support and ideas I would never have made it through the course of graduate school. My situation is an odd one compared to most who attend ISU's chemistry program. I had the rare opportunity within physical chemistry to explore both the experimental and computational aspects of the field. Most people only get the opportunity to travel down one road of physical chemistry so to speak. It is because of the generosity of both Dr. Gordon and Dr. Petrich that I was able to set out on this unique course of study. This is where the inspiration for the title of this dissertation came from. Robert Frost sums it up in his well-known poem "The Road Not Taken."

Two roads diverged in a yellow wood,
And sorry I could not travel both
And be one traveler, long I stood
And looked down one as far as I could
To where it bent in the undergrowth;

Then took the other, as just as fair,
And having perhaps the better claim
Because it was grassy and wanted wear,
Though as for that the passing there
Had worn them really about the same,

And both that morning equally lay
In leaves no step had trodden black.
Oh, I marked the first for another day!
Yet knowing how way leads on to way
I doubted if I should ever come back.

I shall be telling this with a sigh
Somewhere ages and ages hence:
Two roads diverged in a wood, and I,

> I took the one less traveled by,
> And that has made all the difference.

Most don't know which road to take and both seem equally promising. Yet I being fortunate enough have had the opportunity to take what is in hindsight the road less traveled by which has allowed me to explore the experimental and computational aspects of projects and to see the sights along the way. This road, the "one less traveled by" has proven to be both a challenge and a delight. Again, it is thanks to Dr. Petrich and Dr. Gordon who have made the "less traveled by" an option for me.

I also wish to thank my wonderful wife and children whom have supported me so much. Rebecca has been a steadfast supporter and wonderful spouse. My children, Lennell and CarrieAnn, while young have shown such love and have, perhaps unknowingly, sacrificed time with me. I am grateful. My family has also been a big source of support. My parents on both sides and siblings on both sides have been especially supportive and understanding throughout these times. A special thanks goes to Andy and Kate Pearce for their unwavering support professionally, and personally. A man could not ask or dream of someone to be there for him more than Kate and Andy have been.

Of course, the graduate school experience is not complete without fellow graduate students helping along the way. In the Petrich group, thanks to Ram Adhikary and Sayantan Bose who have helped me to learn much of the workings of the lab and concepts. Thanks to Charles Barnes for his support and for always being there to listen to my frustrations. Charles also has provided much needed help on many different research projects as well as ideas and genuine assistance. Life in graduate school would not have

been nearly as bearable without Charles. Also, thanks to Ujjal Bhattacharjee for his help and perspective. The Gordon group has also provided much needed help. Thanks to Spencer Pruitt, Luke Roskop, Justin Conrad and other members who have provided entertainment, gave direction when needed and explained many concepts.

There are many people from the past who have helped me to get where I am today and while I will not mention them by name I am thankful for their contribution as well. I am also thankful for my church family that has supported me throughout my time here in Ames. A heart of thankfulness also goes to the good Lord who has truly worked out more on my behalf than I would have ever imagined.

CHAPTER I: GENERAL INTRODUCTION

A Brief Introduction to Chemistry

The term "chemistry" has a complex long-debated etymology. [1,2,3] One strain of thought derives the word from Greek origin [4] and others from the Egyptian [5] or Arabic. Hilditch in his *A Concise History of Chemistry* states that, "With regard to the origin of the word 'chemistry,' there is a choice of about six very plausible 'derivations,' . . ." [1] He does not go so far as to state which choice he prefers. According to the noted chemical historian and author of a large four volume work on the history of chemistry, Dr. J. R. Partington, "The name 'chemistry' first occurs in an edict of the Emperor Diocletian in A.D. 296 . . ." [6] It appears to come from the Greek term χημεια (*chemeia*) which is derived from the native designation of Hellenized Egypt. [6] Ptolemaic Egypt was known as *chemeia*, which was a reference to its black colored soil. The Arabic form of this term gave rise to the term "alchemy" which was known as "the black arts." With alchemy being the forerunner to chemistry it seems that the term "chemistry" ultimately comes down to etymologically meaning, "the Egyptian art." [6] Chemistry is then derived from the term that was used to describe those who practiced such, what we know as alchemy, in Egypt.

Alchemy was commonly practiced until the time of the renaissance. The alchemists were mostly concerned with transmutating things into gold via the "philospher's stone." This obsession with producing and procuring wealth also extended to the protofield of medicine. They searched for the "elixir of life" which would give

eternal youth. This would have been of immense value given the time period (before the advent of modern medicine and the germ theory of disease) and the ongoing struggle with the bubonic plague. This medicinal side of alchemy eventually became known as iatrochemistry and was practiced in the sixteenth and seventeenth centuries. [6] Alchemy as a whole would have undoubtedly been a fascinating and curious field to work in with its mixture of philosophy, mysticism and pseudoscience yet many grew skeptical of its practice. The proto-science of alchemy, which often contained mysterious elements, was eventually dismissed as pseudoscience and any contributions it made to actual science were incorporated and reformed into the study of chemistry during the renaissance period. [7]

Chemistry is usually taken to be the study of the properties and behavior of matter, where matter refers to the physical materials of the universe that have mass and occupy space. [8] Even this very general definition does not quite capture the full extent of what is studied in the modern field of chemistry. Spectrosocpy for example involves studying light and its interaction with matter. Light (i.e. photons) can not really be said to have mass. [9] Should we still call this chemistry? Given that photons are produced from excited matter perhaps this does fall within some district inside the field of chemistry. While it is not straightforward to catagorize all such areas of study we can say that this definition forms a good generalization of what chemistry is.

Matter is the primary subject of chemistry. Matter was thought to be made up of small indivisible particles called atoms (from the Greek ατομος meaning not-cuttable or indivisble). This concept was held by the ancient Greek philosopher Democritus (460 – 370 BC) but eventually came into obscurity after the teachings of Plato and Aristotle,

who taught that there were no ultimately indivisible particles, became popular. The atomistic theory came back into consideration when the need to explain the behavior and properties of gases arrose. In fact, Isaac Newton described such indivisble corpuscles in his thirty-first query of his *Opticks* by stating, "It seems probable to me, that God in the Beginning form'd matter in solid, massy, hard, impenetrable, moveable Particles, of such Sizes and in such Proportion to Space, as most conduced to the End for which he form'd them." [10] This idea was developed further and proposed by John Dalton (1766-1844). Dalton's atomic theory lays the basis of modern atomic theory yet lacks in a few aspects due to the fact that no direct experimental evidence was avaliable until a century after his ideas were proposed. Experiments started to abound for which no explaination could be offered except that there exists small subatomic particles of negative charge (called electrons). Additional experimentation led to the modern understanding that in most cases matter is composed of molecules, molecules are composed of atoms, atoms are composed of protons, electrons and neutrons. Later developments in physics have led to the understanding that there are even more fundamental particles - among which are quarks. [11] This modern experimentally derived understanding of matter forms the domain for the study of chemistry.

The Rise of Quantum Understanding

The experiments that led to the understanding of atoms being made up of protons and neutrons in the nucleus surrounded by electrons also led to some strange phenomena which could not be explained by the scientific paradigms of the time. When black body radiation was studied based on the ideas of classical physics using the Rayleigh-Jeans

law, [12] it was expected that large amounts of energy should be radiated in the high-frequency region of the electromagnetic spectrum at room temperature. Classical physics predicted that even cool objects should radiate in the visible and ultraviolet regions – that is, they should glow in the dark – there should be no darkness at all. This result is known as the ultraviolet catastrophe.

Planck, a German physicist, offered insight on how to account for the experimental observations regarding black body radiation. [12] He found that if one only allows discrete values for the energy of each electromagnetic oscillator that the experimental results could be accounted for. This idea of the quantization of energy was quite contrary to the prevailing ideas of classical physics wherein all possible values for the energy are allowed. Planck found that integer multiples of hv would correctly describe the experiments. So, $E=nhv$ where n is a positive integer, h is Planck's constant, and v is the frequency of the electromagnetic oscillator. Interestingly, h is an undetermined parameter in this theory and was obtained by varying its value until a best fit was obtained. [12] The currently accepted value for h is $6.6260693 \times 10^{-34}$ Js. This new concept of the quantization of energy was applied to other areas of theory in classical physics and found to successfully account for other phenomena such as the thermal properties of solids. This powerful idea lays the groundwork for understanding much of current science.

Perhaps the most powerful display of the quantization of energy comes from its ability to explain the observations of the frequencies of radiation absorbed and emitted by atoms and molecules. Atoms and molecules absorb and emit energy at discrete frequencies giving rise to their well-known line spectra. These line spectra are easily

accounted for by recognizing that the energy levels in the atoms and molecules must be discrete. Energy can be absorbed or emitted *only* in discrete amounts. This forms the basis for the field of spectroscopy, which will be discussed in more detail later.

The explanation offered by classical physics regarded electromagnetic radiation as mostly wave-like in its nature. However, other experiments led to what the view that light and matter possess both a wave nature and a particle nature. This concept is known as wave-particle duality. The photoelectric effect demonstrates the particle identity of light nicely. Electrons are ejected from metals only when they interact with light of frequency sufficient to provide the interaction necessary for such ejection. If light of an inadequate frequency hits the metal's surface, no electrons would be ejected. If light of a higher frequency than necessary for ejection hits the metal's surface the electron is ejected and the additional energy imparted by the light is transferred to the kinetic energy of the electron. These observations led to the strong conclusion that the photoelectric effect depends on a collision between a particle-like projectile that carries the necessary energy for ejection and an electron. This particle of light is known as the photon.

Matter as Waves

Light can behave as both a wave and as a particle. Oddly enough, matter is found to behave the same way. This was the hypothesis of Louis de Broglie (for which he won a Nobel Prize in 1929) as set forth in 1924 as the subject of his PhD thesis. He retraces his thoughts in a 1970 article when he states:

> When I conceived the first basic ideas of wave mechanics in 1923-1924, I was guided by the aim to perform a real physical synthesis, valid for all

> particles, of the coexistence of the wave and of the corpuscular aspects that Einstein had introduced for photons in his theory of light quanta in 1905. I did not have any doubts at that time about the physical reality of the wave and the localization of the particle in the wave. [13]

Indeed, de Broglie's extension of "wave mechanics" to all particles is rather startling at first. It is deceivingly simple when expressed as: $p = h/\lambda$, where p is the momentum, h is Planck's constant, and λ is the wavelength associated with the particle. It is often helpful to apply this relationship to macroscopic bodies to understand what it means on such a scale. It is quickly seen that macroscopic systems have such high momenta that their associated wavelengths are undetectably small. These very small wavelengths (on the order of 10^{-35} m) leave the wave-like behaviors that we are familiar with on the macroscopic scale unobservable. Yet this idea was supported by numerous experimental results including the radical experiments by Davisson (1881 – 1958, Nobel Prize for this experiment in 1937) and Germer (1896 – 1971). The Davisson-Germer experiment (carried out in 1927) and other experiments have shown de Broglie's hypothesis of the wave nature of matter to be correct. The wave-particle duality of matter is perhaps realized most effectively when considering the results of Young's experiment (the double-slit experiment) when electrons are used (It should be noted that Young's experiment was not performed with electrons until 1961 by Jönsson). [14] When passing electrons through two parallel slits an interference pattern is produced on the detector screen behind the slits. This demonstrates that the electrons are interfering with one another in a wave-like manner. This result is completely inconsistent with how particles would behave in a similar situation. One can easily imagine larger particles (e.g.

baseballs) passing through two slits (e.g. windows), and no evidence of their "interference" from the wave-like nature would be detected. The interference pattern seen when electrons are used in this experiment demonstrates again the wave-particle duality extends to matter and not just light. It is interesting to note that this double-slit experiment has also been performed with C_{60} molecules and an interference pattern was still observed. [15] It is this wave-particle duality of matter – not just light, but all matter – that was ground breaking and led the way to Schrödinger's development of a wave equation to describe quantum systems. The Schrödinger equation is perhaps one of the most well known aspects of quantum theory, and forms the basis for the electronic structure theory on which this dissertation is based.

Electronic Structure Theory

Upon learning of de Broglie's developments, Erwin Schrödinger had a burst of creativity and produced the wave equation that bears his name. He surmised that it ought to be possible to begin with the classical wave equation itself and with it construct a bridge beginning at wave optics and leading to a general wave mechanics capable of accounting for quantum phenomena. [16] A series of papers published in 1926 shows how Schrödinger was able to arrive at his famous equation and detailed how matter behaves as waves. [17] [18] [19] [20] [21] The nonrelativistic time-dependent Schrödinger equation can be see in Eq.1 where the function describing the system as a wave is dependent on time (*t*) and the electronic (r) and nuclear (R) coordinates of the system.

$$i\frac{\partial}{\partial t}\Psi\left(r,R,t\right) = H\Psi(r,R,t) \tag{1}$$

In Eq. (1) $\hbar$ is Planck's constant over 2π; $i = \sqrt{-1}$, H is the Hamiltonian operator, and Ψ(r,R,t) is the wavefunction. It is often sufficient to use the Schrödinger equation in its time-independent form that can be expressed as an eigenvalue problem:

$$H\Psi\left(r,R\right) = E\Psi(r,R) \tag{2}$$

This second-order differential equation depends only on the nuclear and electronic degrees of freedom. E is the eigenvalue corresponding to the total energy of the quantum state and Ψ(r,R) is the eigenfunction which is the stationary state wavefunction that depends on the electronic (r) and nuclear coordinates (R). Here again we see H, which is the Hamiltonian operator.

The Hamiltonian operator (Eq. (3)) assumes the nuclei and electrons to be point masses and neglects spin-orbit and other relativistic interactions that are properly derived using Dirac's relativistic treatment of the electron.

$$H = \underbrace{-\frac{\hbar^2}{2}\sum_{\alpha}\frac{1}{m_\alpha}\nabla_\alpha^2}_{\text{(1) kinetic energy of nuclei}} \underbrace{-\frac{\hbar^2}{2m_e}\sum_{i}\nabla_i^2}_{\text{(2) kinetic energy of electrons}} + \underbrace{\sum_{\alpha}\sum_{\beta>\alpha}\frac{Z_\alpha Z_\beta e'^2}{r_{\alpha\beta}}}_{\text{(3) potential energy of nuclei repulsion}} \underbrace{-\sum_{\alpha}\sum_{i}\frac{Z_\alpha e'^2}{r_{i\alpha}}}_{\text{(4) potential energy of attraction between electrons and nuclei}} + \underbrace{\sum_{j}\sum_{i>j}\frac{e'^2}{r_{ij}}}_{\text{(5) potential energy of electron repulsion}} \tag{3}$$

In Eq (3), α and β refer to nuclei and *i* and *j* refer to electrons. *m* refers to the mass of the particle; $r_{\alpha\beta}$ is the distance between nuclei α and β with atomic numbers Z_α and Z_β; $r_{i\alpha}$ is the distance between electron *i* and nucleus α; r_{ij} is the distance between the electrons *i* and *j*. The potential energy is taken to be zero when all the particles are infinitely far from one another.

The Hamiltonian in Eq 3 includes operators (terms 1, 3) that rely solely on the nuclei. Since the nuclei are much heavier than electrons (roughly three orders of magnitude more massive), electrons move much faster than the nuclei, so it is a good approximation to consider the nuclei to be fixed in the field of the moving electrons. This Born-Oppenheimer approximation [22] serves as the basis for the vast majority of molecular electronic structure calculations performed today.

When the Born-Oppenheimer approximation is employed the Hamiltonian is reduced to terms (2), (4), and (5) of Eq (3). The electronic Hamiltonian is then

$$H_{el} = -\frac{\hbar^2}{2m_e}\sum_i \nabla_i^2 - \sum_\alpha \sum_i \frac{Z_\alpha e'^2}{r_{i\alpha}} + \sum_j \sum_{i>j} \frac{e'^2}{r_{ij}} \tag{4}$$

In atomic units the electronic Hamiltonian becomes

$$H_{el} = -\frac{1}{2}\sum_i \nabla_i^2 - \sum_i \sum_\alpha \frac{Z_\alpha}{r_{i\alpha}} + \sum_i \sum_{j>i} \frac{1}{r_{ij}} \tag{5}$$

The Schrödinger equation for the electrons is:

$$H_{el}\Psi_{el}\left(r\right) = E_{el}\Psi_{el}(r) \tag{6}$$

Within the Born-Oppenheimer approximation, E_{el} corresponds to the total electronic energy of a molecule. The internuclear repulsion term V_{NN} is added as a constant, since the nuclear positions are fixed:

$$V_{NN} = \sum_\alpha \sum_{\beta>\alpha} \frac{Z_\alpha Z_\beta}{r_{\alpha\beta}} \tag{7}$$

A classical point charge model is used to treat the nuclear repulsion term. For each nuclear configuration the electronic Schrödinger equation is solved to get a set of

electronic wavefunctions and corresponding electronic energies. The electronic wavefunctions and energies thus depend parametrically on the nuclear configuration.

Hartree-Fock Theory

A simple approach for solving the complex electronic Schrödinger equation is to use the Hartree-Fock (HF) approximation, which uses a mean field approach [23 24 25] to replace the explicit two-electron repulsion operator. Eq (8) shows $f(i)$ (the Fock operator) in which $v^{HF}(i)$ is the average potential experienced by the ith electron due to the presence of the other electrons.

$$f\left(i\right) = -\frac{1}{2}\nabla_i^2 - \sum_{A=1}^{M}\frac{Z_A}{r_{iA}} + v^{HF}(i) \tag{8}$$

The Hartree-Fock equations (9) are pseudo eigenvalue equations whose solutions are the orbitals and orbital energies.

$$f\left(i\right)\chi\left(x_i\right) = \varepsilon\chi(x_i) \tag{9}$$

The HF equations must be solved iteratively, since the Fock operator depends on the orbitals. The procedure for solving the HF equation is called the self-consistent-field (SCF) method. This iterative procedure yields a set of orthonormal HF spin orbitals $\chi(x_i)$ with orbital energies ε.

Hartree-Fock theory is central to most *ab initio* calculations of electronic structure in atomic and molecular systems. The explicit form of v^{HF} is

$$f(1) = h(1) + \sum_{a}^{N/2}[2J_a(1) - K_a(1)] \tag{10}$$

In Eq (10), $h(1)$ contains the first two terms in Eq (8); $J_a(1)$ is the coulomb operator

$$J_b(1)\chi_a(1) = \left[\int dx_2 \chi_b^*(2) r_{12}^{-1} \chi_b(2)\right]\chi_a(1) \tag{11}$$

and $K_a(1)$ is the exchange operator

$$K_b(1)\chi_a(1) = \left[\int dx_2 \chi_b^*(2) r_{12}^{-1} \chi_a(2)\right]\chi_b(1) \tag{12}$$

The HF SCF procedure produces a set of molecular orbitals that minimize the energy of a molecular system by making use of the variational principle. The calculated energy of any HF wavefunction is guaranteed to be an upper bound to the exact non-relativistic energy.

$$E_{exact} \leq E_{HF} \tag{13}$$

Post Hartree-Fock Methods

HF theory fails for processes like bond breaking, because the motions of the electrons are not correlated with each other. This failure has led to the development of many post-HF methods that provide more reliable potential energy surfaces (PESs) than HF. The difference between the HF predicted energy and the exact non-relativistic energy is defined as the correlation energy.

$$E_{corr} = E_{exact} - E_{HF} \tag{14}$$

The “recovery” of the correlation energy has become the goal of most of these methods.

The Configuration Interaction (CI) Method

The HF method determines the energetically best one-determinant trial wave function within a given basis set. The CI method improves upon the HF method by expnading the wavefunction in a basis of configurations. The CI wavefunction Φ_{CI} is expanded in a finite basis of spin-adapted configuration state functions (CSFs) as follows

$$\Phi_{CI} = C_{HF}\Psi_{HF} + \sum_{S} C_S \Psi_S + \sum_{D} C_D \Psi_D + \sum_{T} C_T \Psi_T + \ldots = \sum_{i} C_i \Psi_i \qquad (15)$$

The HF determinant (Ψ_{HF}) weighted by an appropriate CI coefficient (C_{HF}) is the leading term in this expansion. Each additional term corresponds to a configuration that is classified as a single ($C_S\Psi_S$), double ($C_D\Psi_D$), triple ($C_T\Psi_T$) or higher excitation from occupied to unoccupied molecular orbitals (MOs). Full CI corresponds to all possible excitations and is the exact, non-relativistic solution to the time-independent Schrödinger equation within the Born-Oppenheimer approximation and for a given atomic basis set. [26] Due to computational limitations, the application of CI typically involves a truncated expansion.

The CI method truncated to include only single excitations (CIS) is the simplest implementation of the CI method. The accuracy of the CI method improves upon the inclusion of additional terms, at an appreciable computational cost. Hence, a balance must be obtained between the desired level of accuracy and the computational

requirements. Therefore, typically CI with doubles (CISD) and triples (CISDT) are the most commonly used CI methods that are feasible.

The CI expansion methods have a few shortcomings that should be mentioned. The truncated CI expansion is neither size consistent nor size extensive. A method is size extensive if the energy calculated scales linearly with the number of particles, and size consistent when the energy is consistent when the interaction between the involved molecular system is removed (e.g. by distance). For example, a calculation of two H_2 molecules separated by 100 Å will not give the same energy as twice the results from a calculation on one H_2 molecule. CI is a variational method and hence gives an upper bound to the true energy, it has been shown to be a very effective and useful tool in finding the correlation energy.

Møller-Plesset Perturbation Theory

Another approach to finding the correlation energy is many-body perturbation theory (MBPT). MBPT has better computational scaling then the CI methods and is used more frequently because of this. Perturbation theory is size consistent but is not a variational method. There is no guarantee that the energy calculated is higher than the exact energy. The usual approach is Rayleigh-Schrodinger perturbation theory, in which the exact non-relativistic Hamiltonian, H, is treated as a perturbed independent particle Hamiltonian H_0, with the energy and wavefunction expanded in *n* orders of the perturbation V :[27 28]

$$H = H_0 + \lambda V \tag{17}$$

$$\Psi_{MPn}^{(i)} = \Psi_0 + \sum_{i=1}^{n} \lambda^i \Psi_i \tag{18}$$

$$E_{MPn}^{(i)} = E_0 + \sum_{i=1}^{n} \lambda^i E_i \tag{19}$$

A formulation of MBPT that uses the Fock Hamiltonian as H_0 is second order Møller-Plesset (MP2) perturbation theory. The majority of the studies in this thesis have utilized the MP2 method.

MP2 accounts for about 80-90% of the total correlation energy and is computed by using the following equation. [29]

$$E_{MP2} = \sum_{i<j}^{occ} \sum_{a<b}^{vir} \frac{\left(\left\langle \phi_i \phi_j \middle| \phi_a \phi_b \right\rangle - \left\langle \phi_i \phi_j \middle| \phi_b \phi_a \right\rangle \right)}{\varepsilon_i + \varepsilon_j - \varepsilon_a - \varepsilon_b} \tag{20}$$

The summation in equation 20 runs over all double excitations from occupied to unoccupied (virtual) orbitals. Møller-Plesset perturbation theory can be extended to higher order energy corrections; however, convergence can be slow, rapid, oscillatory, regular, highly erratic or simply non-existent, depending on the system of interest and the basis set. Various properties of molecules have been calculated at MP3 and MP4 levels and have been found to be no better than their MP2 counterparts, even for small molecules. [30] Hence, performing the less expensive (less computationally demanding) MP2 calculation is accurate enough and feasible for most systems of interest where *ab initio* methods are utilized.

There exist a number of other post-HF methods that have been developed and used heavily. These methods, discussed in detail in many textbooks, have both advantages and disadvantages.

The Fragment Molecular Orbital Method

A consideration when performing electronic structure theory calculations is the chemical system size. Most *ab initio* methods are practical for systems comprised of a modest number of atoms (~100 atoms). There is often a need to explore larger systems than this. To treat efficiently a large molecular system on the order of 10^4 or more atoms with only quantum mechanics fragmentation methods provide a practical approach. [31] The fragment molecular orbital (FMO) method has been used in this work. [32]

The FMO method treats a large molecular system by splitting the molecular or system into fragments. Each fragment is refered to as a monomer. A separate quantum mechanical calculation can then be performed for each monomer making *ab initio* calculations on larger systems much more feasible. Each monomer is calculated in the electrostatic field (coulomb field) constructed from calculations performed on the other monomers. This scheme is made more accurate by performing additional calculations corresponding to specific interactions between two monomers (dimer corrections) or three monomers (trimer corrections). The following equation can be used to determine the total energy of a system within the FMO method.

$$E_{FMO} = \sum_{I} E_I + \sum_{I>J}^{N} (E_{IJ} - E_I - E_J) + \sum_{I>J>K}^{N} \left[\left(E_{IJK} - E_I - E_J - E_K \right) - \left(E_{IJ} - E_I - E_J \right) - \left(E_{JK} - E_J - E_K \right) - (E_{KI} - E_K - E_I) \right] + \ldots \quad (21)$$

E_I is the monomer energy, E_{IJ} is the dimer energy, and E_{IJK} is the trimer energy. A major benefits of this method is the ability to use it with a number of different levels of theory. The FMO method has been used and tested in the following chapters and much more is said about it there.

Introduction to Photochemistry and Photophysics

In addition to advanced electronic structure theory calculations and concepts, this dissertation is also based on experimental photochemistry and photophysics. A brief introduction to those central photophysical ideas follows. These concepts are foundational to more advanced concepts that were heavily utilized to study different systems with biological and high-energy materials application.

Figure 1 is a schematic representation of some of the different processes that can transpire within a chemical system.

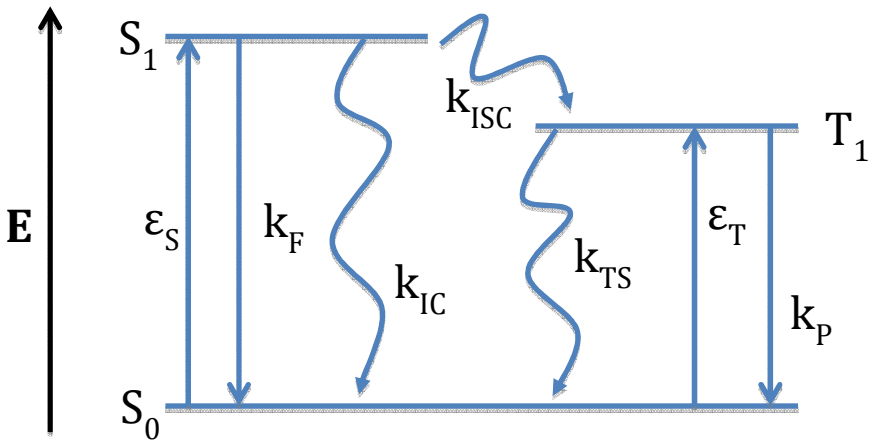

Figure 1 – A schematic representation showing some of the different process that can happen within a molecule. S_0 represents the ground state, S_1 the first excited singlet state and T_1 is the first excited triplet state. See the text for an explanation of the rest of the labels.

This type of diagram is sometimes called a Jablonski diagram. The ground state is represented by S_0 and the first excited singlet state is given as S_1. The T_1 label represents the first excited triplet state. The energy increases from bottom to top. The singlet state is higher in energy than the triplet state. ε_S represents the energy needed to transition from the ground state to the first excited singlet state. This energy is typically probed via an absorption measurement. This transition is a spin-allowed transition and occurs much more frequently than the spin-forbidden singlet-triplet absorption (ε_T). k_F is the rate constant that characterizes fluorescence. k_P is the rate constant that characterizes the phosphorescence process. Fluorescence is defined as a radiative transition from a particular excited spin state to another lower energy state of the same spin (e.g. singlet to singlet). Phosphorescence is a radiative transition from an excited state of one spin to a lower energy state of a different spin (e.g. triplet to singlet).

The processes we have discussed so far are called radiative processes because they involve the absorption or emission of a photon. The nonradiative (or radiationless)

processes are characterized by the k_{IC}, k_{ISC}, and k_{TS} rate constants (see Figure 1). The k_{IC} label is the rate constant associated with the spin-allowed raditionless transition between state of the same spin which is known as internal conversion. Spin-forbidden radiationless transitions between excited states of different spin are known as intersystem crossings and are characterized by the rate constant k_{ISC}. The label k_{TS} is the rate constant for the spin-forbidden radiationless transitions between the triplet and the ground state. This summarizes the nonradiative processes shown in Figure 1.

The values of the various rate constants (k) can usually be easily determined from experiment. These rates determine the probability of the various transitions. Obviously we have multiple processes happening which contribute to the probability of the other transitions taking place. Each system will have different rates for each of these processes depending on a number of factors mostly related to the energetics of the molecules (PES, orbital interactions, stabilizing effects etc.).

Solvation Dynamics

Solvation dynamics involves the investigation of a dielectric solvent response to a perturbation invoked by the dipole change of an appropriate fluorescent probe molecule. [33] The fluorescence spectra of a fluorophore can be significantly impacted by the polarity of a solvent and the local environment. The fluorophore of choice (for most) when studying solvation dynamics is Coumarin 153. This molecule has risen as a reliable fluorescent probe in the study of solvation dynamics for a number of reasons detailed by Horng *et al.* in a very thorough report. [34] Figure 2 presents a diagrammatic representation of the process of solvation dynamics, in which the fluorophore is in the ground state (S_0) and the solvent relaxed around it. Upon a vertical excitation to the Franck-Condon first excited state (S_1) the solvent is initially in the same orientation. The solvent can lower its free energy by "relaxing" around the new dipole produced in the fluorophore upon excitation. As the solvent reorganizes, fluorescence emission occurs at lower and lower energies (red shifts) until the solvent reaches its "relaxed" equilibrium

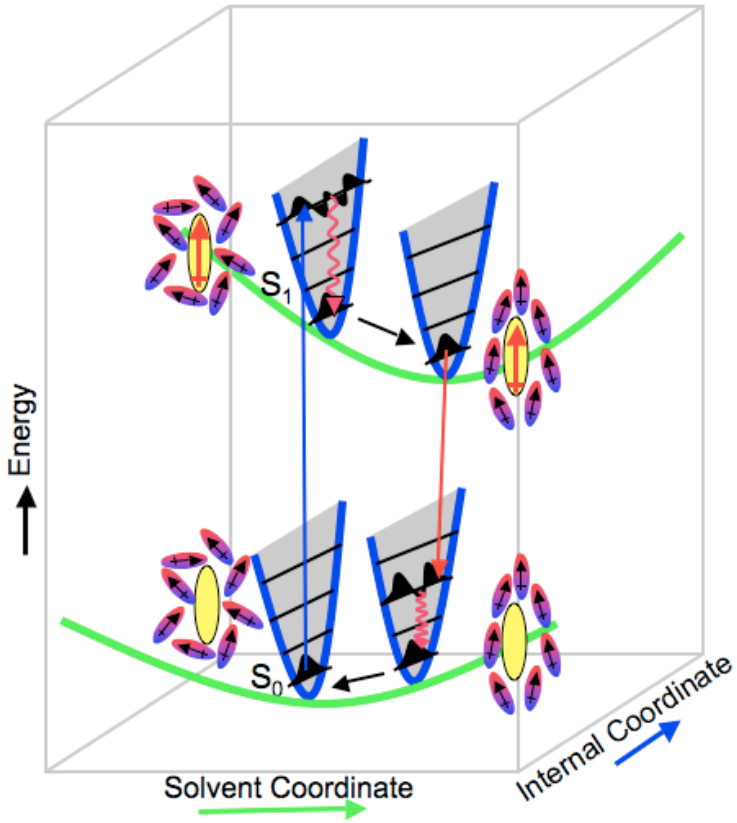

Figure 2 – A diagrammatic representation of solvation dynamics.

state. This is as "red" as the spectrum will shift and is generally congruent with the steady-state spectrum measured with a standard fluorimeter. The effect of solvation is too fast (~1-10 ps) to resolve by steady-state fluorometry; hence, there is need for alternate techniques to resolve the solvent response. [35] A number of techniques allow one to study solvation dynamics; the one most commonly used in the Petrich lab is time correlated single photon counting (TCSPC). [36] This technique allows for time resolution of ~45 ps by using a high repetition rate Ti-Sapphire laser. More will be said about the particular setup in the following chapter. With the appropriate equipment, one can measure the time-resolved fluorescence of the probe molecule, thereby shedding light on the solvation process

Room Temperature Ionic Liquids

The studies carried out which are included in this dissertation involved room temperature ionic liquids (RTILs). Ionic liquids (ILs) are composed of an organic cation and an inorganic anion and are commonly liquid at room temperature. They are not new, having been known since at least 1914. [37] Recently, research on ionic liquids has gained popularity having a steeper than exponential growth in the number of publications since 2000. [38] This is primarily due to the need to replace hazardous solvents in current industrial processes. ILs are thought to be exceptionally environmentally friendly since in most

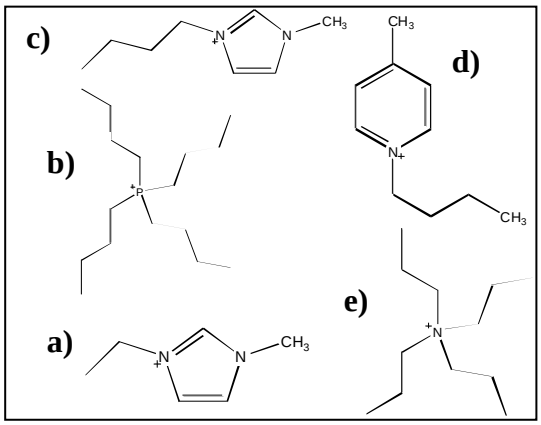

Figure 3 – Common ionic liquid cations **a)** 1-Ethyl-3-methyl-imidazolium [EMIM] **b)** Tetrabutylphosphonium **c)** 1-Butyl-3-methyl-imidazolium [BMIM] **d)** 1-Butyl-4-methylpyridinium

cases they possess a negligible vapor pressure and emit no volatile organic compounds (VOCs). [39] Perhaps the most commonly used and well-understood ionic liquid system is the 1-butyl-3-methyl-imidazolium (BMIM) cation and tetrafluoroborate (BF_4) or hexafluorophosphate (PF_6) anion. This compound and other commonly used IL cations are shown in Figure 3.

Because ILs can be formulated to be very stable and to possess many ideal properties they have been termed "designer solvents". [40] Most studies focus on using ILs in various applications such as catalysis, chromatography, and synthesis. [41] A few reports also detail the use of ILs in more diverse applications. These include using ILs in space propulsion applications, vapor take-off reactors, electropolishing and electroplating, dye sensitized solar cells, nanoclays, an optical thermometer, and even exploiting their nonlinear optical properties. [42] Undoubtedly the reason that ILs have found such varied application is due in part to the tunability of their properties. One can easily tailor an ionic liquid for a particular application. For instance, the water solubility can easily be changed, the melting point can be somewhat varied, the viscosity can be adjusted. [43] These customizations, the environmentally friendly properties and the stability of ILs make them ideal for nearly unlimited applications.

Curcumin

Curcumin, 1,7-bis(4-hydroxy-3-methoxyphenyl)-1,6-heptadiene-3,5-dione, is a naturally occurring yellow-orange pigment derived from the rhizomes of Curcuma longa (turmeric). Turmeric has been traditionally used as a spice and food coloring in Indian cooking and medicine. Its yellow color is primarily caused by a group of structurally

related polyphenols collectively known as curcuminoids, which are composed of curcumin (77%), as the major bioactive component, and two of its derivatives, demethoxycurcumin (17%) and bismethoxycurcumun (3%). Currently, curcumin is the subject of a large number of investigations in the fields of biology, medicine, and pharmacology owing to its profound effects on human health. It exhibits a variety of biological and photochemical properties, including antioxidant, anti-inflammatory, and anticancer activity. Recently, it is also established that curcumin has the ability to prevent protein aggregation in debilitating diseases such as Alzheimer's and Parkinson's.

Concluding Thoughts

There exists some confusion among the general public about the chemical sciences. Despite the fact that all living things are directly composed of chemicals and that every item we interact with on a macroscopic scale on a daily basis are composed of chemicals few nonscientists recognize the importance of chemistry in our daily lives. Many feel that chemicals are "bad for you" and they are just "not natural." They are reacting to what one can only suppose is a stigma created by the media and advertisement for "natural" products and "organic" food. These sources play on the fear that many posses about consuming or using an item that is "man-made" and therefore "unnatural and not healthy." They fail to see that we need chemicals to survive. Some rely daily on "man-made" chemicals to live and have normal lives. The benefits that modern chemistry and "man-made" materials have had on society is incalculable. Consider the current use of plastics in industry, medicine, and in the home. Indeed there does exist chemicals that are harmful – both man-made and natural in origin. Why the desire to abandon all

synthetic chemicals and dismiss them as harmful? Deciscions such as these should only be made by the informed individual who has taken the time to investigate the issues associated with each component and who have taken the inicitive to learn about the topics involved from more than one aspect. Consider the statement that Dr. Raymond Seymour gives in his article *Chemicals in Everyday Life*:

> As consumers, we are dependednt on chemists and farmers for our food, shelter, and clothing and for other needs. Fortunately, the chemist has provided drugs to cure illness, and equipment for our exploration, recreation, ventilation, communication, decoration, snitation, and education. Those critics who are not appreciative fo the accomplishments of chemists should be reminded that today's problems such as contamination and pollution are being solved by chemists, and without chemists the consumer would not be able to enjoy his or her present lifestyle. . . . We are dependednt of chemistry for our everyday living and will be more dependent on this branch of science in the future.[29]

Dissertation Organization

Chapter 1 of this dissertation provides the background necessary to understand the material contained herein. It serves as a general introduction to chemistry and includes the development of quantum mechanics as well as the theoretical concepts of computational chemistry that were used in carrying out this work. Also included is the basics of photophysics which serves to prepare the reader for more advanced concepts used in the following chapters.

Chapter 2 includes experimental methods that were used to analyze the experimental data given and detailed in following chapters.

Chapter 3 discusses the molecule curcumin and its ability to undergo excited state intramolecular hydrogen atom transfer in a micellar environment.

Chapter 4 is a review paper written over curcumin and summarizes the data gathered using experimental techniques.

Chapter 5 shows the characterization of the high-energy HEATN molecule both experimentally and computationally.

Chapter 6 discusses some very recent work on the proton transfer reaction in similar delta pK_a amine systems.

Chapter 7 summarizes this dissertation and provides the general conclusions of the entire work.

References

1. Hilditch, T. P., *A Concise History of Chemistry*, Second, Revised ed. (Methuen & Co. LTD., London, 1922).
2. The etymology of "chemistry". *Journal of Chemical Education* **7** (3), 652 (1930).
3. Hollander, S., Alchemy. *Journal of Chemical Education* **54** (5), 330 (1977).
4. Trimble, R. F., Etymology of Chemistry. *Journal of Chemical Education* **53** (12), 802 (1976).
5. Glackin, J. J., Chemistry: The Black Art? *Journal of Chemical Education* **53** (4), 267 (1976).
6. Partington, J. R., *A Short History of Chemistry* (The Macmillan Company, New York,

1937).

7. Asimov, I., *A Short History of Chemistry* (Anchor Books, Garden City, 1965).
8. Brown, T. L., LeMay, H. E. & Bursten, B. E., *Chemistry the Central Science* (Pearson, Upper Saddle River, 2006).
9. Fischbach, E., Kloor, H., Langel, R. A., Lui, A. T. Y. & Peredo, M., New Geomagnetic Limits on the Photon Mass and on Long-Range Forces Coexisting with Electromagnetism. *Physical Review Letters* **73** (4), 514-517 (1994).
10. Newton, I., *Opticks*, 4th ed. (1730).
11. Nye, M. J., *Before Big Science* (Twayne Publishers, New York, 1996).
12. Atkins, P. & de Paula, J., *Physical Chemistry*, 7th ed. (W. H. Freeman and Co., New York, 2002).
13. de Broglie, L., The Reinterpretation of Wave Mechanics. *Foundations of Physics* **1** (1), 5-15 (1970).
14. Jonsson, C., Electron Diffraction at Multiple Slits. *American Journal of Physics* **42** (1), 4 (1974).
15. Arndt, M. *et al.*, Wave-particle duality of C60 molecules. *Nature* **401**, 680-682 (1999).
16. Pilar, F. L., *Elementary Quantum Chemistry*, 2nd ed. (Dover, Mineola, 2001).
17. Schrodinger, E. *Ann. Phys.* **79**, 361 (1926).
18. Schrodinger, E. *Ann. Phys* **79**, 489 (1926).
19. Schrodinger, E. *Ann. Phys* **79**, 734 (1926).

20. Schrodinger, E. *Ann. Phys* **80**, 437 (1926).

21. Schrodinger, E. *Ann. Phys* **81**, 109 (1926).

22. Born, M. & Oppenheimer, R. *Ann. Phys* **84**, 457 (1927).

23. Hartree, D. *Proc. Cambridege Philos. Soc.* **24**, 89 (1928).

24. Hartree, D. *Proc. Cambridge Philos. Soc.* **24**, 111 (1928).

25. Fock, V. *Z. Phys.* **61**, 126 (1930).

26. Lowdin, P.-O. *Phys. Rev.* **97**, 1509 (1955).

27. Pople, J. A., Brinkley, S. & Seeger, R. *Int. J. Quant. Chem.* **10**, 1 (1976).

28. Lowdin, P. *J. Chem. Phys.* **19**, 1396 (1951).

29. Szabo, A. & Ostlund, N. S., *Modern Quantum Chemistry* (Dover, Mineola, 1989).

30. Jensen, F., *Introduction to Computational Chemistry*, 2nd ed. (John Wiley, West Sussex, 2007).

31. Gordon, M. S. e. a. *J Phys. Chem. B* **113**, 9646 (2009).

32. Fedorov, D. G. & Kitaura, K., *The Fragment Molecular Orbital Method: Practical Applications to Large Molecular Systems* (CRC Press, Boca Raton, 2009).

33. Stratt, R. & Maroncelli, M., Nonreactive dynamics in solution. *J. Phys. Chem.* **100** (31), 12981-12996 (1996).

34. Horng, M. L., Gardecki, J. A., Papazyan, A. & Maroncelli, M., Subpicosecond Measurements of Polar Solvation Dynamics: Coumarin 153 Revisited. *J. Phys. Chem.* **99**, 17311-17337 (1995).

35. Lakowicz, J. R., *Principle of Fluorescence Spectroscopy*, 3rd ed. (Springer, New

York, 2006).

36. O'Connor, D. V. & Phillips, D., *Time-correlated Single Photon Counting* (Academic Press, London, 1984).

37. Forsyth, S. A., Pringle, J. M. & MacFarlane, D. R., Ionic Liquids - An Overview. *Aust. J. Chem.* **57**, 113-119 (2004).

38. Deetlefs, M., Hakala, U., Seddon, K. R. & Wahala, K., in *Ionic Liquids IV: Not just solvents anymore*, edited by Brennecke, J. F., Roers, R. D. & Seddon, K. R. (American Chemical Society, Washington D. C., 2006).

39. Earle, M. J. & Seddon, K. R., Ionic Liquids: Green Solvents for the future. *Pure Appl. Chem.* **72** (7), 1391-1398 (2000).

40. Freemantle, M., Designer Solvents. *Chem. Eng. News* **76** (30th March), 32 (1998).

41. Welton, T., Room-Temperature Ionic Liquids. *Chem. Rev.* **99**, 2071-2083 (1999).

42. Brennecke, J. F., Rogers, R. D. & Seddon, K. R., *Ionic Liquids IV: Not just solvents anymore* (American chemical Society, Washington D.C., 2007).

43. Brennecke, J. F. & Maginn, E. J., Ionic Liquids: Innovative Fluids for Chemical Processing. *AiChE* **47** (11), 2384-2389 (2001).

44. Seymour, R. B., Chemicals in Everyday Life. *Journal of Chemical Education* **64** (1), 63-68 (1987).

45. O'Connor, D. V. & Phillips, D., *Time-correlated single photon counting* (Academic Press, 1984).

46. Adhikary, R., Carlson, P. J., Kee, T. W. & Petrich, J. W. Excited-State Intramolecular Hydrogen Atom Transfer of Curcumin in Surfactant Micelles. *J Phys Chem B* **114**, 2997–3004 (2010).

47. Kee, T. W., Adhikary, R., Carlson, P. J., Mukherjee, P. & Petrich, J. W. Femtosecond Fluorescence Upconversion Investigations on the Excited-State Photophysics of Curcumin. *Aust. J. Chem.* **64**, 23–30 (2011).

CHAPTER II: EXPERIMENTAL METHODS

Time Correlated Single Photon Counting (TCSPC)

Time correlated single photon counting (TCSPC) is one of the most used techniques to gain information about the short time scale on which the majority of photophysical processes occur. There are several good references that discuss this topic to which the reader is referred for additional information and that were also instrumental to the writing of this section of the disseratation.[1-4] A brief overview of the technique follows as well as the specific experimental set-up used in our laboratory.

Basic Principles

As a fluorescence technique, TCSPC relies on the random event of radiative decay following excitation of a molecule. With knowledge of the excitation source and the monitoring of the fluorescence output, one can establish the time delay between an excitation pulse and the fluorescence photon. The fluorophore usually decays following first order kinetics as follows

$$-\frac{d[s_1]}{dt} = k[s_1] \tag{1}$$

Where $[s_1]$ is the first excited singlet state population and k is the rate constant. We can define the lifetime of the excited state that depends on the rate constant k as follows

$$\frac{1}{k} = \tau \tag{2}$$

Here we have the overall rate constant *k* divided into the individual processes that can take place from the excited state (See chapter 1, figure 1 for a schematic representation) where k_{IC} is the rate of internal conversion, k_{rad} is the rate of radiative decay, and k_{ISC} is the rate of intersystem crossing. Finally, τ_f is the fluorescence lifetime. Quickly working through the calculus gives the exponential decay of the fluorophore at time *t*.

$$\left[S_1\right]_t = \left[S_1\right]_0 e^{-\frac{t}{\tau_f}} \tag{3}$$

The TCSPC technique ultimately allows one to record a histogram of this signature exponential decay. This technique relies on the concept that the probability distribution for emission of a single photon after an excitation event yields the actual intensity against time distribution of all the photons emitted as a result of the excitation.[1] The emitted photons are usually collected through a series of electronic components, those being, the constant fraction discriminator (CFD), the time-to-amplitude converter (TAC), and the analog-to-digital converter (ADC). After the signal has passed through each of these components it is then detected by a multichannel plate (MCP).

More specifically, the experiment starts with the excitation pulse that excites the samples and sends a signal to the electronics. This signal is passed through the CFD, which accurately measures the arrival time of the pulse. This signal is passed to the TAC, which generates a voltage ramp that is a voltage that increases linearly with time on the nanosecond timescale. A second channel detects the pulse from the single detected photon. The arrival time of the signal is accurately determined using a CFD, which sends the signal to stop the voltage ramp. The TAC now contains the voltage proportional to the time delay between the excitation and emission signals. The ADC then converts the

signal to a numerical value. A histogram of the decay is measured by repeating this process numerous times with a pulsed-light source.[3] If the operation of the TCSPC electronics follows this “normal mode” the detector will be much to busy detecting the start pulses due to the high repetition rate of the laser source. This results in a very long dead time as the need to “reset” the electronics is constant. With modern laser sources the TCSPC electronics are usually run in “reverse mode.” This is where the emission pulse is used to start the TAC and the excitation pulse is used to stop the TAC. Typically during TCSPC measurements one collects a large number of start-stop cycles and this results in a more complete histogram of the fluorescence decay of the system of interest.

TCSPC Set-up used in our Laboratory

A schematic diagram of the TCSPC experimental set-up used in our laboratory can be seen in figure 1. Using a home-made mode-locked Ti:sapphire oscillator pumped at 532 nm by a Nd:VO_4 Millennia (Spectra-Physics) laser, femtosecond pulses were produced which were tunable from 780 nm – 900 nm having a repetition rate of 82 MHz. With the output selected at 814 nm from the Ti:Sapphire oscillator, the repetition rate was reduced to 8.8 MHz via the use of a Pockels cell (model 350-160 from Conoptics Inc.) and was subsequently frequency doubled through the use of a harmonic generator (model TP-2000B from U-Oplaz Technologies). The produced blue light with a wavelength of 407 nm was used as the primary excitation source for all time-resolved studies. After the harmonic generator a half-wave plate was placed in front of a vertical polarizer to ensure the polarization of the excitation light. The fluorescence was collected at a 90° angle to the excitation source and then passed through an emission polarizer set to the magic angle

(54.7°) with respect to the vertical excitation light. In the case of the anisotropy studies this polarizer was set to 0° and 90° with respect to the vertical excitation light, respectively. A 425 nm cut-off filter was placed before a multichannel plate (MCP) (Hamamatsu) to help remove any unwanted scattered excitation light. When performing the solvation dynamics studies, a monochromator was placed before the MCP to ensure the collection at each selected wavelength. The signal from the MCP detector was amplified and sent to a Becker & Hickl photon counting module (model SPC-630). The instrument response function had a full width at half maximum (FWHM) of ~45 - 50 ps. The FWHM limits the time resolution of the TCSPC apparatus. For more rapid time measurements, the fluorescence upconversion technique is used.

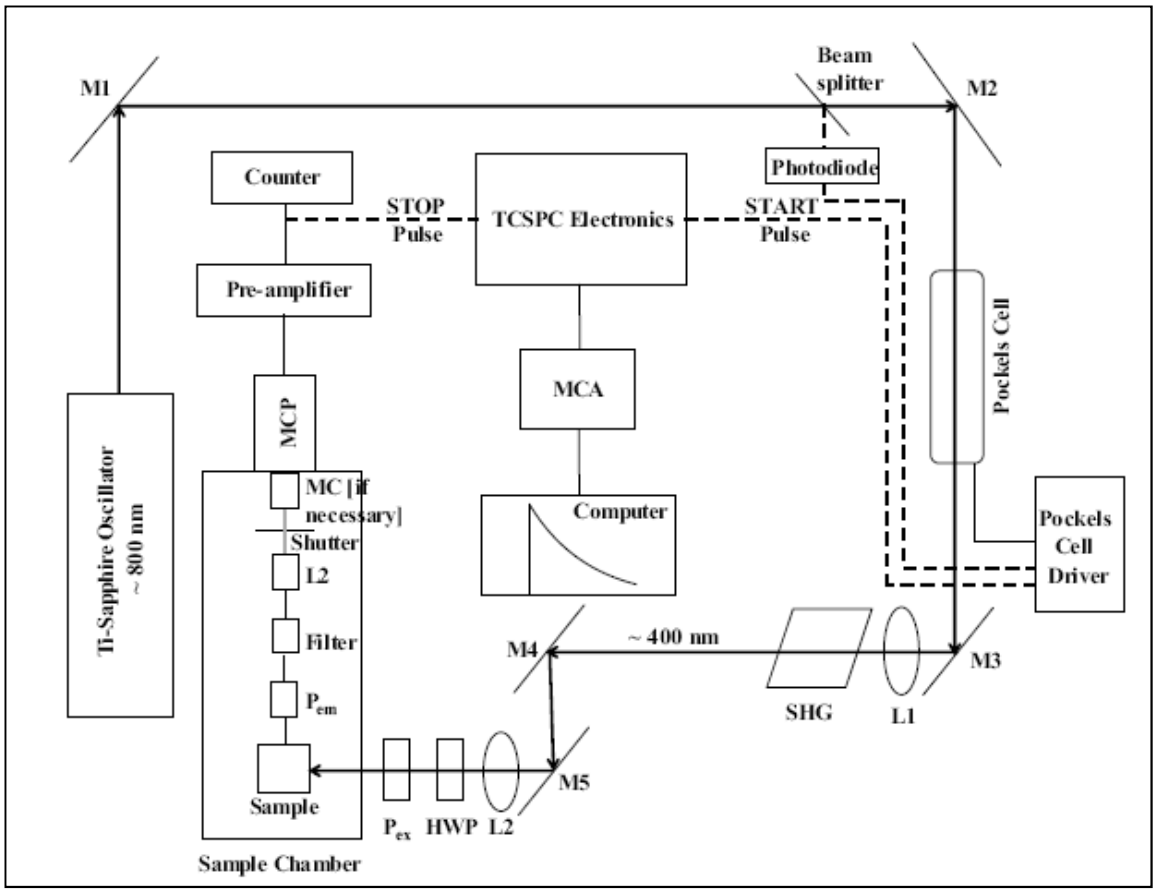

Figure 1 – A schematic diagram of the TCSPC set-up used in our laboratory. See the above text for more details.

Fluorescence Upconversion

Fluorescence upconversion is a valuable fluorescence technique that can allow for ultra-fast time resolution on the order of femtoseconds (10^{-15} s). A basic introduction to the technique follows as well as details on the specific upconversion set-up in our laboratory.

Basic Concepts

Within the framework of the fluorescence upconversion idea is the thought that the fluorescence from the sample is not detected directly. This seems odd, as typically the goal of such techniques is to measure the fluorescence directly from the sample. Often

the limiting factor of that approach is the finite time needed for the detection and processing of that signal by the associated electronics. The idea of fluorescence upconversion is to upconvert the fluorescence signal using the appropriate nonlinear optics. The fluorescence from the sample is mixed with a gate pulse to generate the sum frequency light of both. It is this upconverted sum frequency light that is detected allowing for time resolution due to the detailed knowledge and modulation of the gate pulse.

In an upconversion experiment one pulse is used to excite the sample and the fluorescence (ν_f) is collected and focused along with the gate pulses (ν_g) onto a nonlinear crystal. These two pulses interact with the nonlinear crystal and a new electromagnetic field at the sum frequencies (ν_s) of the two original pulses. Hence we have $\nu_f + \nu_g = \nu_s$. An important consideration for effective sum frequency generation within the nonlinear crystal is that the gate pulse and the fluorescence must be present in the crystal at the same time because the polarization of the electrons is nearly instantaneous. If one of the two essential beams is not present no sum frequency signal can be obtained. Therefore the gate pulse can be delayed for a controlled known amount of time after excitation providing time information about the generated fluorescence. It is also of utmost importance to have the nonlinear crystal at the proper phase matching angle as in figure 2. The delay is typically controlled with a motorized delay stage and is allowed to scan over the desired time range to gain information about the fluorescence decay from the sample (See the lower portion of Figure 2). The time resolution in this technique is limited by the width of the gate beam and the fluorescence signal. Both of these are broadened due to the optics through which they must pass. Therefore, it is beneficial to

make as many of the optics, including the sample cell as thin a possible to avoid broadening the beam.

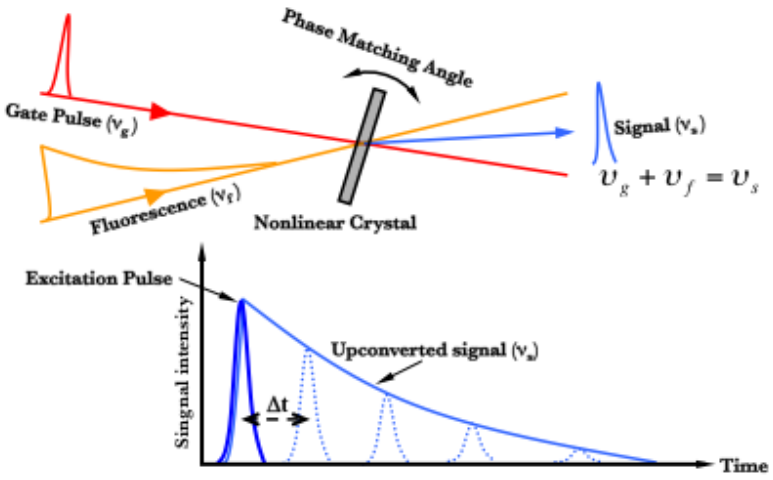

Figure 2 – The upper portion of the diagram shows the nonlinear crystal in which the fluorescence and the gate beam are focused to generate the upconverted signal. The lower poertion of the diagram shows the exponential decay of the excited state as the excitation pulse is scanned over the time delay.

Fluorescence Upconversion Set-up in our Laboratory

A diagram of our fluorescence upconversion set-up can be seen in figure 3 below.[4] The laser source is a homebuilt mode-locked Ti:sapphire oscillator. The fundamental wavelength and repetition rate of the femtosecond output are 814 nm and 88 MHz, respectively. The fundamental output from the oscillator is frequency-doubled by a type-I LBO crystal (2 mm in width). The frequency-doubled pulses (407 nm) are separated from residual fundamental light using a dichroic mirror, and used to excite the sample. The residual of the fundamental is used as the gate pulse to upconvert the fluorescence signal. A filter is used to block trace 407 nm light with the fundamental. The gate pulses pass through a λ/2 plate, turning the polarization by 90° with respect to the

plane of the laser table. The excitation pulses also pass through a λ/2 plate, which is adjusted at the magic angle (54.7°). In our upconversion system, the excitation pulse is delayed with respect to the gate pulse using a motorized delay stage.

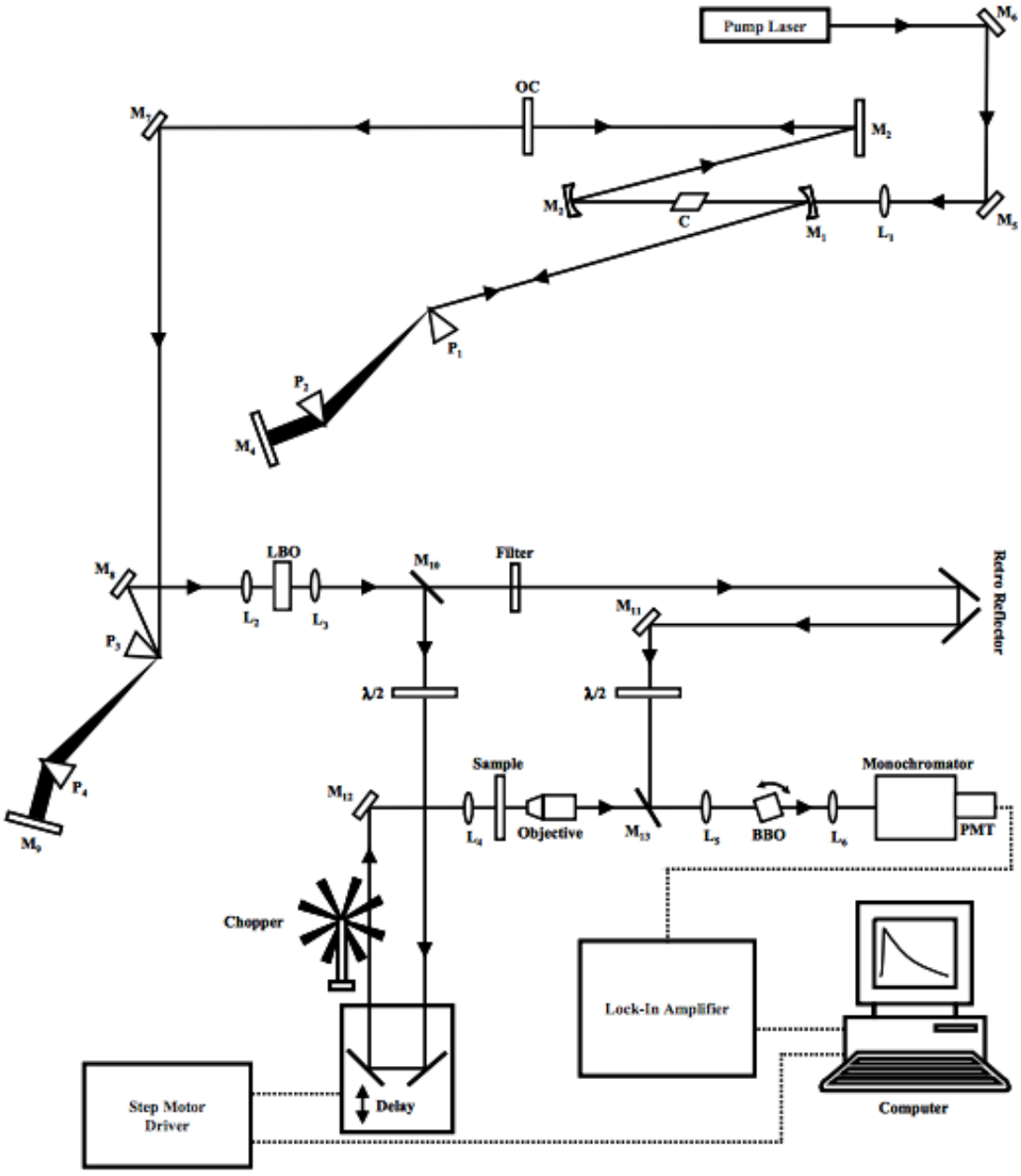

Figure 3 – Schematic diagrm of the fluorescence upconversion system used in our laboratory. M – mirror, L- lens, C- crystal, OC – output coupler, P – prism, BS – beam splitter, BBO – betabarium borate, PMT – photomultiplier tube.

The sample is contained in a rotating glass cell of path length 1 mm mounted perpendicularly to the excitation beam and spins about an axis parallel to the beam. First, the frequency-doubled blue pulses (407 nm) are focused on the sample and the fluorescence signal is collected using a 10x objective lens. Then, the gate pulse and fluorescence signal are focused onto a 0.4 mm type-I BBO crystal to generate the sum frequency light, which is detected by a photomultiplier tube mounted on a monochromator. The upconverted signal is usually weak. In order to pick up the upconverted signal from the background noise, an optical light chopper is set in the excitation beam line. The light is chopped at 1000 Hz, and the signal is counted at this rate using a lock-in amplifier connected to the PMT. The FWHM of the instrument response function is 300 fs, obtained by the cross-correlation function of the frequency doubled and the fundamental light.[5]

Time Resolved Emission Spectra

The emission spectrum of a fluorophore in a polar and viscous environment often shifts to lower energies, longer wavelengths, with time. The intensity decay at each wavelength can be adequately represented by a sum of exponentials,

$$I(\lambda,t) = \sum_{i=1}^{n} \alpha_i(\lambda) e^{-t/\tau_i} \qquad (4)$$

where λ is the emission wavelength, and τ_i the *i*th decay time, and $\alpha_i(\lambda)$ the pre-exponential factor of the *i*th component at the wavelength λ.[6] These decays ($I(\lambda,t)$) are collected at different wavelengths spanning the entire wavelength range of the steady-state emission spectrum. Each of the pre-exponential factors (α_i) sum to 1 representing

100% of the entire decay. The decays at the blue end are faster and those on the red edge show rise times due to the increase in the population of the relaxed state. This rise is indicative of the solvation process. Each I(λ,t) are constructed by normalizing the traces obtained from equation 4 so that the intensity at each wavelength is equal to the steady-state intensity at the wavelength.

$$I\left(\lambda,t\right)=I_{\lambda}^{SS}\frac{I_{\lambda}(t)}{\int_{0}^{\infty}I_{\lambda}(t)} \tag{5}$$

Equation 5 has I_{λ}^{SS} is the steady-state emission intensity at a given wavelength, and $\int_{0}^{\infty}I_{\lambda}(t)$ is the average lifetime at each different wavelength. The time resolved emission spectrum is then obtained by fitting the data points I(λ,t) obtained at each given time to a lognormal function[6]

$$I\left(\nu,t\right)=h\left\{exp\left[-\ln 2\left\{\ln(1+\alpha)/\gamma\right\}^{2}\right]\right\} \tag{6}$$

This is the form of the function used most directly. These lognormal fits provide a good representation of the time-resolved emission spectra in polar solvents. Using these fitting procedures, the peak frequency maxima ν(t) are obtained as a function of time.

The Solvation Correlation Function

Solvation dynamics (see chapter 1) is described well by a normalized correlation function.

$$C\left(t\right)=\frac{\nu\left(t\right)-\nu(\infty)}{\nu(\text{"0"})-\nu(\infty)} \tag{7}$$

This equation is made up of ν(“0”) and ν(∞) are the peak maxima at time t=0 and infinity respectively. The C(t) function is a exponential decay with time and is fitted with a sum of two or three exponentials to obtain the average solvation time τ_s. For C(t) to have standardized meaning, an accurate and universal determination depends on accurate values of ν(“0”) and ν(∞). ν(∞) is usually obtained from the maximum of the steady-state spectrum. The ν(t) are determined from the lognormal fit of the time resolved emission spectra. There is some uncertainty in determining the maxima due to the TRES being very broad at the peak. We have determined the typical uncertainties as follows: “zero-time” ~ steady-state (~ ± 100 cm−1) < time-resolved emission (~ ± 200 cm−1). We use these uncertainties to compute error bars for the C(t). Finally, in generating the C(t), the first point was obtained from the “zero time” spectrum. The second point was taken at the maximum of the instrument response function. Determining the ν(“0”) point is very important and non-trivial to ensuring C(t) is standardized.

Defining and Calculating the “Zero” Time Emission Spectrum

Since all instruments have a finite time resolution and cannot obtain true zero time information it is necessary to determine what the spectrum would look like at zero time in a theoretical way. At zero time the spectrum would come from a molecule that is completely relaxed vibrationally but before any relaxation of the solvent has started. Intramolecular vibrational relaxation occurs on a very fast time scale, on the order of <100 fs. The shift between absorption and emission spectra of a solute before solvation takes place should be equal to the Stokes shift of the same solute in a non-polar solvent.

This has been thoroughly worked through by Fee and Maroncelli and their report is the basis of this explaination.[8] The basic idea is that a molecule has an intrinsic spectra absorption g(ν) and an emission line-shape *f*(ν). These line shapes are related to the absorption (A_{np}) and emission spectra (F_{np}) of the molecule in a non-polar solvent by

$$g(\nu) \propto \nu^{-1} A_{np}(\nu) \tag{8}$$

$$f(\nu) \propto \nu^{-3} F_{np}(\nu) \tag{9}$$

These line shape functions can be used to calculate the absorption and emission spectra of the molecules in an inhomogenously broadened environment. The solvent molecules being distributed around the solute molecule cause broadening (σ) and a shift (δ_0) of the line shape function due to the solvent-solute interactions. Assuming a Gaussian distribution p(δ) of solvent molecules, these effects can be described as a convolution of the line shape function g(ν) with the solvent distribution function p(ν). Based on this assumption, the absorption spectrum in a polar solvent can be written as

$$A_p(\nu) \propto \nu \int g\left(\nu - \delta\right) p\left(\delta\right) d\delta \tag{10}$$

where $p(\delta)=(2\pi\sigma^2)^{-1/2}\exp[-(\delta-\delta_0)^2/2\sigma^2]$. Similarly, the time-zero emission spectrum immediately after excitation (ν_{ex}) in a polar solvent can then be expressed as

$$F_p(\nu, t=0, \nu_{ex}) \propto \nu^3 \nu_{ex} \int g\left(\nu_{ex} - \delta\right) p\left(\delta\right) f(\nu - \delta) k_{rad}(\delta) d\delta \tag{11}$$

Here, ν_{ex} is essentially proportional to the measured absorption spectrum; $\nu^3 f$ is proportional to the emitted quantum distribution over wavenumbers. The k_{rad} is the radiative constant. The terms, $f(\nu-\delta)k_{rad}(\delta)$ leads to emission intensity function and $g(\nu-\delta)p(\delta)$ to convolution of the solvent distribution initially transferred to the excited state.

g(ν) and f(ν) are obtained from the absorption and emission spectra in a non-polar solvent. The broadening and shift by the solvent which define distribution function, p(δ), are determined as a set that yields closest match with the absorption spectra in an polar solvent of interest when convoluted with g(ν). The radiative rate function is calculated with shift using

$$k_{rad}(\delta) \propto \frac{\int f(\nu-\delta)\nu^3 d\nu}{\int f\left(\nu-\delta\right) d\nu} \tag{12}$$

This method was program by Dr. Song and is used in our laboratory to obtain a standardized time zero spectrum. This time zero spectrum is crucial to obtaining an accurate C(t) function and its validity was explored and extolled in a report here.[9] The information discussed in this chapter regarding the time resolved emission spectrum can be summed up graphically as seen in figure 4.

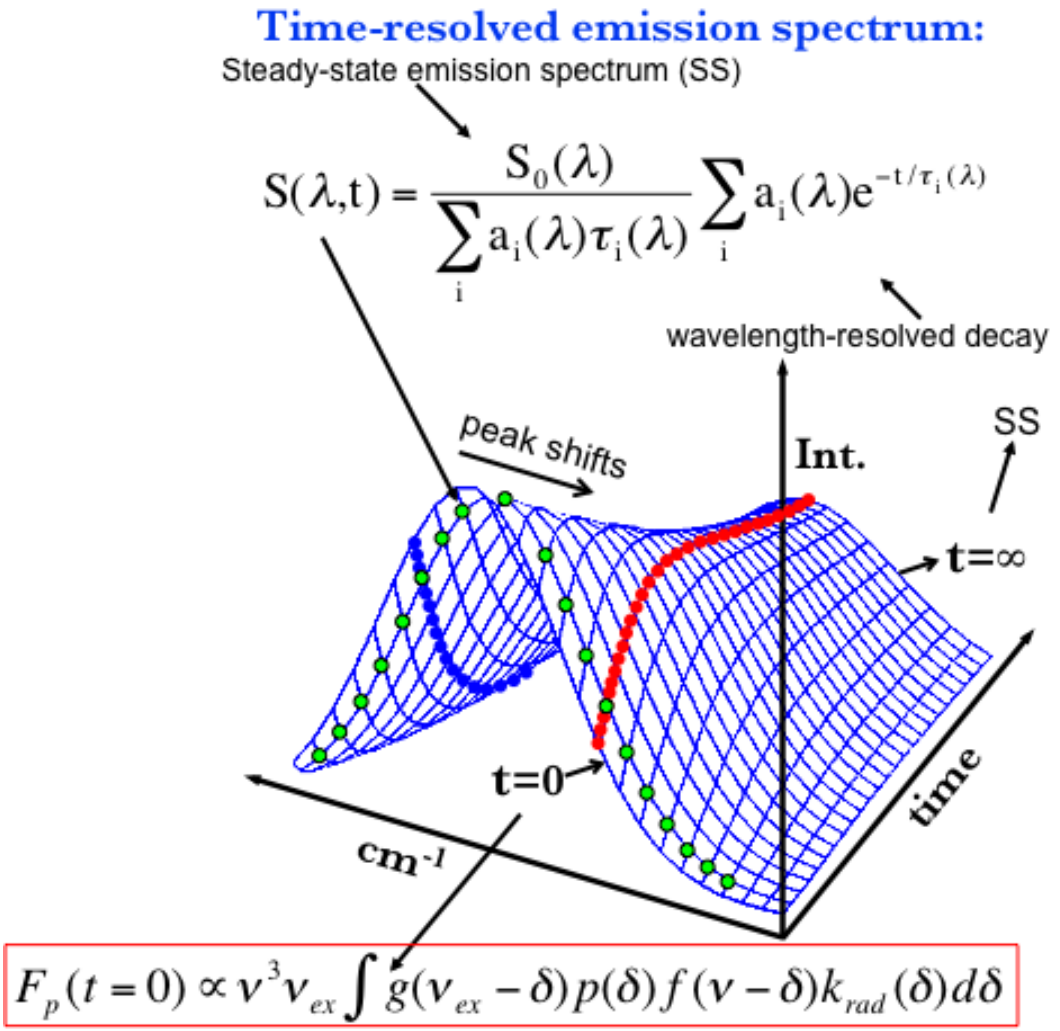

Figure 4 – A diagrammatic description of how each of the pieces involved in constructing the time resolved emission spectrum come together.

References

(1) O'Connor, D. V.; Phillips, D. *Time-correlated Single Photon Counting;* Academic Press, 1984.

(2) Fleming, G. R.; *Chemical Applications of Ultrafast Spectroscopy;* Oxford University Press, 1985.

(3) Lakowicz, J. R. *Principles of fluorescence spectroscopy*, 3rd ed.; Springer New York, 2004.

(4) Birks, J. B. *Photophysics of Aromatic Molecules*; Wiley-Inter- science: London, 1970.

(5) Adhikary, Ramkrishna; *Application of fluorescence spectroscopy: excited-state dynamics, food-safety, and disease diagnosis*, PhD thesis at Iowa State University, 2011.

(6) Lakowicz, J. R., Gratton, E., Cherek, H., Maliwal, B. P. & Laczko, G. *Journal of Biological Chemistry* **259**, 10967–10972 (1984).

(7) HORNG, M., GARDECKI, J., Papazyan, A. & Maroncelli, M. *J Phys Chem* **99**, 17311–17337 (1995).

(8) FEE, R. & Maroncelli, M. *Chem Phys* **183**, 235–247 (1994).

(9) Mukherjee, P. *et al.* *J Phys Chem B* **112**, 3390–3396 (2008).

CHAPTER III: EXCITED-STATE INTRAMOLECULAR HYDROGEN ATOM TRANSFER OF CURCUMIN IN SURFACTANT MICELLES

A Paper Published in the *Journal of Physical Chemistry B*

Ramkrishna Adhikary,[1] Philip J. Carlson,[1] Tak W. Kee[2]* and Jacob W. Petrich[1]*

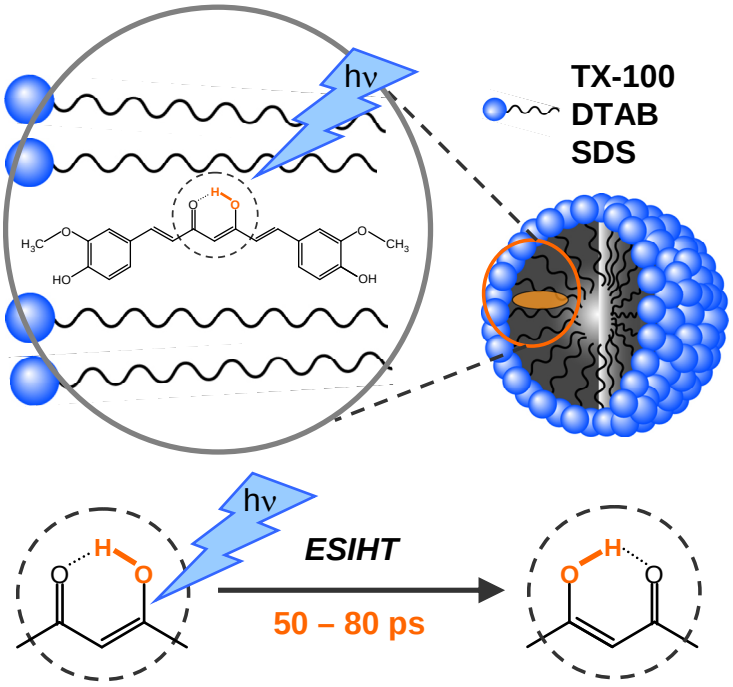

Abstract

Femtosecond fluorescence upconversion experiments were performed on the naturally occurring medicinal pigment, curcumin, in anionic, cationic, and neutral

---

Reprinted with permission from the American Chemical Society copyright (2010) *Journal of Physical Chemistry B*, **2010**, 114, 2997-3004
[1] Department of Chemistry, Iowa State University, Ames, Iowa 50011
[2] School of Chemistry and Physics, University of Adelaide, Adelaide, South Australia, 5005, Australia
*Author to whom correspondence should be addressed.

micelles. The use of surfactant micelles to capture and transport curcumin addresses several challenging issues in the application of this medicinal pigment as a disease treatment agent. The benefits include a high concentration of an aqueous dispersion, significant bioavailability, and prevention of rapid degradation in water. Photodynamic therapy is one of the most recently discovered medicinal applications of curcumin for cancer treatment. It is, therefore, relevant to investigate the photophysics of curcumin in surfactant micelles. In our studies, the micelles are composed of sodium dodecyl sulfate (SDS), dodecyl trimethyl ammonium bromide (DTAB) and triton X-100 (TX-100). We demonstrate that the excited-state kinetics of curcumin in micelles have a fast (3 – 8 ps) and slow (50 – 80 ps) component. While deuteration of curcumin has a negligible effect on the fast component, the slow component exhibits a pronounced isotope effect, indicating that micelle-captured curcumin undergoes excited-state intramolecular hydrogen atom transfer (ESIHT). In addition, the wavelength-dependent fluorescence upconversion results reveal that the short component is due to solvation of curcumin in the micelle.

Introduction

Curcumin, 1,7-bis(4-hydroxy-3-methoxyphenyl)-1,6-heptadiene-3,5-dione, has received considerable attention owing to its numerous medicinal properties.[1-9] Curcumin, whose structure is shown in Figure 1, is the major ingredient of the yellow pigments (curcuminoids) in the Indian spice plant turmeric. While curcuminoids are composed of approximately 77% curcumin, demethoxy curcumin (17%) and bisdemethoxy curcumin (3%) constitute most of the remaining portion. In addition, cyclocurcumin, which was

isolated in 1993, is also present at a trace level.[10] A large number of studies have shown that curcumin possesses anticancer,[3,4] anti-Alzheimer,[6] anti-cystic fibrosis,[7] and other desirable medicinal benefits.[1,8,9] Of particular interest are the prospects of curcumin or curcumin-like nontoxic agents to exhibit anticancer effects without side effects,[3,4] unlike conventional chemotherapy drugs. Several clinical trials are either underway or have recently been completed with curcumin as the treatment agent.[11,12] The preliminary results from these trials are highly promising.

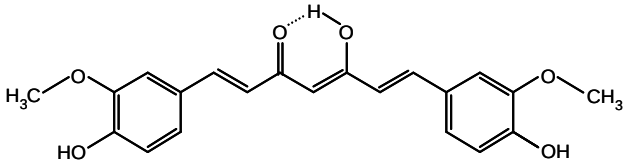

Figure 3 - Structure of keto-enol form of curcumin.

Two major challenges in the application of curcumin as an effective treatment agent are lack of bioavailability and severely limited stability in aqueous environments. Because of the low aqueous solubility, curcumin tends to aggregate and precipitate in water, limiting its bioavailability.[13-16] In addition, curcumin undergoes rapid degradation in water and buffer solutions, with a reaction half-life of 9.5 minutes at pH 7.2.[17] It has been demonstrated that the degradation is mostly due to deprotonation of curcumin, producing the degradation products: vanilin, ferulic acid, and feruroyl methane.[17,18] It is interesting that most of these products have medicinal properties as well. Previous studies have shown that encapsulation of curcumin in surfactant micelles and binding to proteins resolve these two major issues.[14-16]

Micelles are the supramolecular aggregation of surfactant molecules in water, which occurs at a level above the critical micelle concentration (CMC). Owing to the amphiphilic nature of surfactants, the hydrophobic tails form the core of the micelle and the polar head groups constitute the interface with water. The polar head group is either

positively or negatively charged, or uncharged, forming cationic, or anionic, or nonionic micelles, respectively. Micelles are commonly used as drug delivery tools to solubilize hydrophobic drugs and to protect them from reacting with the surrounding environment, including water molecules and ions.[19] In addition to homogeneous micelles, aggregation of multiple types of surfactants also leads to formation of either mixed micelles or vesicles, which also have significant potential for drug delivery applications.[20,21] Recently, developments of block copolymer micelles are attracting interest in the pharmaceutical and pharmacological fields owing to the importance of micellar systems in drug delivery.[22]

Micellar systems may potentially play an important role in leading to improved clinical use of curcumin. It is established that micelle-captured curcumin is well dispersed in aqueous solutions, thereby increasing the bioavailability significantly.[13,15,16] Moreover, curcumin is trapped in the regions of the micelle where the presence of free water molecules is relatively limited, preventing alkaline hydrolysis, which is the major mechanism for degradation.[17,18] It is therefore plausible that association to micelles plays a considerable role in enabling curcumin to exhibit its medicinal characteristics. Apart from preventing degradation, micelles also serve as well defined model systems for biomembranes. It has been shown that a large portion of curcumin is membrane bound in a biological environment.[23] Investigations on the behavior of curcumin in micelles may provide valuable insight into the properties of curcumin in biomembranes.

In addition to the medicinal properties of curcumin mentioned earlier, recent work has demonstrated that curcumin is effective for the treatment of melanoma.[24-28] In particular, studies have shown that the antiskin cancer effects of curcumin are enhanced

significantly with light,[26-28] clearly indicating the importance of light-induced physical and chemical processes of curcumin. Curcumin exists predominantly as the keto-enol tautomer in a number of solvents.[29] It is capable of executing excited state intramolecular hydrogen atom transfer (ESIHT) due to the presence of strong intramolecular hydrogen bonding between the proton donor and the acceptor atom, as indicated in Figure 1. Although there is a general agreement that ESIHT is a major photophysical event of curcumin,[30-32] the exact time scale of this phenomenon was not well established until our recent work.[32] Using deuteration of curcumin and time-resolved fluorescence upconversion as a technique for probing ESIHT, our work has shown that the time constant of ESIHT of curcumin is 70 ps in methanol and 120 ps in ethylene glycol.[32] It has been proposed that the presence of a labile hydrogen as a result of ESIHT plays a role in the medicinal effects of other naturally occurring pigments such as hypericin and hypocrellin.[33-40] As for curcumin, it is possible that ESIHT results in partial deprotonation, which induces fragmentation to yield the medicinal degradation products mentioned earlier. While ESIHT of curcumin in polar organic solvents has been established,[32] it remains unclear if micelle-captured curcumin also undergoes this photoinduced process. It is known that intramolecular proton transfer processes are affected in confined environment due to the structure, various interfaces and dynamics of the environment.[41]

Here we present unambiguous results demonstrating that ESIHT is a major photophysical event of curcumin in micelles. The well studied micellar systems composed of sodium dodecyl sulfate (SDS), dodecyl trimethyl ammonium bromide (DTAB) and triton X-100 (TX-100), which are anionic, cationic and nonionic in nature,

respectively, were chosen for our investigations. These micelles not only serve as model systems for biomembranes, but also enable photophysical investigations as a function of the polarity of the headgroup. By comparing the excited-state decay kinetics of the deuterated and nondeuterated species obtained by fluorescence upconversion spectroscopy, we show that the time constant of ESIHT of curcumin in these micelles ranges from 50 – 80 ps. In addition to ESIHT, a fast component of 3 – 8 ps was also observed. Results from multiwavelength studies reveal that the fast component is due to solvation dynamics of curcumin in the micellar media. In short, the present studies offer the first insights into the photophysical events of curcumin in micelles, which may lead to further understanding of the behavior of curcumin in biomembranes.

Experimental Section

Materials

Curcumin (purity ~ 70% HPLC) and high purity curcumin (≥ 98.5%) were purchased from Sigma Aldrich and Alexis Biochemicals, respectively. High purity curcumin was used for all experiments except in the solvation dynamics studies. We confirmed that curcumin from the two sources produces identical fluorescence upconversion results at 520 nm. Triton X-100 (TX-100, reduced), dodecyltrimethyl ammonium bromide (DTAB, ~99%) and sodium dodecyl sulfate (SDS, ~99%) were obtained from Sigma Aldrich and used without further purification. Tris-d11 solution (1 M in D2O, 98 atom %D), deuterium chloride (35 wt% solution in D2O, 99 atom %D) and D2O (99.9 atom %D) were purchased from Sigma Aldrich. The nondeuterated tris (>99.8% purity) was acquired from AMRESCO. Methanol and Methanol-d4 (purity

99.8%) were obtained from Fisher Scientific and Cambridge Isotope Laboratories, Inc., respectively, and used as received. All solutions were prepared with water from a Millipore Milli-Q NANOpure water system.

Sample Preparation

A 20 mM buffer solution was prepared at either pH or pD = 7.4 for all the experimental work in these studies using tris or tris-d_{11}, respectively. The concentration of surfactant was maintained at 0.1 M, which is above the CMC for each of the micelles, in nondeuterated and deuterated tris buffer. Two stock solutions of curcumin in methanol and methanol-d_4 were used for steady-state, time-correlated single photon counting (TCSPC) measurements. A small quantity (2 μL) of the curcumin stock solution (4.5 or 1.5 mM) was transferred to the micellar solution to yield a solution with a curcumin concentration of 3 or 1 μM for the UV-Vis or fluorescence spectra, respectively. Care was taken to keep the total methanol content of the final sample solution at < 0.1% for all solutions. The solutions were then allowed to equilibrate overnight in either the tris/H_2O or tris-d_{11}/D_2O solution in the dark prior to the optical experiments. Equilibration was particularly important for curcumin in the D_2O micellar solutions to ensure a complete exchange of the enolic hydrogen of curcumin with deuterium, as indicated below. For the upconversion measurements, the required amount of curcumin (powder form) was directly added to the micellar solution to result in a curcumin concentration of 0.5×10^{-3} to 1×10^{-3} M. This solution was then sonicated for an hour in the dark. All the solutions for fluorescence upconversion measurements were allowed to equilibrate overnight. In addition, data collected with the deuterated samples that were equilibrated for 48 hours

are identical to those with only overnight equilibration, indicating completion of H/D exchange.

Steady-State Measurements

Steady-state UV-Vis absorption and emission spectra were acquired on a Hewlett Packard 8453 UV-visible spectrophotometer and Spex Fluoromax-4 with 1-nm resolution at room temperature. The emission spectra were corrected for lamp spectral intensity and detector response. The emission spectra were obtained with an excitation wavelength of 407 nm with 3-nm bandpass for all the samples. A 5-mm path-length quartz cuvette was used for all the absorption and emission measurements.

Time-Resolved Measurements

Excited-state lifetime measurements were performed using the TCSPC technique. A homebuilt mode-locked Ti:sapphire oscillator pumped by a Nd:VO_4 laser (Millennia, Spectra Physics) producing femtosecond pulses tunable from 780 to 900 nm with a repetition rate of 82 MHz was used as the laser source. The fundamental wavelength at 814 nm from the Ti-sapphire oscillator was modulated by a Pockels cell (Model 350-160, Conoptics Inc.) to reduce the repetition rate to approximately 8.8 MHz and was subsequently frequency doubled by using a harmonic generator (Model TP-2000B, U-Oplaz Technologies). The resulting blue light, which had a central wavelength of 407 nm, provided the excitation source. The fluorescence was collected at a 90^o geometry, and passed through an analyzer set at the magic angle (54.7^o) with respect to excitation polarization. A half-wave plate before a vertical polarizer ensured the polarization of the

excitation light. A 425 nm cut-off filter was placed in front of a multichannel plate, MCP (Hamamatsu). The detector output was amplified and fed to the Becker & Hickl photon counting module Model SPC-630. The full-width-at-half-maximum (FWHM) of the instrument response function is ~40 – 45 ps. All the measurements were made in a 3.33 ns time window with a total of 1,024 channels. A total of 65,000 counts were collected at the peak channel for all the lifetime measurements. A cuvette of 1-cm path length was used for all the lifetime measurements.

The apparatus for fluorescence upconversion is described in detail elsewhere.[42] In short, the laser source was also a homebuilt mode-locked Ti:sapphire oscillator. The fundamental wavelength and repetition rate of the femtosecond output were 814 nm and 82 MHz, respectively. The fundamental output from the oscillator was frequency-doubled by a type-I LBO crystal (2 mm). The frequency-doubled pulses (407 nm) were used to excite the sample and the residual of the fundamental was used as the gate pulse to upconvert the fluorescence signal. The polarization of the excitation pulse was at the magic angle relative to that of the gate pulses. First, the frequency-doubled blue pulses (407 nm) were focused onto a rotating cell containing the sample and the fluorescence signal was collected using a 10x objective lens. Then, the gate pulse and fluorescence signal were focused onto a 0.4 mm type-I BBO crystal to generate the sum frequency light, which was detected by a photomultiplier tube mounted on a monochromator. The full-width-at-half-maximum (FWHM) of the instrument response function is 300 fs, obtained by the cross-correlation function of the frequency doubled and the fundamental light. All experiments were performed at room temperature. For most fluorescence upconversion experiments, a time window of 100 ps was used with a step size of 0.2 ps.

The solvation correlation function, *C(t)*, was used to analyze and quantify the solvation dynamics.

$$C(t) = \frac{\nu(t) - \nu(\infty)}{\nu(\text{"0"}) - \nu(\infty)} \quad (1)$$

The ν*("0"),* ν*(t)* and $\nu(\infty)$ in eq 1 denote the peak frequency (typically in cm^{-1}) of the zero time, *t* and infinity emission spectra. Using the approach of Fee and Maroncelli,[43] the "zero time" emission spectrum was approximated by using the emission spectrum of curcumin in hexanes. As for $\nu(\infty)$, the peak frequency of the steady-state fluorescence spectrum was used. In these investigations, fluorescence upconversion measurements were performed at 15 wavelengths, ranging from 470 – 630 nm, with a time window of 10 ps to construct time-resolved emission spectra with sufficient data points to reflect the real spectra. Each of the time-resolved emission spectra was fitted with the log-normal function and the peak frequency $\nu(t)$ was obtained using the procedure outlined by Maroncelli and Fleming.[44] The relatively large width of the time dependent emission spectra typically results in uncertainty in the exact position of the maxima. Therefore, by using the signal-to-noise ratio and width of the spectrum (including "zero-time", steady-state, or time-resolved emission spectrum) as sources of uncertainty, we determined the following typical uncertainties: time-resolved emission (~ ± 200 cm^{-1}), "zero-time" and steady-state (~ ± 100 cm^{-1}). These uncertainties were used to compute error bars for the $C(t)$. Finally, the fractional solvation at 300 fs was calculated using $f_{300fs} = 1 - C(t = 300$ fs).

Results and Discussions

UV-Vis Absorption and Emission Spectra of Curcumin in Micelles

The spectral properties of curcumin in three different micelles were investigated systematically to examine the influence of micellar environments on spectral features. Figure 2 depicts the UV-vis absorption and emission spectra of curcumin in TX-100, DTAB and SDS micelles under deuterated (blue) and non-deuterated (red) condition at pD or pH = 7.4 in tris buffer. Curcumin exhibits a broad and intense absorption peak at 426 nm, 423 nm and 432 nm in the TX-100, DTAB and SDS micelles, respectively. A small shoulder in the absorption band is present at 445 nm and 442 nm in the TX-100 and DTAB micelles, whereas curcumin produces a featureless absorption band in the SDS micelle. The absence of vibronic structure in the absorption band of curcumin, as observed in the SDS micelle, is also observed for curcumin in water. This phenomenon indicates that curcumin may interact strongly with water molecules in the Stern layer of the micelle, as will be discussed

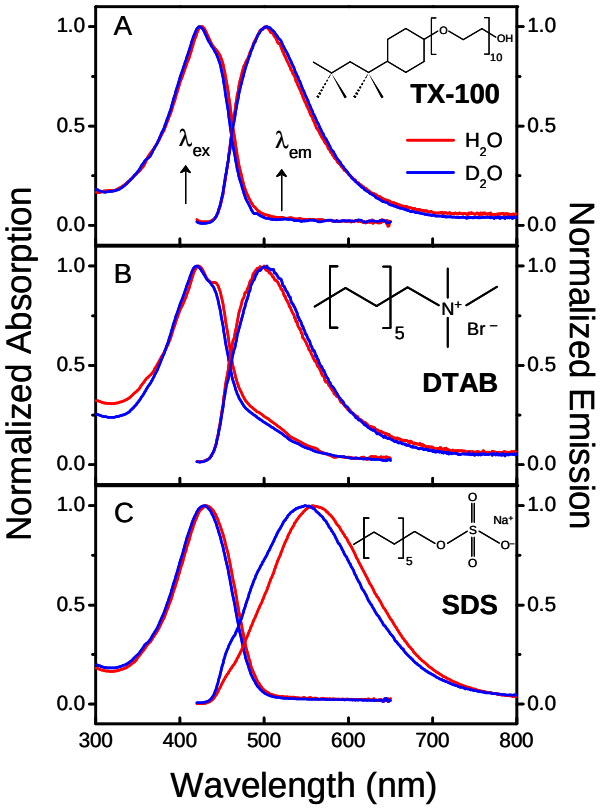

Figure 4 - UV-Vis absorption and emission spectra of curcumin in (A) TX-100, (B) DTAB, and (C) SDS in H2O (red) and D2O (blue).

furthering more detail forthwith. Additionally, a broad spectral shoulder is present around 500 nm for curcumin in the DTAB micelle. This extra shoulder, which is absent in the other two micelles, is due to the presence of a small population of deprotonated curcumin at pH = 7.4.

As for the emission spectrum of each micelle, curcumin shows a broad spectrum peaked at 501 nm, 498 nm and 548 nm in the TX-100, DTAB and SDS micelles, respectively. The peak positions of the UV-vis absorption and emission spectra of curcumin are affected by the isotopic substitution, as shown in Figure 2. While a 3-nm blue shift appears in the UV-vis absorption of curcumin in both the TX-100 and DTAB micelles in D_2O, a red shift with the same magnitude in the emission maximum emerges in these micelles. As for the SDS micelle in D_2O, a 3-nm blue and ~10 nm red shift are found in the absorption and emission maxima, respectively. The changes in absorption and emission peak positions are possibly due to changes in zero-point energies in S_0 and S_1 induced by deuteration.[45,46]

A comparison between the UV-vis absorption and emission spectra of curcumin in micelles with those in a number of organic solvents and water provides valuable insights. The UV-vis absorption spectra of curcumin in the TX-100 and DTAB micelles resemble those of curcumin in aprotic solvents, including chloroform and toluene,[32,47] suggesting similarities between the environments. However, the emission spectra of curcumin in these micelles are red-shifted compared to those in the aprotic solvents, potentially due to interactions with water molecules at the interface and within the micelle,[48-52] as will be discussed further in a later section. It is well established that curcumin exhibits a red-shifted emission spectrum in protic solvents including methanol

and water, with an emission maximum around 550 nm. The overall results suggest that curcumin is likely to be located in the palisade layer of the TX-100 and DTAB micelles, which is consistent with results from another study.[31] As for the SDS micelle, the positions of the UV-vis absorption and emission maxima are identical to those of curcumin in methanol and water, indicating that the micellar environment is analogous to the polar environment in these protic solvents. This suggests that curcumin is probably situated near the Stern layer of the SDS micelle, which facilitates strong interactions with bulk water.

The Stokes shifts of curcumin are 75 nm, 75 nm, and 116 nm in the TX-100, DTAB and SDS micelles, respectively. Interestingly, the value of the Stokes shift for TX-100 and DTAB micelles are similar to those measured for human and bovine serum albumin (HSA and BSA) bound curcumin.[14,53-56] It is established that curcumin binds strongly in the hydrophobic pocket of these proteins. The similar Stokes shift values for TX-100 and DTAB micelles imply that the micellar environment is similar to the hydrophobic regions of HSA and BSA. In contrast, the sizeable Stokes shift observed in the SDS micelle is virtually identical to that observed in a buffer solution, which reflects that the local environment of curcumin in the SDS micelle may have a significant bulk water content, which further supports that curcumin is located near the Stern layer of the micelle.

Fluorescence Upconversion and Excited-State Intramolecular Hydrogen Atom Transfer of Micelle-Captured Curcumin

The fluorescence upconversion results of curcumin in the TX-100, DTAB and SDS micelles are shown in Figure 3. The fluorescence upconversion decay traces of curcumin in both nondeuterated and deuterated micellar environments at pH and pD =7.4, respectively, are illustrated in the figure. The decay kinetics were monitored at 520 nm with an excitation wavelength of 407 nm. Collection of time-resolved florescence at 520 nm for the SDS micelle provides early time excited-state relaxation information as this wavelength is on the blue side of the emission spectrum. In the case of curcumin in TX-100 and DTAB micelles, since 520 nm is on the red side of their emission peak maxima, relaxation processes including solvation could be pronounced as curcumin shows a strong solvatochromatic behavior. All the upconversion decays are well fitted with a biexponential function within the 100 ps time window and the results are summarized in Table 1. Curcumin in the TX-100/H_2O system shows a fast component of 8 ± 2 ps and a slow component of 80 ± 10 ps. Upon deuteration of

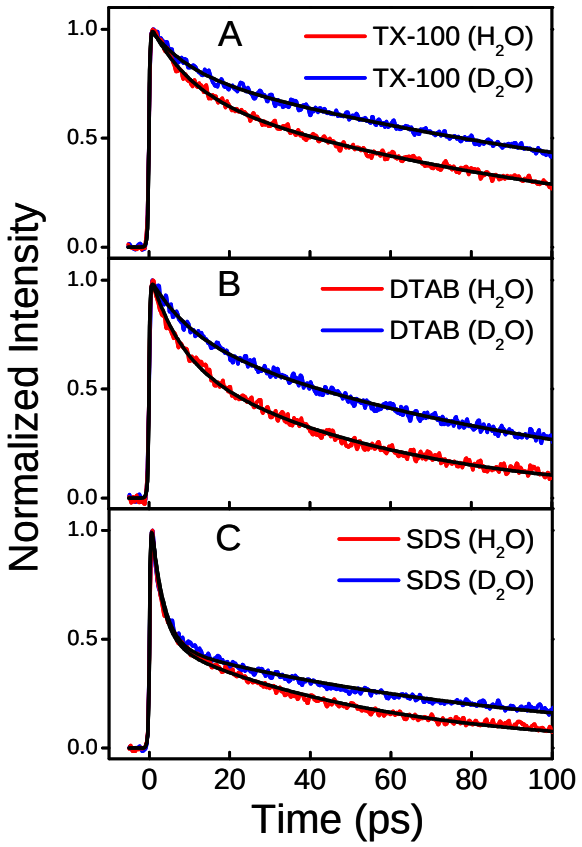

Figure 5 - Fluorescence upconversion decays of curcumin collected at 520 nm in (A) TX-100, (B) DTAB and (C) SDS micelles at pH = 7.4 tris buffer (red) with an excitation wavelength of 407 nm. Corresponding upconversion decays in deuterated micellar environment at pD = 7.4 (blue) are also included. Curcumin shows a prominent isotope effect in all three micellar media.

curcumin in the same micelle, a biexponential decay with time constants of 8 ± 2 and 130 ± 20 ps is obtained. It is important to note that while the fast component remains identical within experimental error in the two results, the slow component shows a significant isotope effect of 1.6. The isotope effect on the slow component clearly indicates that ESIHT occurs with a time constant of 80 ps

Table 1 - Fluorescence upconversion decay parameters for curcumin in different micellar systems. The fluorescence upconversion traces, $f(t)$, were fitted with the multi-exponential function $f(t) = a_1 \exp(-t/\tau_1) + a_2 \exp(-t/\tau_2)$.

Micellar system	a_1	τ_1 (ps)	a_2	τ_2 (ps)
TX-100/H_2O	0.30 ± 0.04	8 ± 2	0.70 ± 0.04	80 ± 10
TX-100/D_2O	0.23 ± 0.03	8 ± 2	0.77 ± 0.03	130 ± 20
DTAB/H_2O	0.36 ± 0.03	6 ± 2	0.64 ± 0.03	50 ± 5
DTAB/D_2O	0.22 ± 0.03	6 ± 2	0.78 ± 0.03	80 ± 5
SDS/H_2O	0.57 ± 0.03	3 ± 2	0.43 ± 0.03	55 ± 3
SDS/D_2O	0.57 ± 0.03	3 ± 2	0.43 ± 0.03	85 ± 6

in TX-100. In DTAB/H_2O and SDS/H_2O, the time-resolved fluorescence also exhibited a distinct biexponential decay. The fast component has time constants of 6 ± 2 and 3 ± 2 ps whereas in the slow component 50 ± 5 and 55 ± 3 ps are obtained for curcumin in the DTAB and SDS micelles, respectively. Deuteration of curcumin induces a similar isotope effect, *i.e.*, an identical fast component and lengthening of the slow component. The time constants of the long component are 80 ± 5 and 85 ± 6 ps in the DTAB/D_2O and SDS/D_2O media, respectively. The presence of an isotope effect of ~1.6 for curcumin in these two micelles reinforces our assignment of the long-lived component to ESIHT. As

for the fast component observed in the results, further discussion will be given in the following section.

Several studies have shown that the ESIHT process in curcumin is highly sensitive to the presence of hydrogen bonding between curcumin and the solvent.[30-32] Nardo et al. and Khopde et al. independently reported that there is a ~50 ps decay component in the fluorescence lifetime (89 and 64 ps, as measured by the two groups, respectively) of curcumin in cyclohexane using TCSPC.[30,31] This decay component is, however, limited by the time resolution of TCSPC apparatus. It is accepted that this fast decay component is due to ESIHT of curcumin.[31] The ESIHT time constant of curcumin in this nonpolar solvent is shorter than that in methanol, which has a value of ~ 70 ps.[32] The results imply that the strength of the intramolecular hydrogen bond of curcurmin is the determining factor in the rate of ESIHT. These authors, furthermore, suggest that in protic solvents, such as methanol and ethanol, the keto-enol group of curcumin forms strong hydrogen bonds with the solvent molecules, in addition to the intramolecular hydrogen bond within the keto-enol group.[30,31] The interactions between curcumin and the protic solvent molecules interfere with the intramolecular hydrogen bond, weakening the bond effectively, thereby decreasing the rate of ESIHT. However, such perturbation in intramolecular hydrogen bonding is absent in nonpolar solvents such as cyclohexane, enabling a strong intramolecular hydrogen bond in the keto-enol moiety of curcumin and facilitating a fast ESIHT.

The ESIHT time constant for curcumin in the TX-100 micelle, with a value of 80 ps as measured in this fluorescence upconversion study, is very similar to that of curcumin in methanol (70 ps), as reported in our previous study using the same

technique.[32] This indicates a substantial level of curcumin-solvent and curcumin-surfactant intermolecular hydrogen bonding in the micelle. This result is consistent with a previous study, suggesting that curcumin is trapped in the palisade layer of the micelle,[31] which is a relatively hydrophilic layer of the micelle.[57] In addition, studies have shown that the C-O groups in TX-100 interact favorably with water, which support that there is a substantial level of water in the micelle.[58,59] Furthermore, curcumin may also have considerable hydrogen bonding with oxygens in the C-O groups in the TX-100 surfactants, as will be discussed below. In short, in the case of the TX-100 micelle, our results indicate that hydrogen bonding between curcumin and the micellar environment is similar to that between curcumin and bulk methanol, which is consistent with results from a previous report.[31]

In the DTAB and SDS micelles, the ESIHT time constants are approximately 50 ps, as shown in Table 1. It appears that the fast ESIHT times observed in these micelles compare well with that in the nonpolar solvent cyclohexane.[30,31] However, as indicated earlier, the ESIHT process of curcumin in cyclohexane is most likely faster than what was measured with TCSPC due to limited temporal resolution. In comparison to curcumin in the TX-100 micelle, the ESIHT process occurs faster in the DTAB and SDS micelles. It is obvious that there is a stronger curcumin intramolecular hydrogen bond, and a weaker curcumin-water or curcumin-surfactant interaction in these micelles compared to TX-100. To gain insight into the higher rates of ESIHT in the DTAB and SDS micelles relative to that of TX-100, we first consider the water content of the micelles. Studies have suggested that the water contents are similar for the DTAB and TX-100 micelles but higher in the SDS micelle.[60] Therefore, it follows that the

curcumin-water hydrogen bonding is likely to play a minor role in leading to a higher rate of ESIHT for curcumin in the DTAB and SDS micelles. An obvious difference between TX-100 and the other two surfactants is that the presence of a high number of C-O groups in the backbone of TX-100, which may interact with curcumin through hydrogen bonding. In contrast, the surfactant backbones of DTAB and SDS are composed of the dodecyl group, which only interacts with curcumin through weak van der Waals forces. It is likely that the presence of a considerable hydrogen bonding network for curcumin in the TX-100 micelle leads to a slower rate of ESIHT. In the DTAB and SDS micelles, however, the ESIHT rate is higher due to the absence of such hydrogen bonding network. While the results in this study are consistent with the notion of additional hydrogen bonding in the TX-100 micelles for curcumin, more work will be necessary to understand this effect fully.

Early Time Solvation Dynamics in Micelles

The fluorescence upconversion results in Figure 3 show that in addition to the component that is attributed to ESIHT, there is an early time decay component with a time constant significantly shorter than the ESIHT component. Table 1 summarizes the time constant of the fast component, showing that values of 8, 6 and 3 ps were obtained for curcumin in TX-100, DTAB, and SDS micelles, respectively. Interestingly, unlikely the ESIHT component which shows an isotope effect, the fast decay component is insensitive to deuteration of curcumin. As shown in Table 1, the τ_1 values are virtually identical for nondeuterated and deuterated curcumin in each of the micelles. In our previous study on curcumin in polar organic solvents, an isotope effect-free fast decay

component was also observed and we demonstrated that the decay component is due to solvation of curcumin in these solvents.[32] Using the previous results as a guide, we conducted a series of fluorescence upconversion experiments with a time window of 10 ps. The results are shown in Figure 4. For curcumin in the TX-100 micelle (Figure 4A), the fluorescence upconversion traces show a clear decay at 470 nm (blue) and this decay slows down considerably at 540 nm (red). However, at 610 nm (green), the fluorescence decay vanishes and a rise component is observed. The presence of the decay and rise components as a function of fluorescence wavelength shown in Figure 4 is a key signature of solvation dynamics. As will be discussed further below, water molecules in the micellar structure play a major role in solvating curcumin. For curcumin in the DTAB micelle (Figure 4B), an almost identical trend in the fluorescence upconversion is shown, with a rise component observed at 610 nm. While a similar behavior of the multiwavelength fluorescence upconversion is shown by curcumin in the SDS micelle, the wavelengths at which the

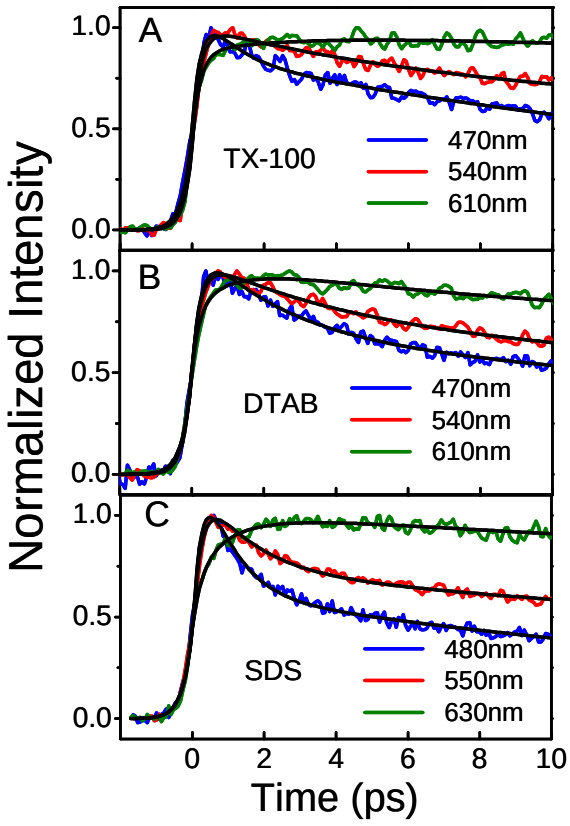

Figure 6 - Representative normalized wavelength resolved fluorescence upconversion decay traces of curcumin at three different wavelengths in (A) TX-100, (B) DTAB, and (C) SDS micelles at pH =7.4 tris buffer. The time-resolved traces at the red end (610 nm for TX-100 and DTAB and 630 nm for SDS micelles) show a rising component, clearly indicating the presence of solvation dynamics.

decays were recorded were set slightly to the red due to a larger Stokes shift observed for curcumin in this micelle. In short, the results indicate the presence of solvation dynamics for curcumin in TX-100, DTAB and SDS micelles.

Using the method outlined in the experimental section, the solvation correlation function, C(t), for curcumin in the three micelles were constructed and are shown in Figure 5. First, it is clear that for curcumin in each micelle, C(t) shows a rapid decay which is followed by a slow decay and an apparent constant offset. Curcumin shows a

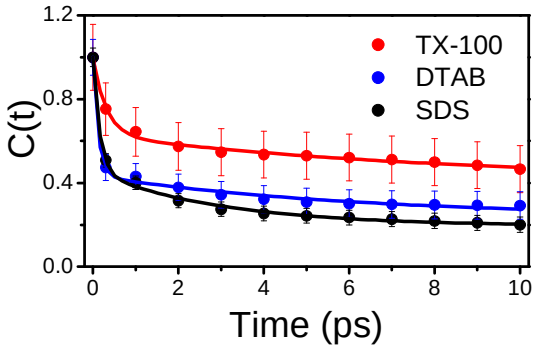

Figure 7 - Solvation correlation function, $C(t)$, of curcumin in TX-100 (red), DTAB (blue), and SDS (black) micelles constructed from multiwavelength fluorescence upconversion results. The $C(t)$ is well fitted with a biexponential function. All three micelles show different fast and slow components, refer to Table 2. Note that the slow component in $C(t)$ for each micelle is identical to the fast component of the corresponding fluorescence upconversion decay at 520 nm within experimental error, see Figure 3 and Table 1.

fractional solvation at 300 fs, f300 fs, of 0.25, 0.53, and 0.50, in the TX-100, DTAB, and SDS micelles, as summarized in Table 2. The C(t) for curcumin in each of the micelles was fitted with a multiexponential function, of which the equation is shown as follows, and the fitting parameters are listed in Table 2.

$$C(t) = a_1 \exp(-t/\tau_1) + a_2 \exp(-t/\tau_2) + a_3 \qquad (2)$$

Initially, a fit to eq 2 was attempted by fixing the τ_2 component to 8, 6, and 3 ps for the TX-100, DTAB, and SDS micelles, respectively and excellent fits were obtained. For curcumin in the TX-100 micelle, the fast decay component in $C(t)$ has a time constant of

0.31 ps, which is as short as the instrument response function (IRF) of our apparatus, and an amplitude of 37%. In the DTAB and SDS micelles, however, the time constants of the fast component have values of 0.12 and 0.15 ps, respectively, which are shorter than the IRF of the instrument.

Table 2 - Solvation correlation function, $C(t)$, decay parameters for curcumin in different micellar systems.

Micellar system	$f_{300\ fs}$[a]	a_1[b]	τ_1 (ps)	a_2	τ_2 (ps)[c]	a_3
TX-100	0.25 ± 0.03	0.37 ± 0.02	0.31 ± 0.04	0.22 ± 0.03	8	0.41 ± 0.02
DTAB	0.53 ± 0.03	0.56 ± 0.02	0.12 ± 0.02	0.20 ± 0.02	6	0.24 ± 0.02
SDS	0.50 ± 0.03	0.54 ± 0.02	0.15 ± 0.02	0.26 ± 0.02	3	0.20 ± 0.01

[a] f_{300fs}: fractional solvation at 300 fs

[b] The $C(t)$ was fitted with the multi-exponential function $C(t) = a_1 \exp(-t/\tau_1) + a_2 \exp(-t/\tau_2) + a_3$.

[c] The τ_2 component was fixed at 8, 6, and 3 ps for the TX-100, DTAB, and SDS micelles, respectively to demonstrate the agreement with the results in Figure 3 and Table 1.

These IRF-limited decay time constants have amplitudes of 56% and 54% in these two micelles. The fast component of $C(t)$ is followed by a slow decay component, of which the time constants are fixed as mentioned above. The amplitudes of this component are nearly the same in the three micelles, ranging from 20% to 26%. In addition to the fast (≤ 300 fs) and slow (3 – 8 ps) components of $C(t)$, it is obvious that solvation dynamics are incomplete within the time window of the experiment, giving rise to a constant offset in

the $C(t)$, as shown in Figure 5 and the a_3 term in the multiexponential equation in Table 2. Alternatively, a good fit to eq 2 can also be obtained by fixing the fast component to 0.1 ps for the three micelles. In this case, the slow component has a time constant of 1.8, 2.6, and 1.9 ps, respectively. The best-fit curves and fitting parameters are provided in the Supporting Information. The significance of the decay components of $C(t)$ are discussed below.

Solvation dynamics in micellar media is currently an intense area of research.[48-51,61-69] Surfactant micelles are excellent model systems for more complex biomembranes and investigations on solvation dynamics in micelles provide critical insight into the behavior of small molecules in biomembranes. First of all, in our study, it is noteworthy that for each of the micelles the value of the time constant τ_2 of $C(t)$, as summarized in Table 2, is virtually identical within experimental error to that of the fast component of the fluorescence upconversion results shown in Figure 3 and Table 1. The excellent agreement strongly indicates that the fast component observed in the fluorescence upconversion results (Figure 3 and Table 1) is due to solvation dynamics of curcumin in micellar media. Second, the decay time constants of $C(t)$ of curcumin in all micelles show a fast component with a time constant that is too short (<300 fs) to be resolved with our apparatus. This fast decay component was also reported for the SDS and DTAB micelles in a study by Dey et al. using coumarin 480 as the probe molecule and a time constant of <300 fs was measured.[61] This fast component of solvation dynamics has been previously attributed to motions of labile or bulklike water molecules at the interface of the micelle,[48-52] which have a longer solvation time constant compared to bulk water (< 1 ps).[66,70,71] As for fast solvation dynamics in TX-100, Mandal et al. showed that the

fastest component has a time constant of 2.1 ps,[67] which is somewhat longer than our measured value of <300 fs. To our knowledge, a < 300 fs solvation dynamics component in the TX-100 micelle is previously unobserved, and our result is the first demonstration of ultrafast solvation dynamics of the TX-100 micelle. Third, the slow component of $C(t)$, which has time constants of 8, 6 and 3 ps, respectively, in the TX-100, DTAB, and SDS micelles, shows reasonable agreement with results from previous studies,[61,67] which has been assigned to solvation of water molecules that are bound to the surface of the micelle by hydrogen bonding or the head group-water interactions.[48-52] Lastly, the constant offset observed in the $C(t)$ of curcumin in the three micelles, which is expressed as a_3 in Table 2, indicates the presence of a decay component with a time constant that is vastly longer than the 10 ps time window of the solvation dynamics studies. Although this decay component of $C(t)$ is too long to be resolved with our solvation dynamics investigations, it has been established in previous studies that $C(t)$ has a long lived component in micelles, with time constants ranging from 165 to 300 ps.[61,67]

Fluorescence Lifetime in Micelles

The excited-state kinetics of curcumin in micelles was also investigated using time-correlated single photon counting (TCSPC). Figure 6 shows the fluorescence decays of curcumin in the TX-100, DTAB and SDS micelles in tris (pH 7.4) and tris-d_{11} (pD 7.4) buffer with a 3-ns time window, in which curcumin produces an isotope effect in each of the micelles. The decays are multiexponential in nature and three exponential functions are necessary to fit the data well. The best fit parameters and the average fluorescence lifetimes are summarized in Table 3. Briefly, in H_2O, the fastest decay

component has a time constant ranging from 50 – 60 ps, which is followed a slower component of ~200 ps and then a long lived 400 – 900 ps component. In contrast, in D_2O, while the two slower components are essentially indistinguishable within experimental error, the fastest component increases to 70 – 85 ps, exhibiting an isotope effect of 1.4 in the three micelles.

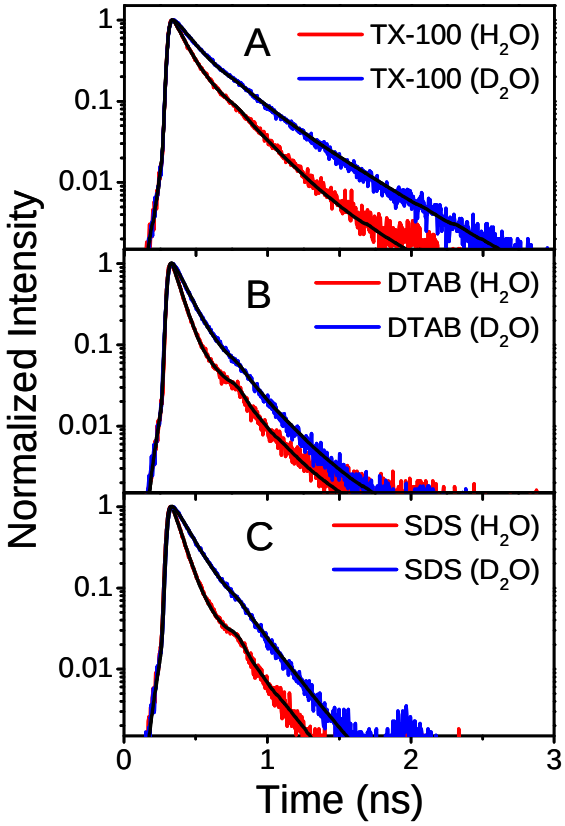

Figure 8 - Fluorescence decays obtained with time-correlated single photo counting for curcumin in (A) TX-100, (B) DTAB and (C) SDS micelle at pH = 7.4 (red) and pD =7.4 (blue) tris buffer. The decays were obtained at λ_{ex} = 407 nm and $\lambda_{em} \geq$ 425 nm with a full time window of 3.33 ns. The decays are well fitted with a triexponentional decay function. The lengthening of the shortest decay component in the deuterated media supports the assignment of this decay component to ESIHT, which shows excellent consistency with the fluorescence upconversion results.

It is noteworthy that there is a close match between the time constants of the ESIHT component, as established in an earlier section on fluorescence upconversion, and the τ_1 component as measured by TCSPC, see Table 1 and 3. Furthermore, similar to the fluorescence upconversion results, this decay component experiences an isotope effect in the deuterated environment. Therefore, the results strongly indicate that the τ_1 component measured by TCSPC is due to ESIHT. Interestingly, the average fluorescence lifetimes of curcumin in the TX-100 micelle is close to that of curcumin in methanol (130 ps), suggesting the similarities of the two environments, as

discussed in a previous section. The shorter average lifetimes of curcumin in the DTAB and SDS micelles imply a greater level of intramolecular hydrogen bonding but lesser extent of intermolecular hydrogen bonding, which was also discussed in the same section.

Table 3 - Fluorescence lifetime results of curcumin in different micellar systems.

Micellar system	a_1[a]	τ_1 (ps)	a_2	τ_2 (ps)[b]	a_3	τ_3 (ps)	$\langle\tau\rangle$ (ps)
TX-100/H_2O	0.68 ± 0.02	60 ± 5	0.30 ± 0.02	210 ± 30	0.02 ± 0.02	510 ± 100	115 ± 15
TX-100/D_2O	0.48 ± 0.02	85 ± 5	0.32 ± 0.02	210 ± 30	0.20 ± 0.01	430 ± 20	195 ± 12
DTAB/H_2O	0.88 ± 0.02	50 ± 5	0.11 ± 0.02	190 ± 50	0.01 ± 0.01	900 ± 200	75 ± 12
DTAB/D_2O	0.72 ± 0.03	70 ± 5	0.27 ± 0.03	190 ± 50	0.01 ± 0.01	730 ± 300	110 ± 17
SDS/H_2O	0.91 ± 0.01	55 ± 5	0.08 ± 0.01	185 ± 10	0.01 ± 0.01	415 ± 80	70 ± 6
SDS/D_2O	0.55 ± 0.02	75 ± 5	0.44 ± 0.02	185 ± 10	0.01 ± 0.01	405 ± 20	125 ± 8

[a] The fluorescence decay traces, f(t), were fitted with the multi-exponential function $f(t) = a_1 \exp(-t/\tau_1) + a_2 \exp(-t/\tau_2) + a_3 \exp(-t/\tau_3)$.

[b] The τ_2 values were limited to the range specified.

Conclusion

We have presented unambiguous results to demonstrate that excited-state intramolecular hydrogen atom transfer (ESIHT) is a major photophysical process of curcumin in the TX-100, DTAB and SDS micelles. The fluorescence upconversion trasient of curcumin in each micelle shows a biexponential decay, with time constants of 3 – 8 ps (fast) and 50 – 80 ps (slow). The slow component exhibits a pronounced isotope

effect, producing a decay time constant of 80 – 130 ps in the micelles, which is assigned to ESIHT. The ESIHT rate of curcumin in the TX-100 micelle is lower than those in the other two micellar system. The hydrogen bonding between curcumin and the TX-100 surfactant may contribute to this effect. The fast decay component, unlike the ESIHT process, is insensitive to deuteration of curcumin and has been attributed to solvation dynamics using results from multiwavelength fluorescence upconversion studies. The water molecules in the micellar structure give rise to solvation dynamics of curcumin. The solvation dynamics observed in the micelles are slower than that in bulk water, which are attributed to water molecules at the micelle interface that are labile or bulklike and those that are bound to the surface of the micelles.

Acknowledgments

T.W.K. acknowledges a research grant from the Australian Research Council and National Health and Medical Research Council Network “Fluorescence Applications in Biotechnology and Life Sciences.

Supporting Information

Time-Resolved Emission Spectra of Curcumin in Micelles

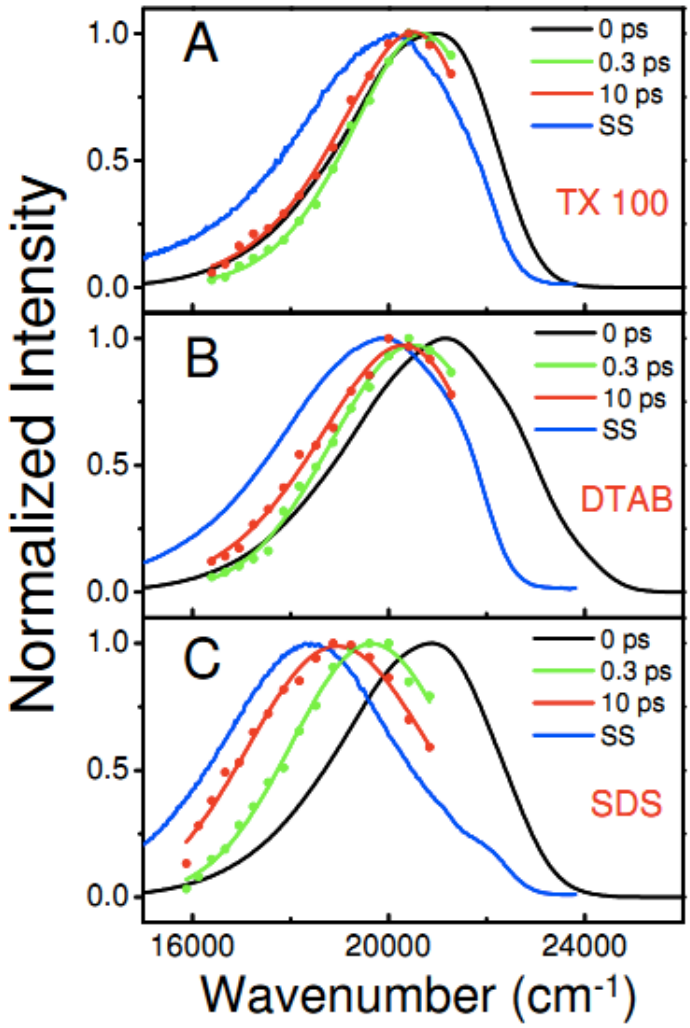

Figure 1. Time-resolved emission spectra of curcumin in TX-100, DTAB and SDS micelles.

Table 1. Solvation correlation function, $C(t)$, decay parameters (alternative fitting) for curcumin in different micellar systems.

Micellar system	$f_{300\ fs}$ [a]	a_1 [b]	τ_1 (ps)[c]	a_2	τ_2 (ps)	a_3
TX-100	0.25 ± 0.03	0.23 ± 0.03	0.1	0.28 ± 0.03	1.8 ± 0.3	0.49 ± 0.01
DTAB	0.53 ± 0.03	0.52 ± 0.01	0.1	0.20 ± 0.01	2.6 ± 0.3	0.28 ± 0.01
SDS	0.50 ± 0.03	0.48 ± 0.02	0.1	0.32 ± 0.01	1.9 ± 0.1	0.20 ± 0.01

[a] f_{300fs}: fractional solvation at 300 fs

[b] The $C(t)$ was fitted with the multi-exponential function $C(t) = a_1 \exp(-t/\tau_1) + a_2 \exp(-t/\tau_2) + a_3$.

[c] The fast component (τ_1) was fixed at 0.1 ps to reflect the portion of unresolved solvation.

References

(1) Ruby, A. J.; Kuttan, G.; Babu, K. D.; Rajasekharan, K. N.; Kuttan, R. *Cancer Lett.* **1995**, *94*, 79.

(2) Lantz, R. C.; Chen, G. J.; Solyom, A. M.; Jolad, S. D.; Timmermann, B. N. *Phytomedicine* **2005**, *12*, 445.

(3) Aggarwal, B. B.; Kumar, A.; Bharti, A. C. *Anticancer Res.* **2003**, *23*, 363.

(4) Shi, M.; Cai, Q.; Yao, L.; Mao, Y.; Ming, Y.; Ouyang, G. *Cell Biol. Int.* **2006**, *30*, 221.

(5) Yang, F.; Lim, G. P.; Begum, A. N.; Ubeda, O. J.; Simmons, M. R.; Ambegaokar, S. S.; Chen, P. P.; Kayed, R.; Glabe, C. G.; Frautschy, S. A.; Cole, G. M. *J. Biol. Chem.* **2005**, *280*, 5892.

(6) Masuda, M.; Suzuki, N.; Taniguchi, S.; Oikawa, T.; Nonaka, T.; Iwatsubo, T.; Hisanaga, S.-i.; Goedert, M.; Hasegawa, M. *Biochemistry* **2006**, *45*, 6085.

(7) Egan, M. E.; Pearson, M.; Weiner, S. A.; Rajendran, V.; Rubin, D.; Glockner-Pagel, J.; Canny, S.; Du, K.; Lukacs, G. L.; Caplan, M. J. *Science* **2004**, *304*, 600.

(8) Jagetia, G. C.; Rajanikant, G. K. *J. Surg. Res.* **2004**, *120*, 127.

(9) Maheshwari, R. K.; Singh, A. K.; Gaddipati, J.; Srimal, R. C. *Life Sci.* **2006**, *78*, 2081.

(10) Kiuchi, F.; Goto, Y.; Sugimoto, N.; Akao, N.; Kondo, K.; Tsuda, Y. *Chem. Pharm. Bull.* **1993**, *41*, 1640.

(11) http://clinicaltrials.gov/ct2/show/NCT00094445.

(12) http://clinicaltrials.gov/ct2/show/NCT00099710.

(13) Bisht, S.; Feldmann, G.; Soni, S.; Ravi, R.; Karikar, C.; Maitra, A.; Maitra, A. *J. Nanobiotechnol.* **2007**, *5*, 3.

(14) Leung, M. H. M.; Kee, T. W. *Langmuir* **2009**, *25*, 5773.

(15) Tønnesen, H. H. *Pharmazie* **2002**, *57*, 820.

(16) Leung, M. H. M.; Colangelo, H.; Kee, T. W. *Langmuir* **2008**, *24*, 5672.

(17) Wang, Y.-J.; Pan, M.-H.; Cheng, A.-L.; Lin, L.-I.; Ho, Y.-S.; Hsieh, C.-Y.; Lin, J.-K. *J. Pharm. Biomed. Anal.* **1997**, *15*, 1867.

(18) Tønnesen, H. H.; Karlsen, J. *Z. Lebensm.-Unters. Forsch.* **1985**, *180*, 132.

(19) Rangel-Yagui, C. O.; Pessoa, A.; Tavares, L. C. *J. Pharm. Pharm. Sci.* **2005**, *8*, 147.

(20) Kaler, E. W.; Herrington, K. L.; Murthy, A. K.; Zasadzinski, J. A. N. *J. Phys. Chem.* **1992**, *96*, 6698.

(21) Wang, X.; Danoff, E. J.; Sinkov, N. A.; Lee, J. H.; Raghavan, S. R.; English, D. S. *Langmuir* **2006**, *22*, 6461.

(22) Kataoka, K.; Harada, A.; Nagasaki, Y. *Adv. Drug Deliv. Rev.* **2001**, *47*, 113.

(23) Kunwar, A.; Barik, A.; Pandey, R.; Priyadarsini, K. I. *Biochim. Biophys. Acta, Gen. Subj.* **2006**, *1760*, 1513.

(24) Menon, L. G.; Kuttan, R.; Kuttan, G. *Cancer Lett.* **1999**, *141*, 159.

(25) Odot, J.; Albert, P.; Carlier, A.; Tarpin, M.; Devy, J.; Madoulet, C. *Int. J. Cancer* **2004**, *111*, 381.

(26) Koon, H.; Leung, A. W. N.; Yue, K. K. M.; Mak, N. K. *J. Environ. Pathol. Toxicol. Oncol.* **2006**, *25*, 205.

(27) Park, K.; Lee, J.-H. *Oncol. Rep.* **2007**, *17*, 537.

(28) Chan, W.-H.; Wu, H.-J. *J. Cell. Biochem.* **2004**, *92*, 200.

(29) Payton, F.; Sandusky, P.; Alworth, W. L. *J. Nat. Prod.* **2007**, *70*, 143.

(30) Nardo, L.; Paderno, R.; Andreoni, A.; Masson, M.; Haukvik, T.; Tønnesen, H. H. *Spectroscopy* **2008**, *22*, 187.

(31) Khopde, S. M.; Priyadarsini, K. I.; Palit, D. K.; Mukherjee, T. *Photochem. Photobiol.* **2000**, *72*, 625.

(32) Adhikary, R.; Mukherjee, P.; Kee, T. W.; Petrich, J. W. *J. Phys. Chem. B* **2009**, *113*, 5255.

(33) Miskovsky, P. *Curr. Drug Targets* **2002**, *3*, 55.

(34) Das, K.; English, D. S.; Petrich, J. W. *J. Phys. Chem. A* **1997**, *101*, 3241.

(35) Das, K.; English, D. S.; Petrich, J. W. *J. Am. Chem. Soc.* **1997**, *119*, 2763.

(36) English, D. S.; Das, K.; Ashby, K. D.; Park, J.; Petrich, J. W.; Castner, E. W., Jr. *J. Am. Chem. Soc.* **1997**, *119*, 11585.

(37) English, D. S.; Zhang, W.; Kraus, G. A.; Petrich, J. W. *J. Am. Chem. Soc.* **1997**, *119*, 2980.

(38) Petrich, J. W. *Int. Rev. Phys. Chem.* **2000**, *19*, 479.

(39) Smirnov, A. V.; Das, K.; English, D. S.; Wan, Z.; Kraus, G. A.; Petrich, J. W. *J. Phys. Chem. A* **1999**, *103*, 7949.

(40) Gai, F.; Fehr, M. J.; Petrich, J. W. *J. Am. Chem. Soc.* **1993**, *115*, 3384.

(41) Zhong, D. P.; Douhal, A.; Zewail, A. H. *Proc. Natl. Acad. Sci. USA* **2000**, *97*, 14056.

(42) Chowdhury, P. K.; Halder, M.; Sanders, L.; Calhoun, T.; Anderson, J. L.; Armstrong, D. W.; Song, X.; Petrich, J. W. *J. Phys. Chem. B* **2004**, *108*, 10245.

(43) Fee, R. S.; Maroncelli, M. *Chem. Phys.* **1994**, *183*, 235.

(44) Maroncelli, M.; Fleming, G. R. *J. Chem. Phys.* **1987**, *86*, 6221.

(45) Barik, A.; Goel, N. K.; Priyadarsini, K. I.; Mohan, H. *J. Photosci.* **2004**, *11*, 95.

(46) Douhal, A.; Lahmani, F.; Zewail, A. H. *Chem. Phys.* **1996**, *207*, 477.

(47) Chignell, C. F.; Bilski, P.; Reszka, K. J.; Motten, A. G.; Sik, R. H.; Dahl, T. A. *Photochem. Photobiol.* **1994**, *59*, 295.

(48) Bagchi, B. *Chem. Rev.* **2005**, *105*, 3197.

(49) Bhattacharyya, K. *Chem. Commun.* **2008**, 2848.

(50) Bhattacharyya, K. *Acc. Chem. Res.* **2003**, *36*, 95.

(51) Nandi, N.; Bhattacharyya, K.; Bagchi, B. *Chem. Rev.* **2000**, *100*, 2013.

(52) Pal, S. K.; Zewail, A. H. *Chem. Rev.* **2004**, *104*, 2099.

(53) Reddy, A. C. P.; Sudharshan, E.; Rao, A. G. A.; Lokesh, B. R. *Lipids* **1999**, *34*, 1025.

(54) Barik, A.; Mishra, B.; Kunwar, A.; Priyadarsini, K. I. *Chem. Phys. Lett.* **2007**, *436*, 239.

(55) Barik, A.; Priyadarsini, K. I.; Mohan, H. *Photochem. Photobiol.* **2003**, *77*, 597.

(56) Mitra, S. P. *J. Surf. Sci. Technol.* **2007**, *23*, 91.

(57) Silva, A. M. S.; Filipe, P.; Seixas, R.; Pinto, D.; Patterson, L. K.; Hug, G. L.; Cavaleiro, J. A. S.; Maziere, J. C.; Santus, R.; Morliere, P. *J. Phys. Chem. B* **2008**, *112*, 11456.

(58) Kimura, N.; Umemura, J.; Hayashi, S. *J. Colloid Interface Sci.* **1996**, *182*, 356.

(59) Wang, X.; Wang, J.; Wang, Y.; Chen, Z. Z.; Tang, B. *J. Photochem. Photobiol., A* **2007**, *186*, 194.

(60) Melo, E. C. C.; Costa, S. M. B.; Maçanta, A. L.; Santos, H. *J. Colloid Interface Sci.* **1991**, *141*, 439.

(61) Dey, S.; Sasmal, D. K.; Das, D. K.; Bhattacharyya, K. *ChemPhysChem* **2008**, *9*, 2848.

(62) Pal, S.; Bagchi, B.; Balasubramanian, S. *J. Phys. Chem. B* **2005**, *109*, 12879.

(63) Kumbhakar, M.; Nath, S.; Mukherjee, T.; Pal, H. *J. Chem. Phys.* **2004**, *121*, 6026.

(64) Shirota, H.; Tamoto, Y.; Segawa, H. *J. Phys. Chem. A* **2004**, *108*, 3244.

(65) Sen, P.; Mukherjee, S.; Halder, A.; Bhattacharyya, K. *Chem. Phys. Lett.* **2004**, *385*, 357.

(66) Pal, S. K.; Peon, J.; Bagchi, B.; Zewail, A. H. *J. Phys. Chem. B* **2002**, *106*, 12376.

(67) Mandal, D.; Sen, S.; Bhattacharyya, K.; Tahara, T. *Chem. Phys. Lett.* **2002**, *359*, 77.

(68) Balasubramanian, S.; Bagchi, B. *J. Phys. Chem. B* **2001**, *105*, 12529.

(69) Pal, S. K.; Sukul, D.; Mandal, D.; Sen, S.; Bhattacharyya, K. *Chem. Phys. Lett.* **2000**, *327*, 91.

(70) Fleming, G. R.; Cho, M. H. *Annu. Rev. Phys. Chem.* **1996**, *47*, 109.

(71) Maroncelli, M.; Fleming, G. R. *J. Chem. Phys.* **1988**, *89*, 5044.

CHAPTER IV: FEMTOSECOND FLUORESCENCE UPCONVERSION INVESTIGATIONS ON THE EXCITED-STATE PHOTOPHYSICS OF CURCUMIN

A Paper Published in the *Australian Journal of Chemistry*

Tak W. Kee,[A,C] Ramkrishna Adhikary,[B] Philip J. Carlson,[B] Prasun Mukherjee,[B] and Jacob W. Petrich[B,C]

Abstract

The demonstration of curcumin as a photodynamic therapy agent has generated a high level of interest in understanding the photoinduced chemical and physical properties of this naturally occurring, yellow-orange medicinal compound. Important photophysical

---

Reprinted with permission from CSIRO Publishing copyright (2011)
Australian Journal of Chemistry, **2011**, 64, 23-30
[A] Department of Chemistry, University of Adelaide, Adelaide, SA 5005, Australia.
[B] Department of Chemistry, Iowa State University, Ames, IA 50011, USA.
[C] Corresponding authors

processes that may be related to photodynamic therapy effects including excited-state intramolecular hydrogen atom transfer (ESIHT) occur within the femtosecond to picosecond time scales. Femtosecond fluorescence upconversion spectroscopy has sufficient time resolution to resolve and investigate these important photophysical processes. In this review, recent advances in using femtosecond fluorescence upconversion to reveal ultrafast solvation and ESIHT of curcumin are presented. The excited-state photophysics of curcumin has been investigated in alcohols and micellar solutions. The results of curcumin in methanol and ethylene glycol reveal the presence of two decay components in the excited-state kinetics with time scales of 12–20 ps and ~100 ps. Similarly, in a micellar solution, biphasic kinetics are present with the fast decay component having a time constant of 3–8 ps, the slow decay component 50–80 ps. Deuteration of curcumin in both media leads to a pronounced isotope effect in the slow decay component, which suggests that ESIHT is an important photophysical process on this time scale. The results of multiwavelength fluorescence upconversion studies show that the fast component in the excited-state kinetics is due to ultrafast solvation. These advances form a part of the continuing efforts to elucidate the photodynamic therapy properties of curcumin.

Introduction

Curcumin, the yellow pigment in the rhizome of turmeric, has been shown to possess a large number of medicinal effects. Most notably, studies[1,2] have suggested that the low incidence of cancers in the gastrointestinal tract in the population of the Indian subcontinent is related to the intake of curcuminoids, which form a family of

yellow polyphenols including curcumin (77%), demethoxycurcumin (17%), bisdemethoxycurcumin (3%), and cyclocurcumin (trace level). In addition to anticancer properties,[3,4] curcumin has anti-inflammatory,[5] antioxidant,[6] anti-Alzheimer's disease,[7] anti-cystic fibrosis,[8] and wound healing effects.[9–11] Recent work shows that curcumin has significant potential as an effective photodynamic therapy agent,[12–19] particularly for melanoma treatment.[20–26] The presence of light has been shown to greatly enhance the destruction of tumour cells.[16,18,19] Although it has been established that stable photoproducts are not the source of medicinal effects of curcumin,[14] photolytically produced reactive oxygen species including singlet oxygen, hydroxyl radical, superoxide, or hydrogen peroxide may be responsible for the photoinduced activity.[13,14,27–31] From the photophysical viewpoint, a study by Jovanovic et al. demonstrates that H-atom transfer is a preferred antioxidant mechanism of curcumin using laser flash photolysis and pulse radiolysis.[32] Currently, there are significant interests in developing a detailed level of understanding of the photophysical and photochemical processes of curcumin in order to further exploit its light-induced medicinal effects.

There are two major challenges in the application of curcumin as an effective treatment agent, namely the lack of bioavailability and the limited stability in aqueous environments. Owing to the low aqueous solubility, curcumin has a tendency to aggregate and precipitate in water, thereby limiting its bioavailability. Moreover, curcumin degrades rapidly in water and buffer solutions with a reaction half-life of 9.5 min at pH 7.2.[33] The degradation involves a retro-aldol condensation reaction catalyzed by the hydroxide anion, to produce products including vanilin, ferulic acid, and

feruroyl methane,[34] which have been shown to possess medicinal properties as well. Our studies have shown that encapsulation of curcumin in surfactant micelles and binding to proteins and diamide linked γ-cyclodextrin dimers resolve these two major issues.[35–38]

Micellar systems may play a critical role in enabling the clinical applications of curcumin. These molecular assemblies address the issue of low bioavailability because micelle-captured curcumin is well dispersed in aqueous solutions. Association with the micelle also enables curcumin to be present in a water-free environment,[17,35,37–41] thereby preventing degradation. Investigations on the behaviour of curcumin in micellar systems are crucial because it is largely membrane bound in a biological environment.[42] These studies provide valuable insight into the properties of curcumin in a biologically relevant environment.

Curcumin exists in two tautomeric forms, namely the β-diketone and keto-enol. Payton et al. have shown that curcumin is predominantly a keto-enol tautomer (Fig. 1) in several solvents with various polarities using results from NMR spectroscopy.[43] This is

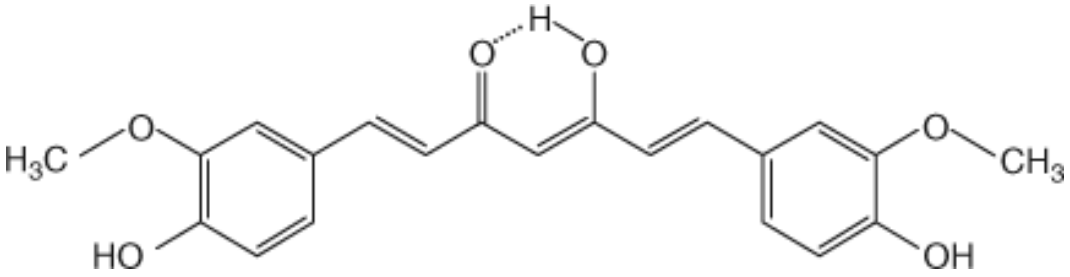

Figure 1 – Structure of keto-enol form of curcumin.

because a strong intramolecular hydrogen bond is present in the keto-enol tautomer, resulting in stabilization of this tautomeric form. As the keto-enol tautomer, curcumin has the capability to undergo excited state intramolecular hydrogen atom transfer (ESIHT)

due to close proximity of the proton donor and the acceptor, as shown in Fig. 1. Our recent work has not only established that ESIHT is a major photophysical event of curcumin, but we have also assigned the time scale of this phenomenon.[44,45] The ESIHT process of curcumin was investigated in two classes of environments. First, studies were performed on curcumin in methanol, ethylene glycol, and chloroform to understand the effect of intermolecular hydrogen bonding on ESIHT.[44] Second, micellar systems composed of sodium dodecyl sulfate (SDS), dodecyl trimethyl ammonium bromide (DTAB), and triton X-100 (TX-100) were chosen to investigate the effect of interfacial water and the charge of the surfactant headgroup on ESIHT.[45] Using deuteration of curcumin and femtosecond fluorescence upconversion spectroscopy, our results show that the time constant of ESIHT of curcumin is 70 ps in methanol and 120 ps in ethylene glycol. In addition, there is a 12–20 ps component in the excited state kinetics that is attributed to ultrafast solvation. In the micellar systems, the results show that the time constant of ESIHT of curcumin in these micelles ranges from 50 to 80 ps. Additionally, a fast component of 3–8 ps, which is due to solvation dynamics of curcumin in the micellar media, was also observed. It has been suggested that the presence of a labile hydrogen as a result of ESIHT plays a role in the medicinal effects of other naturally occurring pigments such as hypericin and hypocrellin.[46–53] In the case of curcumin, ESIHT may result in partial deprotonation, which induces fragmentation to yield the medicinal degradation products mentioned earlier.

Fluorescence Upconversion Technique

Fluorescence upconversion is one of the most attractive time-resolved fluorescence methods. Compared with similar techniques, it provides the highest time resolution in resolving the decay of fluorescence signals. Typically, the time resolution of fluorescence upconversion is ~300 fs or less. In contrast, although time correlated single photon counting, which is another popular time-resolved fluorescence method, provides a simpler solution to data acquisition, the time resolution is significantly poorer (~50 ps or longer). The apparatus for fluorescence upconversion in our studies is described in detail elsewhere.[54] In short, the laser source was a homebuilt mode-locked Ti:sapphire oscillator. The fundamental wavelength and repetition rate of the femtosecond output were 814 nm and 82 MHz, respectively. The fundamental output of the oscillator was frequency-doubled by a type-I lithium triborate crystal (2 mm). The frequency-doubled pulses (407 nm) were used to excite the sample and the residual of the fundamental was used as the gate pulse to upconvert the fluorescence signal. The polarization of the excitation pulse was at the magic angle relative to that of the gate pulses. First, the frequency-doubled blue pulses (407 nm) were focussed onto a rotating cell containing the sample and the fluorescence signal was collected using a 10× objective lens. Then, the gate pulse and fluorescence signal were focussed onto a 0.4 mm type-I beta barium borate crystal to generate the sum frequency light, which was detected by a photomultiplier tube mounted on a monochromator. The full-width-at-half-maximum of the instrument response function is 300 fs, obtained by the cross-correlation function of the frequency doubled and the fundamental light. All experiments were performed at

room temperature. For most fluorescence upconversion experiments, a time window of 100 ps was used with a step size of 0.2 ps.

Solvation Correlation Function

The solvation correlation function, C(t), which reveals the time constants of the solvation process, was used to analyze and quantify the solvation dynamics.

$$C(t) = \frac{\nu(t) - \nu(\infty)}{\nu(''0'') - \nu(\infty)} \quad (1)$$

The v('0'), v(t), and v(∞) in Eqn 1 denote the peak frequency (typically in cm–1) of the zero-time, t and infinity emission spectra, respectively. Using the approach of Fee and Maroncelli,[55] the 'zero-time' emission spectrum was approximated by using the emission spectrum of curcumin in hexanes. As for v(∞), the peak frequency of the steady-state fluorescence spectrum was used. In these investigations, fluorescence upconversion measurements were performed at 11–17 wavelengths depending upon the system, ranging from 470 to 630 nm, with a time window of 10 ps to construct time-resolved emission spectra with sufficient data points to reflect the real spectra. Each of the time-resolved emission spectra was fitted with the log-normal function and the peak frequency v(t) was obtained using the procedure outlined by Maroncelli and Fleming.[56] The relatively large width of the time dependent emission spectra typically results in uncertainty in the exact position of the maxima. Therefore, by using the signal-to-noise ratio and width of the spectrum (including 'zero-time', steady-state, or time-resolved emission spectrum) as sources of uncertainty, we determined the following typical uncertainties: time-resolved emission (~±200 cm–1), 'zero-time', and steady-state

(~±100 cm–1). These uncertainties were used to compute error bars for the C(t). Finally, the fractional solvation at 300 fs was calculated using f300 fs = 1 – C(t = 300 fs).

Excited-State Intramolecular Hydrogen Atom Transfer of Curcumin in Methanol, Ethylene Glycol and Chloroform

The excitation and probe wavelengths in the fluorescence upconversion experiments for curcumin in methanol, ethylene glycol, and chloroform are 407 nm and 520 nm, respectively. The excitation wavelength of 407 nm is near the absorption maximum (see "Accessory Publication" below), which enables efficient promotion of curcumin from the ground state to the excited state. The fluorescence of curcum in in these solvents at 520 nm is relatively, intense (see "Accessory Publication" below). Because it is situated on the blue side of the spectrum, the signal reflects early time events in the excited state relaxation process. Fig. 2a shows the fluorescence upconversion signals of curcumin in methanol and deuterated methanol. The signal of curcumin in methanol, which is shown in red, was fitted with a bi-exponential decay function with time constants of 12 ± 2 ps and 70 ± 10 ps with nearly equal amplitudes. In deuterated methanol, which is shown in blue, while the fast decay component remains identical within noise level, a significant isotope effect is present in the slow component. As a result, the decay time constant of the slow component is increased to 120 ± 20 ps. The fitting parameters are summarized in Table 1.

Fig. 2b shows the time-resolved fluorescence signal of curcumin in ethylene glycol (red). Similar to methanol, the signal also exhibits a bi-exponential decay. In contrast, the time constants of the decays are longer, which are 20 ± 3 ps and

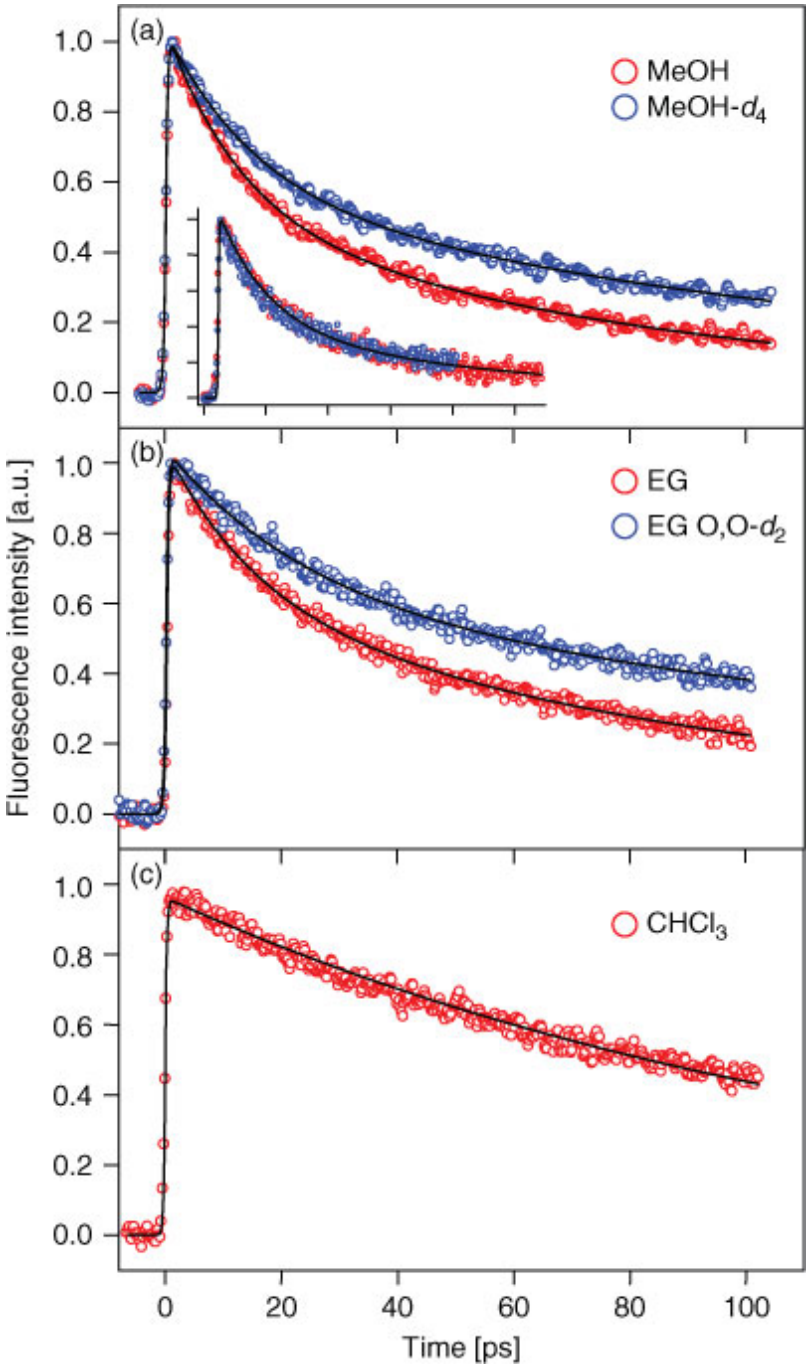

Figure 2 - Fluorescence upconversion decays of curcumin in (a) methanol (MeOH), (b) ethylene glycol (EG) and (c) chloroform ($CHCl_3$); corresponding decays in the deuterated analogs in (a) and (b) show a prominent isotope effect. The inset in (a) shows the virtually identical traces before the H/D exchange (equilibration time of ~15 min), which indicates that the isotope effect observed after equilibration (48 h) is independent of solvent effects. While the decays in (a) and (b) exhibit bi-exponential nature, the trace in (c) is nearly single exponential. All samples were excited at 407 nm and fluorescence was collected at 520 nm. This figure is adapted from ref. [44] and used with permission of the ACS.

Table 1 - Fluorescence upconversion decay parameters for curcumin in different solvents and micellar systems[A]

Solvent/micellar system	a_1	τ_1 [ps]	τ_2 [ps]
Methanol	0.45 ± 0.07	12 ± 2	70 ± 10
Methanol-d_4	0.45 ± 0.07	12 ± 2	120 ± 18
Ethylene glycol	0.45 ± 0.07	20 ± 3	105 ± 15
Ethylene glycol O,O-d_2	0.45 ± 0.07	20 ± 3	220 ± 33
Chloroform[B]	1.0 ± 0.15	130 ± 20	–
TX-100/H_2O	0.30 ± 0.04	8 ± 2	80 ± 10
TX-100/D_2O	0.23 ± 0.03	8 ± 2	130 ± 20
DTAB/H_2O	0.36 ± 0.03	6 ± 2	50 ± 5
DTAB/D_2O	0.22 ± 0.03	6 ± 2	80 ± 5
SDS/H_2O	0.57 ± 0.03	3 ± 2	55 ± 3
SDS/D_2O	0.57 ± 0.03	3 ± 2	85 ± 6

[A]The fluorescence upconversion decays, $f(t)$, were fitted with the multi-exponential function: $f(t) = a_1 \exp(-t/\tau_1) + a_2 \exp(-t/\tau_2)$, where $a_1 + a_2 = 1$.
[B]Chloroform was dried over molecular sieves before use. Water content was assessed with a coulometric Karl Fischer Titration (Mettler Toledo DL 39). % wt $H_2O = 0.002$.

105 ± 15 ps, with amplitudes of 45% and 55%, respectively. The time-resolved fluorescence of curcumin in deuterated ethylene glycol also produces an isotope effect. While the fast decay component remains unchanged, the time constant of the slow component shows an isotope effect of 2.1. The fluorescence upconversion decay trace of curcumin in chloroform is shown in Fig. 2c, which is best fitted with a single exponential decay function with a time constant of 130 ± 20 ps.

The emergence of the isotope effect of 1.7 of curcumin in methanol (Fig. 2a) requires equilibration of curcumin in deuterated methanol for ~48 h. It is possible that

exchange of the enolic hydrogen of curcumin with the deuterium of methanol-d4 takes such a long period due to strong intramolecular hydrogen bonding, which is similar to deuteration of a similar system.[57] The inset of Fig. 2a shows the fluorescence upconversion results of curcumin in methanol and deuterated methanol with an equilibration time of only 15 min. In contrast, the two decay traces are identical within experimental error, clearly indicating the absence of an isotope effect. The dependence of the isotope effect on equilibration time offers important insights. First, the absence of any isotope effect with a short equilibration time suggests that the associated excited state process is intramolecular in nature, in contrast to intermolecular processes such as hydrogen bonding interactions between curcumin and the solvent molecules. Second, the observed isotope effect shows a direct correspondence to the enolic H/D exchange of curcumin, supporting the excited state hydrogen atom transfer properties of the kinetics owing to the following reasons. First, it follows that the isotope effect is associated to a non-radiative process as the fluorescence quantum yield of curcumin in methanol has a low value of <10%.[58] Second, it is unlikely that the formation of an excited triplet state by intersystem crossing plays a big role because the triple yield of curcumin is only ~3%.[58] Finally, other non-radiative processes including photoisomerization and ESIHT may also lead to an isotope effect in the excited state kinetics. It is well established that photoisomerization exhibits a strong dependence on solvent viscosity.[59–63] Owing to a weak dependence of the excited state dynamics of curcumin on solvent viscosity, as is discussed below, it is unlikely for photoisomerization to give rise to the observed isotope effect. However, the isotope effect is substantially more likely to arise from ESIHT, which is expected to play a significant role in the deactivation of excited state curcumin

due to the presence of a strong intramolecular hydrogen bond in the keto-enol moiety. Because only the slow component in Fig. 2a exhibits an isotope effect, the 70-ps decay component is therefore attributed to ESIHT, which forms a non-radiative decay pathway of curcumin. In the case of curcumin in ethylene glycol, as shown in Fig. 2b, the presence of an isotope effect in the long-lived decay component (105 ± 15 ps) supports the assignment of this component to ESIHT. The ESIHT time constants of curcumin reported in this study are comparable to that of 7-azaindole in methanol.[64]

The solvent viscosities of methanol and ethylene glycol are 0.59 cP and 16.1 cP, respectively at 20°C. Although the viscosities are different by a factor of ~30 between these solvents, the ESIHT time constants of curcumin in these solvents are relatively similar. The apparent lack of dependence of the ESIHT time constant on viscosity implies that small amplitude molecular motions are involved, which are virtually independent of the surrounding solvent molecules. This phenomenon has been observed in an analogous system, hypericin, of which the ESIHT time constant is unrelated to solvent viscosity.[48,51]

Fluorescence upconversion investigations were also performed on curcumin in chloroform. The results of these studies provide a useful contrast to those of curcumin in methanol and ethylene glycol. Chloroform is a polar aprotic solvent hence unable to form any intermolecular hydrogen bonding with curcumin. In these studies, water was strictly excluded because a trace level of water is able to quench the fluorescence of curcumin.[43] The 130 ± 20-ps decay component is assigned to ESIHT instead of solvation because the time constants of solvation are 0.285 ps and 4.15 ps. This ESIHT time constant is similar to those of curcumin in methanol and ethylene glycol, which

implies that intermolecular hydrogen bonding between curcumin and solvent may only play a minor role in ESIHT of curcumin.

Excited-State Intramolecular Hydrogen Atom Transfer of Curcumin in Surfactant Micelles

Fig. 3 presents the femtosecond fluorescence upconversion results of curcumin in the TX-100, DTAB, and SDS micelles. The results of curcumin in both non-deuterated (pH 7.4, 20 mM tris buffer in H2O, red) and deuterated (pD 7.4, 20 mM tris-d11 in D2O, blue) micellar environments are shown. Similar to curcumin in alcohols, the decay kinetics were monitored at 520 nm with an excitation wavelength of 407 nm. For the SDS micelle, the time-resolved florescence at 520 nm reflects the early time excited-state relaxation dynamics because it is on the blue side of the emission spectrum (see the Accessory Publication section below). However, for curcumin in the TX-100 and DTAB micelles, because 520 nm is to the red of the fluorescence maxima, the relaxation dynamics also contain solvation owing to a strong solvatochromatic behaviour of curcumin. The upconversion decays in Fig. 3 are well fitted with a biexponential function within the 100 ps time window and the results are summarized in Table 1. Curcumin in the TX-100, DTAB, and SDS micelles shows a fast component of 8 ± 2 ps, 6 ± 2, and 3 ± 2 ps, respectively, and a slow component of 80 ± 10 ps, 50 ± 5, and 55 ± 3 ps, respectively. Upon deuteration of curcumin in these micelles, the fast component remains unchanged but the slow component experiences a significant isotope effect of 1.6.

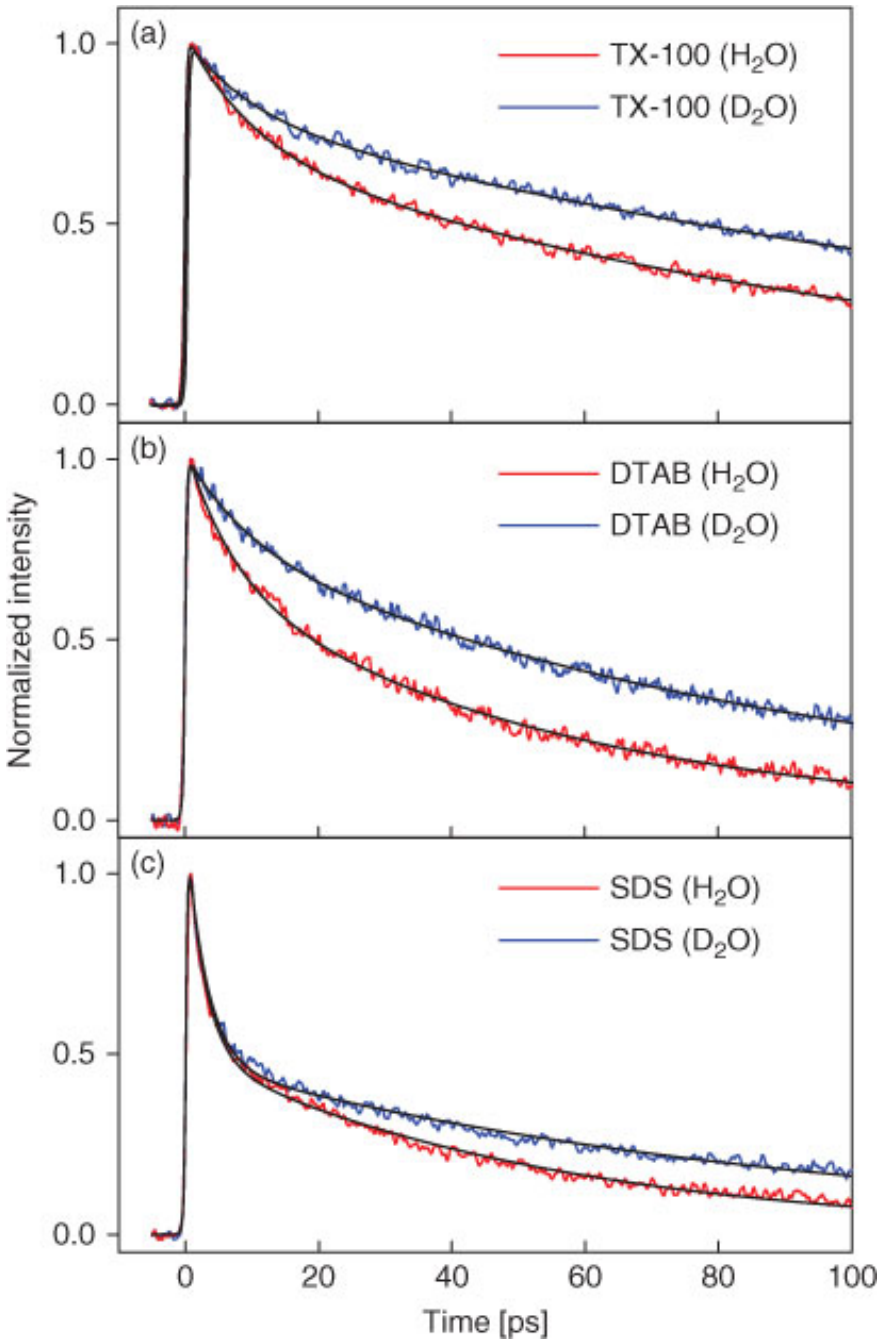

Figure 3 - Fluorescence upconversion decays of curcumin collected at 520 nm in (a) TX-100, (b) DTAB, and (c) SDS micelles at pH = 7.4 tris buffer (red) with an excitation wavelength of 407 nm. Corresponding upconversion decays in deuterated micellar environment at pD = 7.4 (blue) are also included. Curcumin shows a prominent isotope effect in all three micellar media. This figure is adapted from ref. [45] and used with permission of the ACS.

The ESIHT time constant of curcumin in the TX-100 micelle, which has a value of 80 ps, is very similar to that of curcumin in methanol (70 ps). It is well accepted that ESIHT of curcumin in methanol is influenced by the interaction between curcumin and the protic solvent molecules.[44,58,65] The agreement in these values indicates the presence of curcumin-water and curcumin-TX-100 intermolecular hydrogen bonding. The presence of these interactions is expected because it has been suggested that curcumin is captured in the palisade layer of the micelle,[58] where a relatively hydrophilic environment is found.[66] Furthermore, curcumin may form hydrogen bonding interactions with the C–O groups of TX-100, giving rise to an environment that is similar to that of bulk methanol. In the DTAB and SDS micelles, the ESIHT time constants are ~50 ps, which are considerably faster than that in the TX-100 micelle. This faster ESIHT time constant implies a stronger curcumin intramolecular hydrogen bond, and a weaker curcumin-water and/or curcumin-surfactant interaction(s) in these micelles compared with TX-100. First, the water content in the micelles is considered. Results from a study indicate that the water contents of the DTAB and TX-100 micelles are similar but higher in the SDS micelle.[67] Although the DTAB and SDS micelles have different water contents, the nearly identical ESIHT time constants in these micelles imply that the curcumin-water hydrogen bonding only plays an insignificant role in ESIHT. In contrast, the major difference between TX-100 and the other two surfactants is the presence of a high number of C–O groups. As a comparison, DTAB and SDS have the dodecyl group, which is only capable of interacting with curcumin by van der Waals forces. Therefore, it is conceivable that hydrogen bonding between curcumin and TX-100

results in a slower rate of ESIHT, whereas in the DTAB and SDS micelles the ESIHT rate is higher due to the absence of curcumin-surfactant hydrogen bonding.

Solvation Dynamics of Curcumin in Methanol and Ethylene Glycol – Ultrafast Solvent Motions

Solvation, the rearrangement of solvent molecules surrounding a dipole, is expected to play a role in the excited state relaxation dynamics of curcumin due to a large dipole moment change of $\Delta\mu$ = 6.1 D relative to ground-state curcumin.[58] This magnitude of $\Delta\mu$ is similar to that of Coumarin 153,[56,68] which is commonly used as a standard probe for solvation dynamics. As shown in the Accessory Publication (below), the fluorescence spectra have a peak shift that is highly sensitive to solvent polarity, which further indicates that solvation plays a major role in the relaxation of the excited state. The presence of solvation can be detected by a multiwavelength fluorescence upconversion investigation. In our study, fluorescence upconversion experiments were performed at up to 11 wavelengths within 500 nm to 600 nm in methanol and ethylene glycol. Several representative decay traces are shown in Fig. 4. The general trend is that on the blue side of the emission spectrum (e.g. 500 nm) the results show a fast and a slow decay component. However, as the wavelength of the fluorescence upconversion experiment increases, the fast decay component gradually transforms into a growth component. The transition from decay to growth in the time-resolved fluorescence signal is due to a decrease in energy of the excited state due to solvation. As mentioned earlier, excited-state curcumin has a significantly higher dipole moment and the excited state in the initial solvent configuration is relatively high in energy. Solvation, which involves rearrangement of the surrounding solvent molecules, takes place in time and it leads to a

decrease in the energy of the excited state. The behavior of the results is an established indication that solvation dynamics are present in the relaxation dynamics of excited state curcumin. A similar behavior is also observed for curcumin in ethylene glycol.

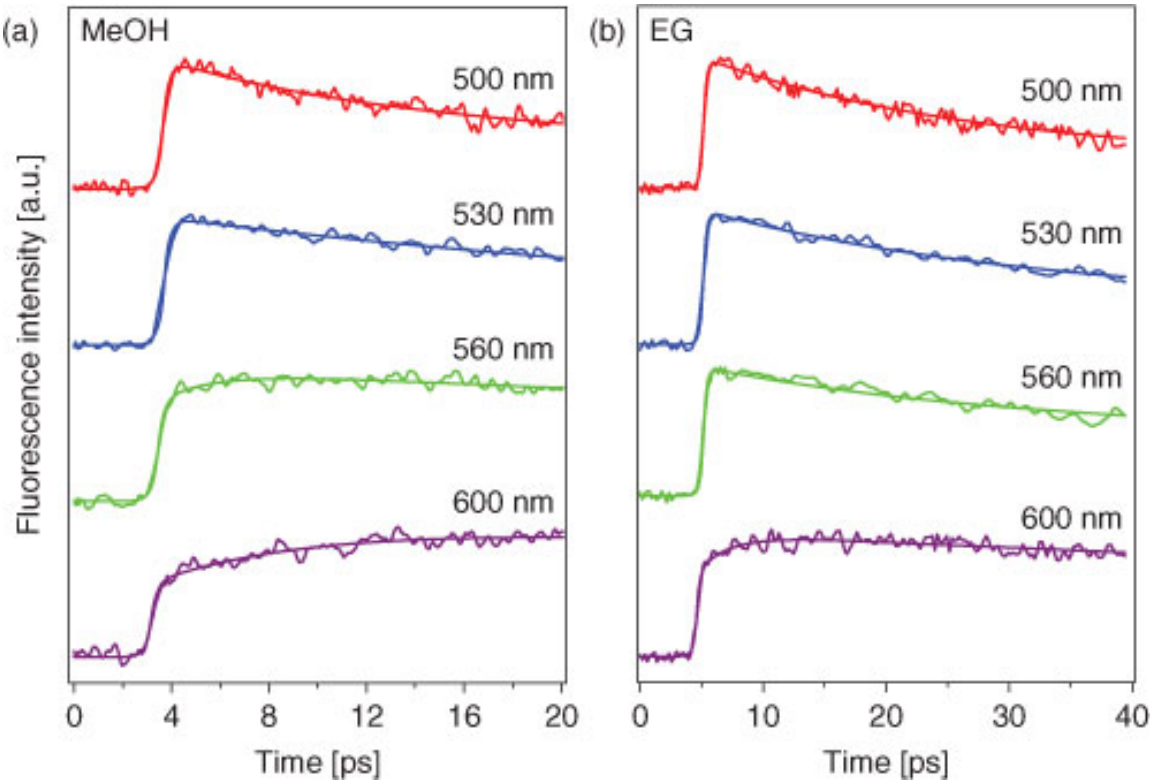

Figure 4 - Representative normalized wavelength resolved fluorescence upconversion traces of curcumin in (a) methanol and (b) ethylene glycol. Time-resolved emission spectra were constructed by collecting upconversion traces over a range from 500 to 600 nm at intervals of 10 nm. The time-resolved traces at the red end (600 nm) show a growing component, which is the signature of solvation dynamics. This figure is adapted from ref. [44] and used with permission of the ACS.

The wavelength resolved fluorescence upconversion traces are used to construct the time-resolved fluorescence spectra (See the accessory publication section below) from which the necessary parameters are extracted to generate the solvation correlation function, C(t) which reveals the time constants of solvation dynamics. The C(t) of curcumin in methanol and ethylene glycol are presented in Fig. 5a and the solvation

parameters are shown in Table 2. The f300 fs values for curcumin in alcohols show that more than 70% of solvation is completed in both the solvents within the time resolution (300 fs) of the instrument. The C(t) of curcumin in methanol and ethylene glycol shows an initial fast response (50 fs, fixed) followed by a slow response; the C(t) for curcumin in these alcohols was fitted with the following multiexponential function and the fitting parameters are listed in Table 2.

$$C(t) = a_1 \exp\left(-t/\tau_1\right) + a_2 \exp\left(-t/\tau_2\right) + a_3 \qquad (2)$$

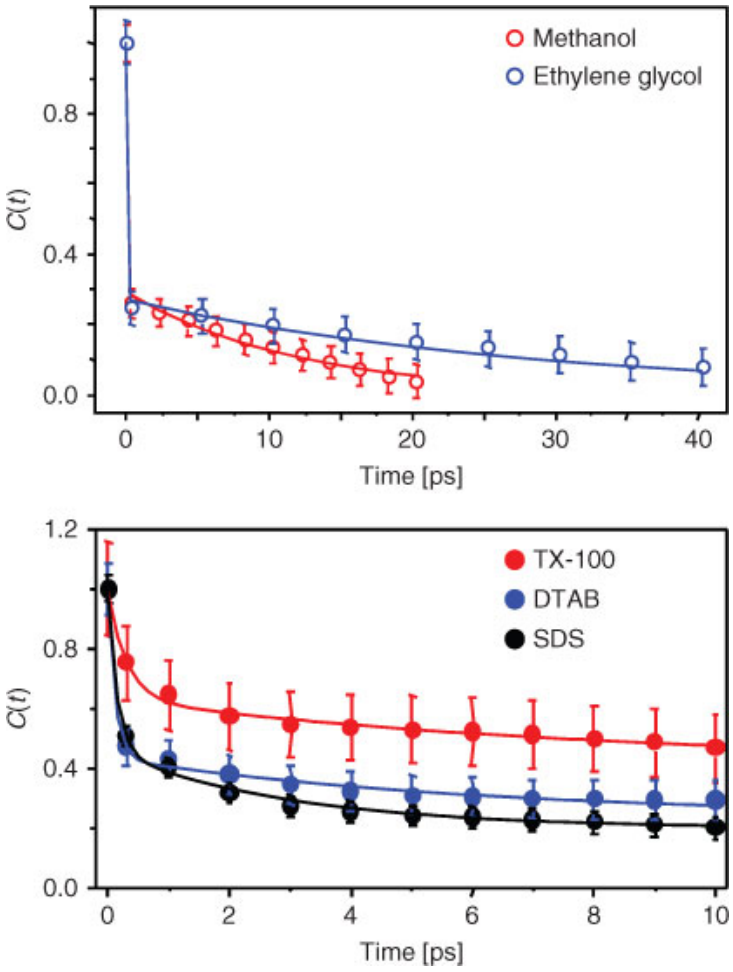

Figure 5- (Top) The solvation correlation function, *C*(*t*) of curcumin in methanol and ethylene glycol obtained from fluorescence upconversion experiments. The *C*(*t*) is fitted with a bi-exponential decay function. Both the solvents showed a same initial fast component of 50 fs but a different slow component of 12 ps (methanol) and 30 ps (ethylene glycol). This figure is adapted from ref. [45]. (Bottom) Solvation correlation function, *C*(*t*), of curcumin in TX-100 (red), DTAB (blue), and SDS (black) micelles constructed from multiwavelength fluorescence upconversion results. The *C*(*t*) is well fitted with a bi-exponential function. All three micelles show different fast and slow components, refer to Table 2. Note that the slow component in *C*(*t*) for each micelle is identical to the fast component of the corresponding fluorescence upconversion decay at 520 nm within experimental error. This figure is adapted from ref. [45]. These figures are used with permission of the ACS.

Table 2 - Solvation correlation function, $C(t)$, decay parameters for curcumin in different systems

	$f_{300\,fs}$[A]	a_1[B]	τ_1[C] [ps]	a_2	τ_2 [ps][D]	a_3	$\langle\tau\rangle$ [ps]
Methanol	0.75 ± 0.04	0.71 ± 0.02	0.05	0.29 ± 0.02	12 ± 2	–	3.5
Ethylene glycol	0.75 ± 0.05	0.73 ± 0.02	0.05	0.27 ± 0.02	30 ± 5	–	8.2
TX-100	0.25 ± 0.03	0.37 ± 0.02	0.31 ± 0.04	0.22 ± 0.03	8	0.41 ± 0.02	1.9
DTAB	0.53 ± 0.03	0.56 ± 0.02	0.12 ± 0.02	0.20 ± 0.02	6	0.24 ± 0.02	1.3
SDS	0.50 ± 0.03	0.54 ± 0.02	0.15 ± 0.02	0.26 ± 0.02	3	0.20 ± 0.01	0.9

[A] $f_{300\,fs}$: fractional solvation at 300 fs.
[B] The $C(t)$ was fitted with the multiexponential function $C(t) = a_1 \exp(-t/\tau_1) + a_2 \exp(-t/\tau_2) + a_3$.
[C] The faster component was fixed at 0.05 ps during fitting.
[D] The τ_2 component was fixed at 8, 6, and 3 ps for the TX-100, DTAB, and SDS micelles, respectively to demonstrate the agreement with the results in Fig. 3 and Table 1.

Previous studies on solvation dynamics of similar systems have shown that the 50-fs component is attributed to ultrafast librational motion of the solvents.[68–70] The slow component in the C(t) has time constants of 12 ± 2 ps and 30 ± 5 ps in methanol and ethylene glycol, respectively. These time constants show excellent agreement with the fast component in the fluorescence upconversion results shown in Fig. 2 and Table 1. Therefore, the fast component in the fluorescence upconversion results for curcumin in methanol and ethylene glycol is assigned to solvation. Furthermore, curcumin in methanol and ethylene glycol have average solvation times of 3.5 ps and 8.2 ps, respectively, showing good agreement with a previous study.[68]

Solvation Dynamics of Curcumin in Surfactant Micelles – Ultrafast Solvation by Interfacial Water

Solvation dynamics in the micellar media is an intense area of research because micelles are realistic models for complex biomembranes. Investigations on solvation dynamics in micelles offer crucial insight into the behaviour of molecules in biomembranes.[71–84] Using the results of curcumin in alcohols as a guide,[44] a series of fluorescence upconversion experiments were conducted with a time window of 10 ps (Fig. 6). For curcumin in the TX-100 micelle (Fig. 6a), the fluorescence upconversion traces show a clear decay at 470 nm (blue) and this decay is lengthened significantly at 540 nm (red). At 610 nm (green), however, the fluorescence decay disappears completely and a rise in fluorescence intensity is observed. As mentioned above, the presence of this behaviour is a clear signature of solvation dynamics. For curcumin in the DTAB and SDS

micelles (Fig. 6b and 6c), a nearly identical trend in the fluorescence upconversion result

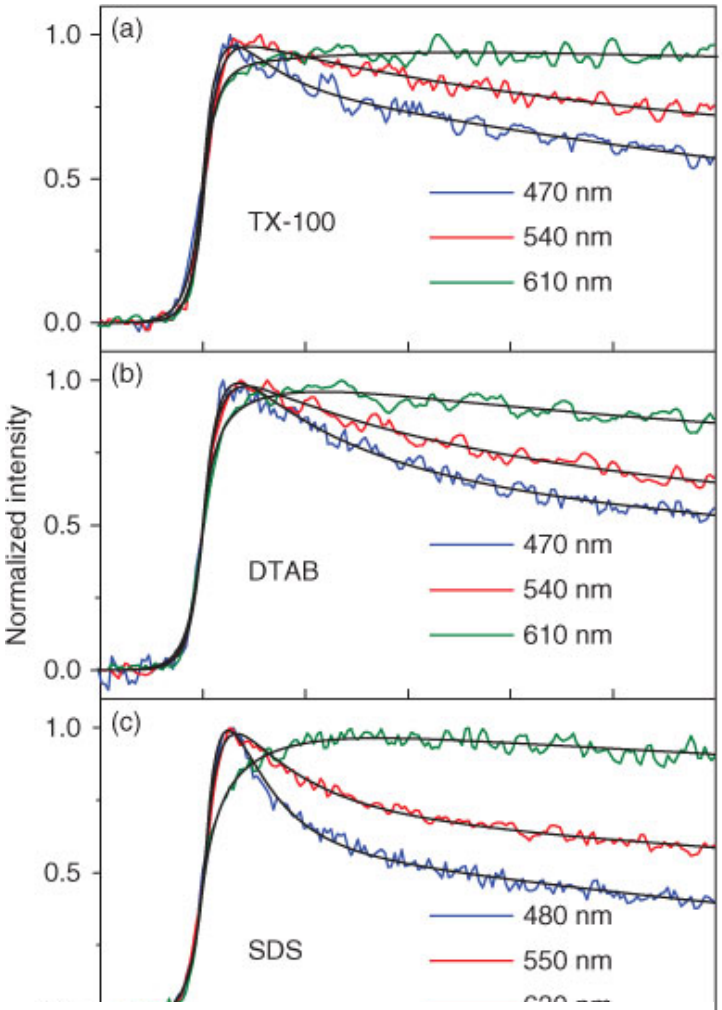

Figure 6- Representative normalized wavelength resolved fluorescence upconversion decay traces of curcumin at three different wavelengths in (a) TX-100, (b) DTAB, and (c) SDS micelles at pH = 7.4 tris buffer. The time-resolved traces at the red end (610 nm for TX-100 and DTAB and 630 nm for SDS micelles) show a rising component, clearly indicating the presence of solvation dynamics. This figure is adapted from ref. [45] and used with permission of the ACS.

is observed. As a whole, the results indicate that solvation dynamics is present for curcumin in TX-100, DTAB, and SDS micelles. Curcumin in the micelles has a C(t) with a rapid decay, a slow decay, and a constant offset (Fig. 5b). The fractional solvation values of curcumin in the TX-100, DTAB, and SDS micelles at 300 fs, (f300 fs), are 0.25, 0.53, and 0.50, respectively (Table 2). Similar to the cases of curcumin in alcohols,

the C(t) for curcumin in each micelle was fitted with Eqn 2. Excellent fits were obtained by fixing the τ2 component to 8, 6, and 3 ps for the TX-100, DTAB, and SDS micelles, respectively. In our study, the τ2 value of C(t) for each micelle is virtually identical within experimental error to that of the fast component of the corresponding fluorescence upconversion results (Fig. 3 and Table 1). The agreement indicates that the fast component in the fluorescence upconversion results is due to solvation dynamics of curcumin in the micellar media. The time constants of the fast component in the C(t) are 0.31 ps, 0.12 ps, and 0.15 ps for curcumin in the TX-100, DTAB, and SDS micelles. These time constants are close to or less than the instrument response function (IRF) of our apparatus, with an amplitude of 37%, 56%, and 54%, respectively. This rapid decay of C(t) is followed by a slow decay component, of which the time constants are fixed as mentioned above. The amplitudes of this component are nearly the same in the three micelles, ranging from 20 to 26%. The results in Fig. 5b also show that solvation dynamics are incomplete within the detection time window, resulting in a constant offset in the C(t), which is represented as the a3 component in Eqn 2.

The decay of C(t) of curcumin in the TX-100, DTAB, and SDS micelles show a fast component with a time constant that is equal or faster than the IRF (300 fs) our apparatus. For the DTAB and SDS micelles, this fast solvation dynamics has been previously observed and attributed to motions of labile or bulk-like water molecules at the interface of the micelle.[71–74,84] However, for TX-100 micelle, the fastest component observed before our work has a time constant of 2.1 ps,[81] which is longer than the measured value of ~300 fs in our study. This ~300 fs solvation dynamics is previously unobserved, and our result is the first demonstration of ultrafast solvation

dynamics of the TX-100 micelle. The fastest component in the C(t) is a likely result of interaction of curcumin with the bulk-like water molecules at the aqueous/micelle interface. A previous study shows that the hydration layer of the SDS and DTAB-like micelles is considerably thinner (6–9 Å) than that of the TX-100 micelle (20 Å),[72] indicating that curcumin is more exposed to the bulk-like water molecules in the former two micelles than in the latter. As a result, faster solvation dynamics are observed in the SDS and DTAB micelles than TX-100. The 8, 6, and 3-ps component of C(t) in the TX-100, DTAB, and SDS micelles, respectively, shows good agreement with previous results, which has been attributed to solvation of water molecules that are bound to the surface of the micelle by hydrogen bonding.[75,81] The presence of a constant offset in the C(t) of curcumin in the micelles, a3 (Table 2), indicates that there is a solvation dynamics component that is substantially longer than the time window (10 ps) of the studies. It has been established in previous studies that C(t) has a long lived component in micelles, with time constants ranging from 165 to 300 ps.[75,81]

Conclusion

We have demonstrated with fluorescence upconversion that curcumin undergoes ESIHT and it plays a major role in the photophysics of curcumin. Photoexcitation of curcumin in methanol and ethylene glycol produces a fluorescence signal that decays with a bi-exponential fashion on the order of 12–20 ps and 70–105 ps. The long-lived signal, which exhibits a prominent isotope effect in deuterated solvents, is attributed to ESIHT. We have also shown that curcumin exhibits a long solvation component of ~12 ps in methanol and ~30 ps in ethylene glycol. In addition to alcohols, ESIHT is also a

major photophysical process of curcumin in the TX-100, DTAB, and SDS micelles. The fluorescence upconversion transient shows a bi-exponential decay, with time constants of 3–8 ps (fast) and 50–80 ps (slow). Similar to the cases of curcumin in alcohols, the slow component exhibits a pronounced isotope effect, producing a decay time constant of 80–130 ps, which is assigned to ESIHT. The ESIHT rate of curcumin in the TX-100 micelle is lower than those in the other two micellar system because the hydrogen bonding between curcumin and the TX-100 surfactant may contribute to this effect. The fast decay component, however, is insensitive to deuteration of curcumin and has been attributed to solvation dynamics. The water molecules at the micelle interface, which are labile or bulk-like, and those that are bound to the surface of the micelle give rise to solvation dynamics of curcumin. Our work in this area forms a part of the continuing efforts to elucidate the photodynamic therapy properties of curcumin.

Accessory Publication

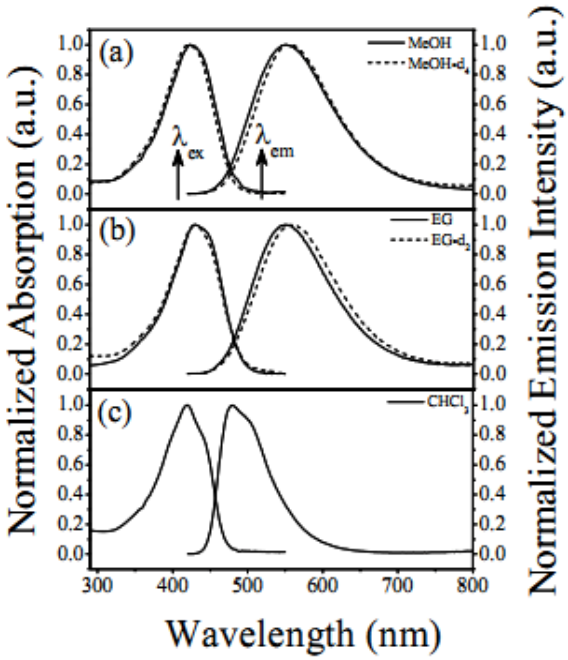

Figure 1. Normalized absorption and fluorescence spectra of curcumin in (a) methanol (MeOH), deuterated methanol (MeOH-d_4), (b) ethylene glycol (EG), deuterated ethylene glycol (EG-d_2) and (c) chloroform ($CHCl_3$). This figure is adapted from ref 44 in the main text and used with permission of the ACS.

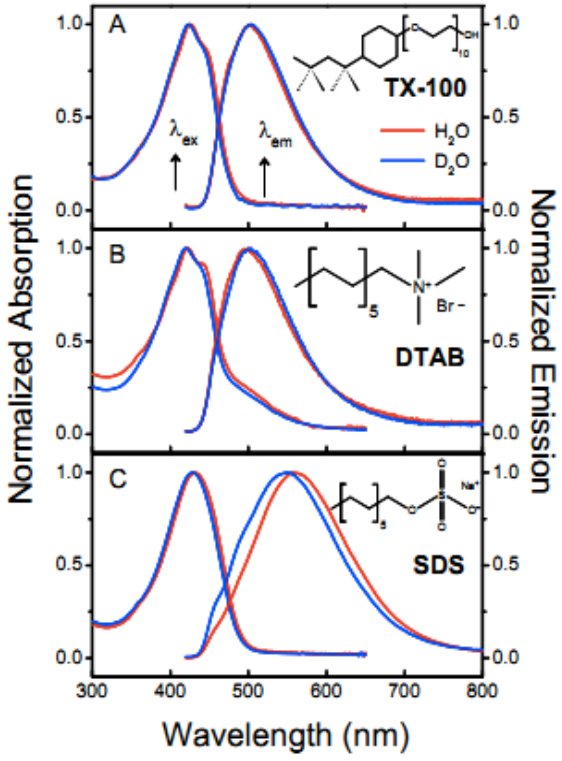

Figure 2. UV-Vis absorption and emission spectra of curcumin in (A) TX-100, (B) DTAB, and (C) SDS in H_2O (red) and D_2O (blue). This figure is adapted from ref 45 in the main text and used with permission of the ACS.

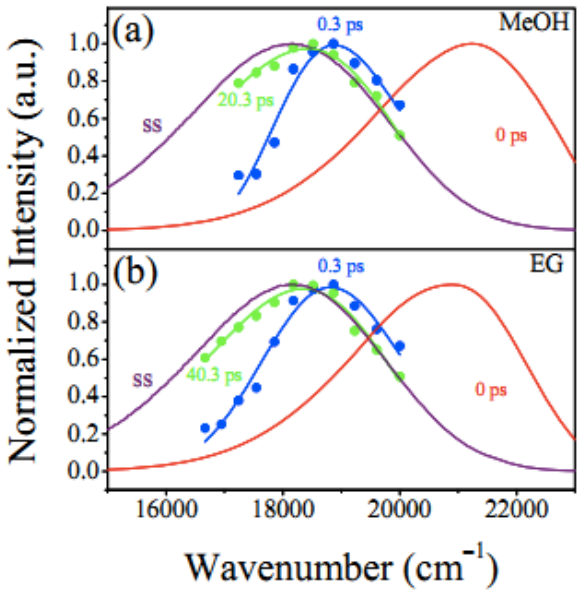

Figure 3. Normalized time resolved emission spectra of curcumin in methanol (MeOH) and ethylene glycol (EG). Steady-state (ss) and "zero-time" (t = 0 ps) spectra are included. Almost 70 % of the solvation is complete in both systems within the time resolution of our instrument (300 fs). This figure is adapted from ref 44 in the main text and used with permission of the ACS.

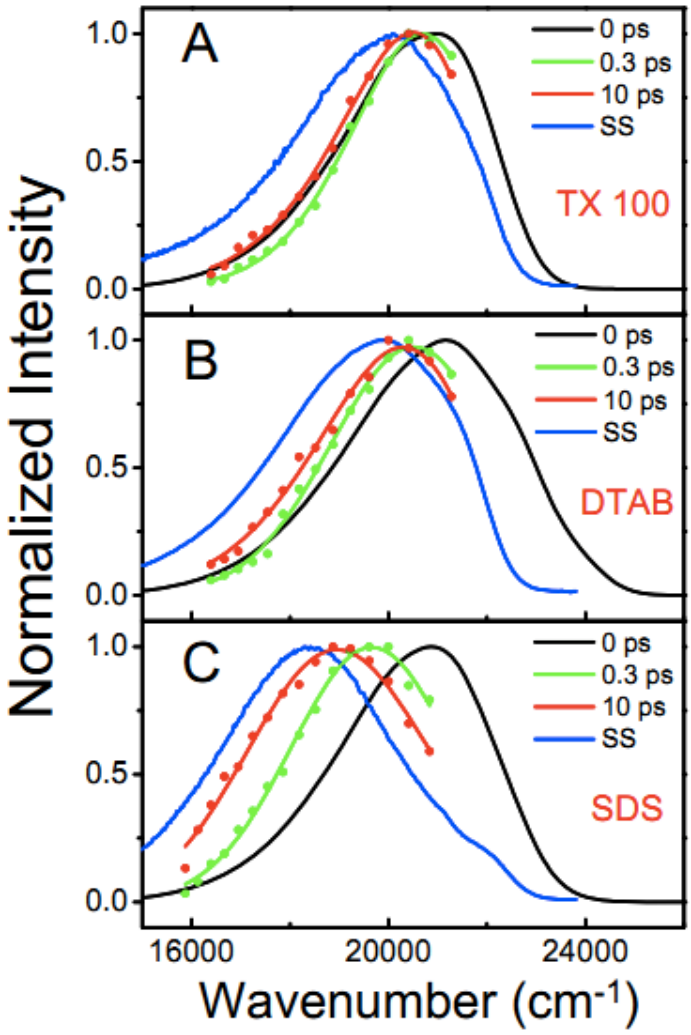

Figure 4. Time-resolved emission spectra of curcumin in TX-100, DTAB and SDS micelles. This figure is adapted from ref 45 in the main text and used with permission of the ACS.

References

[1] K. M. Mohandas, D. C. Desai, Indian J. Gastroenterol. 1999, 18, 118.

[2] L. Moragoda, R. Jaszewski, A. P. N. Majumdar, Anticancer Res. 2001, 21, 873.

[3] B. B. Aggarwal, A. Kumar, A. C. Bharti, Anticancer Res. 2003, 23, 363.

[4] M. Shi, Q. Cai, L. Yao, Y. Mao, Y. Ming, G. Ouyang, Cell Biol. Int. 2006, 30, 221. doi:10.1016/J.CELLBI.2005.10.024

[5] R. C. Lantz, G. J. Chen, A. M. Solyom, S. D. Jolad, B. N. Timmermann, Phytomedicine 2005, 12, 445. doi:10.1016/J.PHYMED.2003.12.011

[6] A. J. Ruby, G. Kuttan, K. D. Babu, K. N. Rajasekharan, R. Kuttan, Cancer Lett. 1995, 94, 79. doi:10.1016/0304-3835(95)03827-J

[7] F. Yang, G. P. Lim, A. N. Begum, O. J. Ubeda, M. R. Simmons, S. S. Ambegaokar, P. P. Chen, R. Kayed, C. G. Glabe, S. A. Frautschy, G. M. Cole, J. Biol. Chem. 2005, 280, 5892. doi:10.1074/JBC. M404751200

[8] M. E. Egan, M. Pearson, S. A. Weiner, V. Rajendran, D. Rubin, J. Glockner-Pagel, S. Canny, K. Du, G. L. Lukacs, M. J. Caplan, Science 2004, 304, 600. doi:10.1126/SCIENCE.1093941

[9] D. Gopinath, M. R. Ahmed, K. Gomathi, K. Chitra, P. K. Sehgal, R. Jayakumar, Biomaterials 2004, 25, 1911. doi:10.1016/S0142-9612 (03)00625-2

[10] G. C. Jagetia, G. K. Rajanikant, Plast. Reconstr. Surg. 2005, 115, 515. doi:10.1097/01.PRS.0000148372.75342.D9

[11] R. K. Maheshwari, A. K. Singh, J. Gaddipati, R. C. Srimal, Life Sci. 2006, 78, 2081. doi:10.1016/J.LFS.2005.12.007

[12] T. A. Dahl, P. Bilski, K. J. Reszka, C. F. Chignell, Photochem. Photobiol. 1994, 59, 290. doi:10.1111/J.1751-1097.1994.TB05036.X

[13] T. A. Dahl, W. M. McGowan, M. A. Shand, V. S. Srinivasan, Arch. Microbiol. 1989, 151, 183. doi:10.1007/BF00414437

[14] H. H. Tønnesen, H. de Vries, J. Karlsen, G. B. van Henegouwen, J. Pharm. Sci. 1987, 76, 371. doi:10.1002/JPS.2600760506

[15] A. A. Gorman, I. Hamblett, V. S. Srinivasan, P. D. Wood, Photochem. Photobiol. 1994, 59, 389. doi:10.1111/J.1751-1097.1994.TB05053.X

[16] W.-H. Chan, H.-J. Wu, J. Cell. Biochem. 2004, 92, 200. doi:10.1002/JCB.20059

[17] C. F. Chignell, P. Bilski, K. J. Reszka, A. G. Motten, R. H. Sik, T. A. Dahl, Photochem. Photobiol. 1994, 59, 295. doi:10.1111/J.1751-1097.1994.TB05037.X

[18] H. Koon, A. W. N. Leung, K. K. M. Yue, N. K. Mak, J. Environ. Pathol. Toxicol. Oncol. 2006, 25, 205.

[19] K. Park, J.-H. Lee, Oncol. Rep. 2007, 17, 537.

[20] M. L. van Iersel, J. P. Ploemen, I. Struik, C. van Amersfoort, A. E. Keyzer, J. G. Schefferlie, P. J. van Bladeren, Chem. Biol. Interact. 1996, 102, 117. doi:10.1016/S0009-2797(96)03739-8

[21] C. D. Lao, M. F. Demierre, V. K. Sondok, Expert Rev. Anticancer Ther. 2006, 6, 1559. doi:10.1586/14737140.6.11.1559

[22] Y. E. Marı´n, B. A. Wall, S. Wang, J. Namkoong, J. J. Martino, J. Suh, H. J. Lee, A. B. Rabson, C. S. Yang, S. Chen, J.-H. Ryu, Melanoma Res. 2007, 17, 274. doi:10.1097/CMR.0B013E3282ED3D0E

[23] L. G. Menon, R. Kuttan, G. Kuttan, Cancer Lett. 1995, 95, 221. doi:10.1016/0304-3835(95)03887-3

[24] J. Odot, P. Albert, A. Carlier, M. Tarpin, J. Devy, C. Madoulet, Int. J. Cancer 2004, 111, 381. doi:10.1002/IJC.20160

[25] D. R. Siwak, S. Shishodia, B. B. Aggarwal, R. Kurzrock, Cancer 2005, 104, 879. doi:10.1002/CNCR.21216

[26] M. Zheng, S. Ekmekcioglu, E. T. Walch, C.-H. Tang, E. A. Grimm, Melanoma Res. 2004, 14, 165. doi:10.1097/01.CMR.0000129374. 76399.19

[27] S. M. Khopde, K. I. Priyadarsini, P. Venkatesan, M. N. A. Rao, Biophys. Chem. 1999, 80, 83. doi:10.1016/S0301-4622(99)00070-8

[28] E. Kunchandy, M. N. A. Rao, Int. J. Pharm. 1989, 57, 173. doi:10.1016/0378-5173(89)90307-4

[29] E. Kunchandy, M. N. A. Rao, Int. J. Pharm. 1990, 58, 237. doi:10.1016/0378-5173(90)90201-E

[30] K. I. Priyadarsini, Free Radic. Biol. Med. 1997, 23, 838. doi:10.1016/ S0891-5849(97)00026-9

[31] O. P. Sharma, Biochem. Pharmacol. 1976, 25, 1811. doi:10.1016/

0006-2952(76)90421-4

[32] S. V. Jovanovic, S. Steenken, C. W. Boone, M. G. Simic, J. Am. Chem. Soc. 1999, 121, 9677. doi:10.1021/JA991446M

[33] Y. J. Wang, M. H. Pan, A. L. Cheng, L. I. Lin, Y. S. Ho, C. Y. Hsieh, . K. Lin, J. Pharm. Biomed. Anal. 1997, 15, 1867. doi:10.1016/S0731-7085(96)02024-9

[34] H. H. Tønnesen, J. Karlsen, Z. Lebensm. Unters. Forsch. 1985, 180, 402. doi:10.1007/BF01027775

[35] M. H. M. Leung, H. Colangelo, T. W. Kee, Langmuir 2008, 24, 5672. doi:10.1021/LA800780W

[36] M. H. M. Leung, T. W. Kee, Langmuir 2009, 25, 5773. doi:10.1021/LA804215V

[37] Z. Wang, M. H. M. Leung, T. W. Kee, D. S. English, Langmuir 2010, 26, 5520. doi:10.1021/LA903772E

[38] T. Harada, D.-T. Pham, M. H. M. Leung, H. T. Ngo, S. F. Lincoln, C. J. Easton, T. W. Kee, J. Phys. Chem. B 2011, in press. doi:10.1021/JP1096025

[39] H. H. Tønnesen, Pharmazie 2002, 57, 820.

[40] E. M. Bruzell, E. Morisbak, H. H. Tønnesen, Photochem. Photobiol. Sci. 2005, 4, 523. doi:10.1039/B503397G

[41] M. O. Iwunze, J. Mol. Liq. 2004, 111, 161. doi:10.1016/J.MOLLIQ.2003.12.013

[42] A. Kunwar, A. Barik, R. Pandey, K. I. Priyadarsini, Biochim. Biophys. Acta, Gen. Subj. 2006, 1760, 1513. doi:10.1016/J.BBAGEN.2006.06.012

[43] F. Payton, P. Sandusky, W. L. Alworth, J. Nat. Prod. 2007, 70, 143. doi:10.1021/NP060263S

[44] R. Adhikary, P. Mukherjee, T. W. Kee, J. W. Petrich, J. Phys. Chem. B 2009, 113, 5255. doi:10.1021/JP901234Z

[45] R. Adhikary, P. J. Carlson, T. W. Kee, J. W. Petrich, J. Phys. Chem. B 2010, 114, 2997. doi:10.1021/JP9101527

[46] P. Miskovsky, Curr. Drug Targets 2002, 3, 55. doi:10.2174/1389450023348091

[47] K. Das, D. S. English, J. W. Petrich, J. Phys. Chem. A 1997, 101, 3241. doi:10.1021/JP9630479

[48] K. Das, D. S. English, J. W. Petrich, J. Am. Chem. Soc. 1997, 119, 2763. doi:10.1021/JA962923T

[49] D. S. English, K. Das, K. D. Ashby, J. Park, J. W. Petrich, E. W. Castner, Jr, J. Am. Chem. Soc. 1997, 119, 11585. doi:10.1021/JA9721071

[50] D. S. English, W. Zhang, G. A. Kraus, J. W. Petrich, J. Am. Chem. Soc. 1997, 119, 2980. doi:10.1021/JA962476H

[51] J. W. Petrich, Int. Rev. Phys. Chem. 2000, 19, 479. doi:10.1080/01442350050034207

[52] A. V. Smirnov, K. Das, D. S. English, Z. Wan, G. A. Kraus, J. W.

Petrich, J. Phys. Chem. A 1999, 103, 7949. doi:10.1021/JP992436A

[53] F. Gai, M. J. Fehr, J. W. Petrich, J. Am. Chem. Soc. 1993, 115, 3384. doi:10.1021/JA00061A069

[54] K. Das, A. V. Smirnov, J. Wen, P. Miskovsky, J. W. Petrich, Photochem. Photobiol. 1999, 69, 633. doi:10.1111/J.1751-1097.1999.TB03339.X

[55] R. S. Fee, M. Maroncelli, Chem. Phys. 1994, 183, 235. doi:10.1016/0301-0104(94)00019-0

[56] M. Maroncelli, G. R. Fleming, J. Chem. Phys. 1987, 86, 6221. doi:10.1063/1.452460

[57] P. Fita, N. Urbanska, C. Radzewicz, J. Waluk, Z. Phys. Chem. 2008, 222, 1165. doi:10.1524/ZPCH.2008.5380

[58] S. M. Khopde, K. I. Priyadarsini, D. K. Palit, T. Mukherjee, Photochem. Photobiol. 2000, 72, 625. doi:10.1562/0031-8655(2000)072o0625:EOSOTE42.0.CO;2

[59] S. Abrash, S. Repinec, R. M. Hochstrasser, J. Chem. Phys. 1990, 93, 1041. doi:10.1063/1.459168

[60] L. Nikowa, D. Schwarzer, J. Troe, J. Schroeder, J. Chem. Phys. 1992, 97, 4827. doi:10.1063/1.463837

[61] J. K. Rice, A. P. Baronavski, J. Phys. Chem. 1992, 96, 3359. doi:10.1021/J100187A034

[62] D. C. Todd, G. R. Fleming, J. Chem. Phys. 1993, 98, 269. doi:10.1063/

1.464672

[63] D. C. Todd, J. M. Jean, S. J. Rosenthal, A. J. Ruggiero, D. Yang, G. R. Fleming, J. Chem. Phys. 1990, 93, 8658. doi:10.1063/1.459252

[64] R. S. Moog, M. Maroncelli, J. Phys. Chem. 1991, 95, 10359. doi:10.1021/J100178A023

[65] L. Nardo, R. Paderno, A. Andreoni, M. Masson, T. Haukvik, H. H. Toennesen, Spectroscopy 2008, 22, 187. doi:10.3233/SPE-2008-0335

[66] A. M. S. Silva, P. Filipe, R. Seixas, D. Pinto, L. K. Patterson, G. L. Hug, J. A. S. Cavaleiro, J. C. Maziere, R. Santus, P. Morliere, J. Phys. Chem. B 2008, 112, 11456. doi:10.1021/JP805889G

[67] E. C. C. Melo, S. M. B. Costa, A. L. Mac¸anta, H. Santos, J. Colloid Interface Sci. 1991, 141, 439. doi:10.1016/0021-9797(91)90341-5

[68] M. L. Horng, J. A. Gardecki, A. Papazyan, M. Maroncelli, J. Phys. Chem. 1995, 99, 17311. doi:10.1021/J100048A004

[69] R. Jimenez, G. R. Fleming, P. V. Kumar, M. Maroncelli, Nature 1994, 369, 471. doi:10.1038/369471A0

[70] G. R. Fleming, M. Cho, Annu. Rev. Phys. Chem. 1996, 47, 109. doi:10.1146/ANNUREV.PHYSCHEM.47.1.109

[71] B. Bagchi, Chem. Rev. 2005, 105, 3197. doi:10.1021/CR020661þ

[72] K. Bhattacharyya, Acc. Chem. Res. 2003, 36, 95. doi:10.1021/AR020067M

[73] K. Bhattacharyya, Chem. Commun. 2008, 2848. doi:10.1039/B800278A

[74] N. Nandi, K. Bhattacharyya, B. Bagchi, Chem. Rev. 2000, 100, 2013. doi:10.1021/CR980127V

[75] S. Dey, D. K. Sasmal, D. K. Das, K. Bhattacharyya, ChemPhysChem 2008, 9, 2848. doi:10.1002/CPHC.200800658

[76] S. Pal, B. Bagchi, S. Balasubramanian, J. Phys. Chem. B 2005, 109, 12879. doi:10.1021/JP0510793

[77] S. K. Pal, J. Peon, B. Bagchi, A. H. Zewail, J. Phys. Chem. B 2002, 106, 12376. doi:10.1021/JP0213506

[78] M. Kumbhakar, S. Nath, T. Mukherjee, H. Pal, J. Chem. Phys. 2004, 121, 6026. doi:10.1063/1.1784774

[79] H. Shirota, Y. Tamoto, H. Segawa, J. Phys. Chem. A 2004, 108, 3244. doi:10.1021/JP035861J

[80] S. Balasubramanian, B. Bagchi, J. Phys. Chem. B 2001, 105, 12529. doi:10.1021/JP012640þ

[81] D. Mandal, S. Sen, K. Bhattacharyya, T. Tahara, Chem. Phys. Lett. 2002, 359, 77. doi:10.1016/S0009-2614(02)00704-2

[82] P. Sen, S. Mukherjee, A. Halder, K. Bhattacharyya, Chem. Phys. Lett. 2004, 385, 357. doi:10.1016/J.CPLETT.2003.12.115

[83] S. K. Pal, D. Sukul, D. Mandal, S. Sen, K. Bhattacharyya, Chem. Phys. Lett. 2000, 327, 91. doi:10.1016/S0009-2614(00)00847-2

[84] S. K. Pal, A. H. Zewail, Chem. Rev. 2004, 104, 2099. doi:10.1021/CR020689L

CHAPTER V: STRUCTURE AND DYNAMICS OF THE 1-HYDROXYETHYL-4-AMINO-1,2,4-TRIAZOLIUM NITRATE HIGH-ENERGY IONIC LIQUID SYSTEM

A Paper Published in the *Journal of Physical Chemistry B*

Philip J. Carlson,[1] Sayantan Bose,[1] Daniel W. Armstrong,[2] Tommy Hawkins,[3]

Mark S. Gordon,[1*] and Jacob W. Petrich[1*]

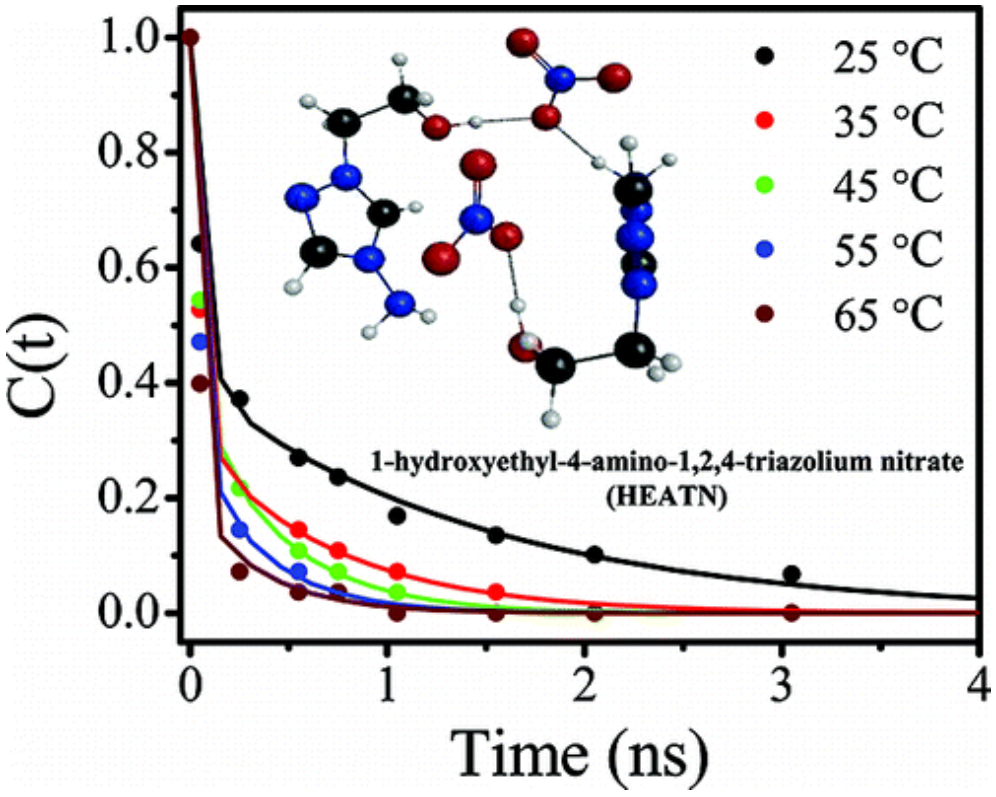

Reprinted with permission for the American Chemical Society copyright (2012)
Journal of Physical Chemistry B, **2012,** 116, 503-512
[1] U.S. Department of Energy Ames Laboratory, and Department of Chemistry, Iowa State University, Ames, Iowa 50011
[2] Department of Chemistry and Biochemistry, University of Texas, Arlington, Box 19065 Arlington, Texas 76019
[3] Air Force Research Laboratory, 10 East Saturn Boulevard, Building 8451, Edwards Air Force Base, California 93524
[*] Authors to whom correspondence should be addressed

Abstract

An investigation of the structure and dynamics of the high-energy ionic liquid, 1-hydroxyethyl-4-amino-1,2,4-triazolium nitrate (HEATN) was undertaken. Both experimental and computational methods were employed to understand the fundamental properties, characteristics, and behavior of HEATN. The charge separation, according to the electrostatic potential derived charges was assessed. The MP2 (second order perturbation theory) geometry optimizations find six dimer and five tetramer structures and allow one to see the significant highly hydrogen bonded network predicted within the HEATN system. Due to the prohibitive scaling of *ab initio* methods, the fragment molecular orbital (FMO) method was employed and assessed for feasibility with highly energetic ionic liquids using HEATN as a model system. The FMO method was found to adequately treat the HEATN ionic liquid system as evidenced by the small relative error obtained. The experimental studies involved the investigation of the solvation dynamics of the HEATN system via the coumarin 153 (C153) probe at five different temperatures. The rotational dynamics through the HEATN liquid were also measured using C153. Comparisons with previously studied imidazolium and phosphonium ionic liquids show surprising similarity. To the authors' knowledge, this is the first experimental study of solvation dynamics in a triazolium based ionic liquid.

Introduction

There has been a steeper than exponential growth in the number of publications related to ionic liquids since the year 2000.[1] The interest in ionic liquids reflects their versatility and their environmentally friendly properties in comparison to

commonly used compounds.[2-4] Ionic liquids are molten salts, commonly composed of an organic cation and an inorganic anion that can often be liquid at room temperature. These low-melting salts are considered to be green solvents, in contrast to volatile organic compounds, due to their high chemical and thermal stabilities, negligible vapor pressure,[5] and high recoverability and reusability.[6,7] Ionic liquids can be customized by varying the identity of the substituents on the cation or by adapting the moiety of the anion.[8] This versatility and these unique properties have piqued the interest of the scientific community, and a variety of fundamental studies[9-16] have been performed on ionic liquids to obtain a better understanding of their characteristics.

One interesting application of ionic liquids is in the high energy density matter (HEDM) community, where many different molten salts have been explored and reported.[17] It is important to understand what characteristics make ionic liquids suited to HEDM applications. This very problem was explored computationally in a series of studies,[18-20] as well as experimentally in a few reports.[21] These studies show that triazolium ionic liquids appear to have more suitable characteristics for HEDM applications than other nitrogen rich ionic liquid species.

A recent report by Drake and co-workers[22] on low-melting, potentially energetic, salts lists their desired characteristics, as well as potential benefits, that might be derived from using them in energetic materials applications. The same authors have discussed the 1-*R*-4-amino-1,2,4-triazolium family of salts[23] that are of interest owing to their high nitrogen content. One interesting room temperature ionic liquid in this family is 1-hydroxyethyl-4-amino-1,2,4-triazolium nitrate (HEATN), depicted in Figure 1a. To use the HEATN ionic liquid in various applications, it is beneficial to employ both

experimental and computational methods to understand the fundamental properties, characteristics, and behavior of HEATN.

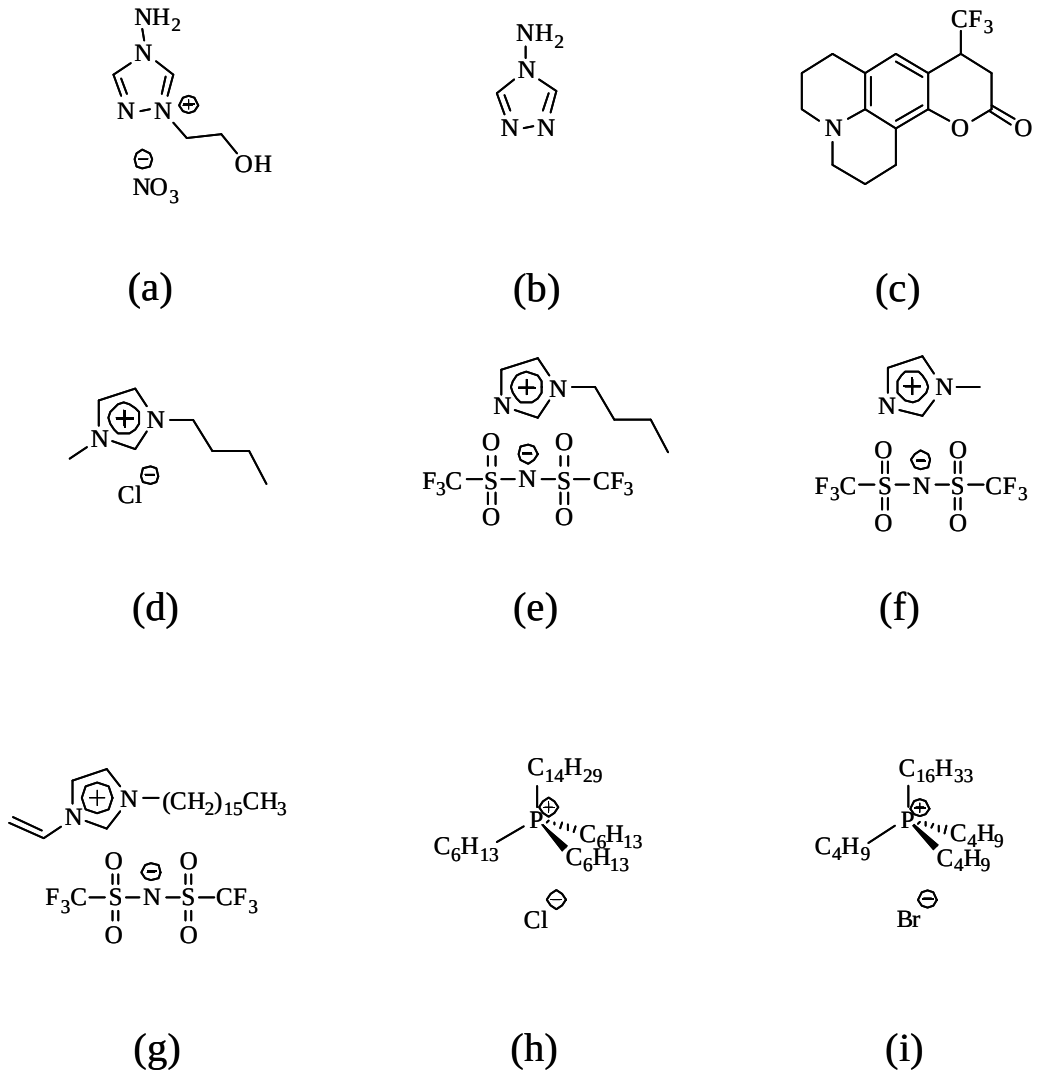

Figure 1- The structures of (a) 1-hydroxyethyl-4-amino-1,2,4-triazolium nitrate (HEATN), (b) 4-amino-1,2,4-triazole, (c) solvatochromic probe Coumarin 153 (C153), (d) 1-butyl-3-methylimidazolium chloride ($BMIM^+$ Cl^-), (e) 1-butylimidazolium bis(trifluoromethylsulfonyl)imide (BIM^+ NTf_2^-), (f) 1-methylimidazolium bis(trifluoromethylsulfonyl)imide (MIM^+ NTf_2^-), (g) 1-cetyl-3-vinylimidazolium bis(trifluoromethylsulfonyl)imide ($CVIM^+$ NTf_2^-), (h) tetradecyl trihexyl phosphonium chloride, and (i) hexadecyl tributyl phosphonium bromide ($(C_4)_3C_{16}P^+$ Br^-).

This present work focuses on the physical chemistry of the high-energy ionic liquid system HEATN. The HEATN system was recently investigated using molecular dynamics simulations for the prediction of bulk properties.[24] The studies presented here assess this ionic liquid at a molecular level, using *ab initio* electronic structure methods, to gain insight into the structure, energetics, and charge delocalization in the component ions. These properties have been shown to be of significance in relation to the physical and chemical properties of ionic liquids,[25] and *ab initio* electronic structure methods have provided excellent agreement with X-ray structures of triazole salts, giving bond lengths that are within 0.003 nm of the experimental values in the case of the common 3,4,5-triamino-1,2,3-triazole salts.[26] Performing electronic structure calculations on large systems of ionic liquids can be difficult given the fact that *ab initio* electronic structure theory methods scale ~N^4 or worse, depending on the chosen method, where N measures the size of the system. This means that correlated electronic structure methods become computationally prohibitive for very large systems with more than 100 heavy atoms. A common approach for large systems is to treat the most important part of the system using quantum mechanics (QM) and the remainder (bulk) using molecular mechanics (MM). These combined QM/MM methods have had some success for large systems. However, not all large species of interest have an obvious separation between QM and MM regions, and the electronic effects of the MM region cannot usually be captured by MM calculations. In such cases, a fully QM treatment is preferable. A fully QM treatment can be made feasible if one can divide (fragment) the system of interest into smaller fragments in such a manner that QM accuracy is retained.[27,28] For example, the fragment molecular orbital (FMO) method[28-32] divides the system into fragments and

computes each fragment (monomer) in the presence of the electrostatic potential of the other fragments. The FMO method is suited for larger systems and has been applied to systems such as polypeptides and proteins,[33] a heavy metal system containing 3596 atoms,[34] and clusters of thousands of water molecules. [35] Large systems can be treated at a high level of theory, thereby allowing valuable insight into large systems of ionic liquids. The use of the FMO method with ionic liquid systems [36] has been limited and is explored in this report.

Additional studies used to investigate the dynamics of the HEATN system include the use of fluorescence spectroscopy to compare this high-energy ionic liquid to other more commonly used ionic liquids. Steady-state and time-resolved fluorescence measurements were performed to assess how HEATN behaves as a solvent at short time scales. In particular, solvation dynamics experiments were carried out using the fluorescent probe coumarin 153 (C153) in HEATN. The structure of C153 is given in Figure 1c. C153 is an ideal probe, and has been used extensively in a large number of solvation dynamics studies in various media.[37-48] The pervasive use of C153 permits facile comparison of HEATN with other ionic liquid systems. A summary of the various solvation dynamics studies in ionic liquids has recently been published,[49] as well as a report of some of the applications of such explorations.[50] Until now there have been no explorations of the solvation dynamics of triazolium ionic liquid systems. The solvation dynamics of the HEATN system were investigated via the C153 probe at five different temperatures, and the rotational dynamics were measured by exploiting the anisotropic nature of the fluorescence of the probe through this viscous ionic liquid as a function of

temperature. Comparisons with previously studied imidazolium and phosphonium ionic liquids are presented.

Materials and Methods

Computational Methods

Molecular structures were obtained by performing geometry optimizations using second-order Moller-Plesset perturbation theory (MP2)[51] and the 6-31++G(d,p) basis set.[52,53] Hessians (matrices of the energy second derivatives) were determined to ensure that each stationary point is a minimum (no negative eigenvalues) or a transition state (one negative eigenvalue). All calculations presented in this work are gas phase cluster calculations. Population analysis was carried out using electrostatic potentials (ESP) following the geodesic approach. Studies of two cation-anion pairs (tetramers) were carried out using the FMO2 and FMO3 method, at the MP2 level of theory.[29] In the FMO2 method, all single fragments (monomers) and pairs of fragments (dimers) are calculated explicitly in the electrostatic field of the remainder of the system. The FMO2 energy may be written as $E = \sum_{I}^{N} E_I + \sum_{I>J}^{N} (E_{IJ} - E_I - E_J)$, where E_I and E_{IJ} are the monomer and dimer energies, respectively.[30] Likewise, the FMO3 energy includes the explicit QM calculations of all trimers, so that three-body interactions are included explicitly. The computational efficiency of the FMO method can be exploited by the use of the generalized distributed data interface (GDDI) allowing two levels of parallelism.[54] With the ionic liquid system studied in this work, each fragment (monomer) was taken to be one cation or one anion. All calculations were performed using the electronic structure

theory program GAMESS (General Atomic and Molecular Electronic Structure System),[55,56] and were visualized when possible with MacMolPlt.[57]

Materials

Coumarin 153 (C153) (Exciton Inc., Dayton, OH) was used as received. 4-Amino-1,2,4-triazole was purchased from Sigma. The production of 1-substituted-4-amino-1,2,4-triazolium nitrate ionic liquid molecules through a metathesis of heterocyclic halide and nitrate salts is well established.[23,58] The specific synthesis of 1-hydroxyethyl-4-amino-1,2,4-triazolium bromide (HEATB) and 1-hydroxyethyl-4-amino-1,2,4-triazolium nitrate (HEATN) from metathesis of HEATB with silver nitrate follows the procedure described by Drake, Hawkins and Tollison.[59]

The synthesis of the other ionic liquids shown in Figure 1 is described elsewhere [11,60,61] and they were decolorized according to the procedure described previously.[62] Briefly, the impure ionic liquid was diluted and was allowed to elute through a column packed with celite, silica gel and activated charcoal. After the excess solvent was removed, the ionic liquid was dried under vacuum with mild heating. The water content of the HEATN sample was determined using a Mettler Toledo DL 39 coulometric Karl Fischer titrator. The viscosity of the HEATN sample was measured at each of the five temperatures ± 0.1 °C using a ViscoLab 4000 viscometer from Cambridge Applied Systems.

Steady-state Measurements

Steady-state absorption spectra were obtained using a Hewlett-Packard 8453 UV-visible spectrophotometer with 1-nm resolution. Steady-state fluorescence

measurements were taken using a SPEX flurormax-4 spectrofluorometer (HORIBA Jobin Yvon) with 1-nm resolution. The emission spectra were corrected for detector response and the lamp spectral intensity. All emission spectra were obtained with an excitation wavelength of 407 nm and a 3 nm band-pass. A 3 mm path length quartz cuvette was used for all measurements.

Time-resolved measurements

Fluorescence lifetime measurements were made using the time-correlated single-photon counting (TCSPC) apparatus described previously.[9,47] A summary is included here. Using a home-made mode-locked Ti:sapphire oscillator pumped at 532 nm by a Nd:VO_4 Millennia (Spectra-Physics) laser, femtosecond pulses were produced which were tunable from 780 nm – 900 nm having a repetition rate of 82 MHz. With the output selected at 814 nm from the Ti:Sapphire oscillator, the repetition rate was reduced to 8.8 MHz via the use of a Pockels cell (model 350-160 from Conoptics Inc.) and was subsequently frequency doubled through the use of a harmonic generator (model TP-2000B from U-Oplaz Technologies). The produced blue light with a wavelength of 407 nm was used as the primary excitation source for all time-resolved studies. After the harmonic generator a half-wave plate was placed in front of a vertical polarizer to ensure the polarization of the excitation light. The fluorescence was collected at a 90° angle to the excitation source and then passed through an emission polarizer set to the magic angle (54.7°) with respect to the vertical excitation light. In the case of the anisotropy studies this polarizer was set to 0° and 90° with respect to the vertical excitation light, respectively. A 425 nm cut-off filter was placed before a multichannel plate (MCP)

(Hamamatsu) to help remove any unwanted scattered excitation light. When performing the solvation dynamics studies, a monochromator was placed before the MCP to ensure the collection at each selected wavelength. The signal from the MCP detector was amplified and sent to a Becker & Hickl photon counting module (model SPC-630). The instrument response function had a full width at half maximum (FWHM) of ~45 - 50 ps. The parallel and perpendicular-polarized fluorescence anisotropy decay curves were collected in a 22 ns time-window and fitted simultaneously following the method described by Cross and Fleming.[63] This method takes full advantage of the statistical properties of the measured curves. The solvation dynamics studies involved recording fifteen single wavelength decays from 490 nm to 630 nm in 10 nm intervals, in a time-window of 9 ns. Typically, 1024 channels of data were collected giving 8.8 ps/ch. The wavelength-resolved fluorescence transients were fit to sums of exponentials (typically 2 or 3, as necessary to fit the data), and time-resolved emission spectra (TRES) were reconstructed as described in previous reports.[9,47]

The traditional approach was used for fitting the time-resolved emission spectra to a log-normal function, [9,37,61] from which the peak frequency $\nu(t)$ is extracted as a function of time. The solvation dynamics is described by the following normalized correlation function:

$$C(t) = \frac{\nu(t) - \nu(\infty)}{\nu(\text{"0"}) - \nu(\infty)}. \qquad (1)$$

Because *C(t)* is a *normalized* function, the accurate determination of *C(t)* depends upon accurate values for ν(“0”) and ν(∞). ν(“0”) is the frequency at zero-time, estimated using the method of Fee and Maroncelli,[64] who have described a robust, model independent,

and simple procedure for generating this "zero-time" spectrum. ν("0") represents the emission spectrum expected prior to any solvent relaxation but after complete intramolecular vibrational redistribution. The validity of this approach has been checked using a different method for estimating the "zero-time" reorganization energy in a previous report,[60] and was shown to be reliable. ν(∞) is (usually[65,66]) the frequency at infinite time, obtained from the maximum of the steady state spectrum. (This is not, however, true in the case of very slowly relaxing solvents, as has been demonstrated in the case of certain ionic liquids,[11,65,66] for which the emission spectrum at ~3 times the fluorescence lifetime of the probe is *red-shifted* to that of the equilibrium spectrum.) The ν(t)s are determined from the maxima of the log-normal fits of the time resolved emission spectra. In most of the cases, however, the spectra are broad, so there is some uncertainty in the exact position of the emission maxima. Thus, the range of the raw data points in the neighborhood of the maximum needed to estimate an error for the maximum obtained from the log-normal fit was considered. Depending on the width of the spectrum (i.e., "zero-time", steady-state, or time-resolved emission spectrum), the typical uncertainties were determined to be: "zero-time" ~ steady-state (~ ± 100 cm^{-1}) < time-resolved emission (~ ± 200 cm^{-1}). These uncertainties were used to compute error bars for the *C(t)* graph (giving a maximum error of ± 0.04). Finally, in generating the *C*(*t*) curve, the first point was obtained from the "zero-time" spectrum. The second point was taken at the maximum of the instrument response function. The fractional solvation was also computed at 50 ps by taking $f_{50ps}=1-C(t = 50ps)$. The experiments were also carried out at five different temperatures (25 °C, 35 °C, 45 °C, 55 °C and 65 °C) that were obtained using a variable temperature sample cell holder.

Results and Discussion

HEATN Structures

A previous *ab initio* investigation[18] of triazolium ionic liquid systems, especially triazolium dinitramide, showed a tendency for proton transfer from the cation to the anion in an ionic dimer to form neutral pairs. This proton transfer was found to have a very low energy barrier and was often spontaneous. This tendency was investigated for the HEATN system by performing geometry optimizations on the different pairs of cations and anions. The geometric structures of both single cation-anion pairs (dimers) and two cation-anion pairs (tetramers) were investigated. Six structures labeled I, II, III, IV, V, and VI were found for the HEATN dimer (Table 1) at the MP2 level of theory. These structures are ordered with respect to their relative energies with structure "I" having the lowest energy. The relative energies are given in Table 1, along with the hydrogen bond distances, and the electrostatic potential derived charges. Interestingly, no spontaneous proton transfer from the cation to the anion ions is found to occur. The magnitudes of the charges are ~0.8 in each structure, so these are clearly ionic species. There are two hydrogen bonds, OH---O and NH---O, that connect each cation-anion pair. The corresponding hydrogen bond distances are listed in Table 1. The hydrogen bonds may contribute to a larger density than these species might otherwise have. High density is a desirable property of high-energy species. [67]

The HEATN tetramer was also investigated using the MP2 method. Each tetramer structure was found by taking the dimer geometries and combining them to form tetramers. The MP2 geometry optimizations using these starting structures yielded the

five geometries seen in Figure 2. The relative energies, hydrogen bond distances, and the electrostatic potential derived charges are given in Table 2. [27] The computed charges are all above 0.7 in magnitude, so that all of the species are ionic as expected.

The FMO method was used to evaluate the feasibility of using this method with larger (hexamer and higher) ionic liquid clusters. The structures discussed above provide benchmarks against which the FMO2-MP2 and the FMO3-MP2 method may be compared, as shown in Table 3. For each system one molecule

Table 1 – MP2 dimer HEATN Properties

Dimer*	E_{rel}[a] (kcal/mol)	OH---O[b] (Å)	NH---O[b] (Å)	ESP Charges (cation, anion)[c]
 I	0	1.85	1.90	0.82, -0.82
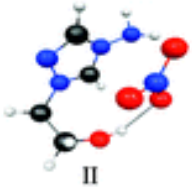 II	0.6	1.84	1.96	0.79, -0.79
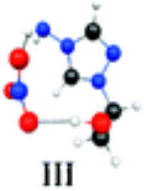 III	3.3	1.87	1.93	0.83, -0.83
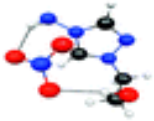 IV	3.6	1.88	1.91	0.80, -0.80
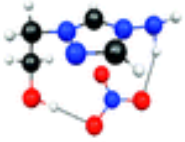 V	4.0	1.84	1.93	0.80, -0.80
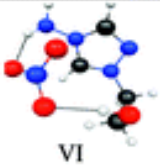 VI	5.0	1.86	1.84	0.82, -0.82

[a] Energies relative to dimer "I".
[b] OH---O & NH---O refer to the distance between the OH/NH group on the cation and the nearest O atom on the anion.
[c] Electrostatic Potential (ESP) Charges on each cation and anion are reported listing the cation first and the anion second.
* MP2 optimized dimer structures of HEATN using the 6-31++G(d,p) basis arranged in order of increasing energy with "I" being the lowest energy structure found. The atom color codes are: nitrogen is blue, oxygen is red, carbon is black and hydrogen is white.

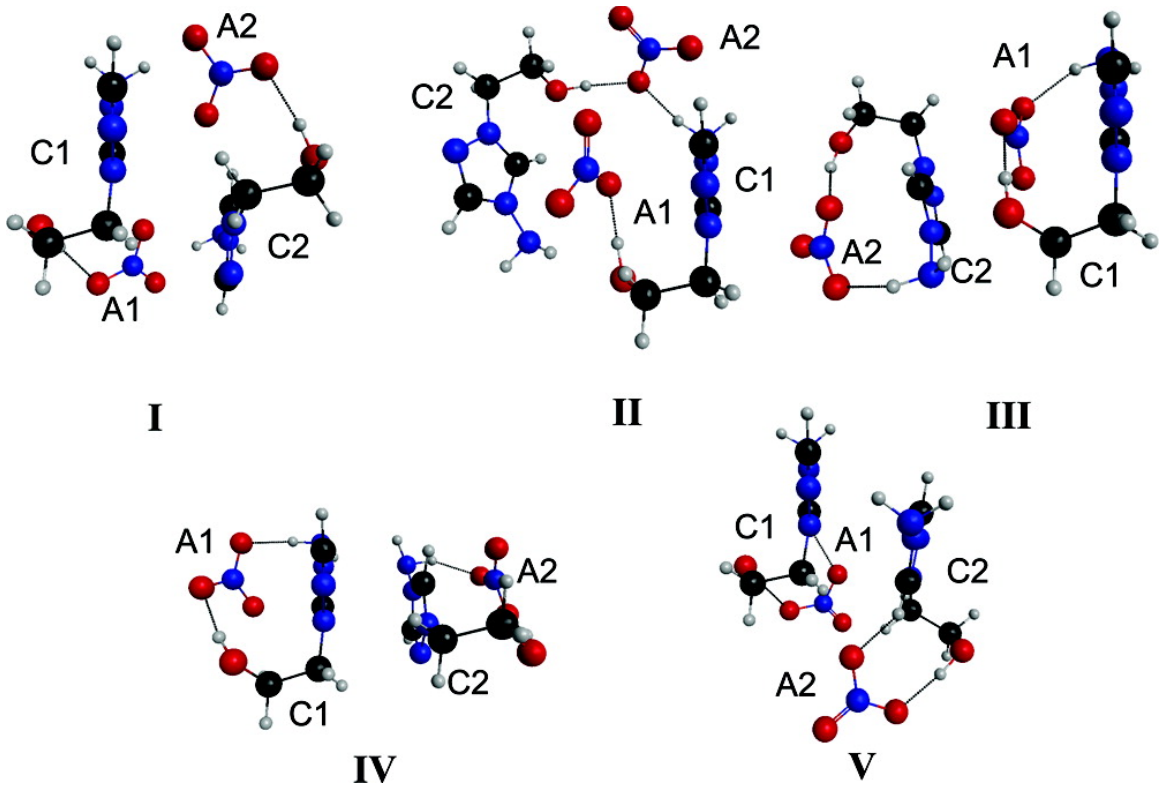

Figure 2 - Tetramer structures of HEATN obtained using the MP2 method with the 6-31++G(d,p) basis. They are labeled in order of increasing energy. Red represents oxygen, blue represents nitrogen, black represents carbon and white represents hydrogen. Additional data obtained from these calculations can be seen in Tables 2 and 3.

was assigned to each fragment, giving one ion per FMO monomer. As expected, the FMO3-MP2 method has smaller errors, but both FMO2 and FMO3 are within 1 kcal/mol or less of the full MP2 relative energies. Thus, the less computationally demanding FMO2 method provides sufficient accuracy for these species, suggesting that three-body effects are minor. Of equal importance is the memory required for the calculations. The full MP2 method uses 8.00 GB of RAM per node of eight cores, while the FMO2-MP2 and FMO3-MP2 methods use 1.93 GB and 1.12 GB respectively. The ESP charges derived from the FMO2 and FMO3 single point calculations are in good agreement with the MP2 values (See Table 3).

Table 2 – MP2 optimized HEATN tetramers (see Figure 2).

Tetramer	E_{rel}[a] (kcal/mol)	Ion[b]	NH---O[c] (Å)	OH---N[c] (Å)	ESP Charge
I	**0.0**	**C1**	2.00	1.84	0.86
		A1			-0.86
		C2	2.00	1.84	0.86
		A2			-0.86
II	**10.1**	**C1**	1.77	1.70	0.86
		A1			-0.74
		C2	1.73	2.45	0.78
		A2			-0.91
III	**18.8**	**C1**	1.93	1.78	0.93
		A1			-0.92
		C2	1.88	1.89	0.82
		A2			-0.84
IV	**27.8**	**C1**	1.89	1.81	0.81
		A1			-0.78
		C2	1.86	1.80	0.73
		A2			-0.76
V	**39.4**	**C1**	5.05	1.73	0.95
		A1			-0.90
		C2	4.74	1.75	0.83
		A2			-0.88

[a] Energies (kcal/mol) relative to tetramer "I"

[b] These ions are defined in Figure 2

[c] OH---O & NH---O refer to the distance between the OH/NH group on the cation and the nearest O atom on the associated anion (see Figure 2)

Table 3. Comparison of MP2 and FMO-MP2 for the tetramer geometries in Figure 2.

Tetramer	E_{rel}[a] (kcal/mol)			Ion[b]	FMO2-MP2	FMO3-MP2
	MP2	FMO2-MP2 Error[c]	FMO3-MP2 Error[d]		ESP Charge	ESP Charge
I	0.00	-0.30	0.02	C1	0.93	0.83
				A1	-0.93	-0.83
				C2	0.94	0.83
				A2	-0.93	-0.83
II	10.13	0.63	0.02	C1	0.97	0.92
				A1	-0.80	-0.78
				C2	0.87	0.82
				A2	-1.03	-0.96
III	18.76	0.55	-0.09	C1	0.85	0.91
				A1	-0.92	-0.88
				C2	0.93	0.81
				A2	-0.86	-0.84
IV	27.75	0.98	-0.28	C1	0.80	0.75
				A1	-0.78	-0.73
				C2	0.74	0.68
				A2	-0.77	-0.71
V	39.43	0.40	0.13	C1	1.01	0.93
				A1	-0.93	-0.89
				C2	0.91	0.83
				A2	-0.99	-0.86

[a] E_{rel} reports the energies (kcal/mol) relative to tetramer "I"
[b] These ions are defined in Figure 2
[c] The FMO2-MP2 energy error relative to the MP2 energy
[d] The FMO3-MP2 energy error relative to the MP2 energy

Solvation Dynamics of C153 in HEATN

HEATN was investigated using the fluorescent probe molecule C153. The absorption and emission spectrum maximum is at 431 nm and 546 nm respectively and there was no temperature dependent shift of the spectra of C153 in HEATN. The fluorescence of C153 underwent a monotonic red shift depending upon the increase in excitation wavelength from 400 to 500 nm. This excitation wavelength dependence, or red edge excitation effect, has also been observed in other ionic liquids.[68,69] This effect observed in ionic liquids is due to its inherent heterogeneity. This heterogeneity is attributed to the presence of nanostructural assemblies and different microenvironments within the neat ionic liquid.[70,71] Thus, exciting at different wavelengths selectively excites molecules in different local environments and thus the solvent response around the excited probe differs from one to another. In order to construct the solvation correlation function $C(t)$, time-resolved fluorescence decays were collected at different wavelengths spanning the entire range of the emission spectrum of the probe as shown in Figure 3. The decays on the blue end of

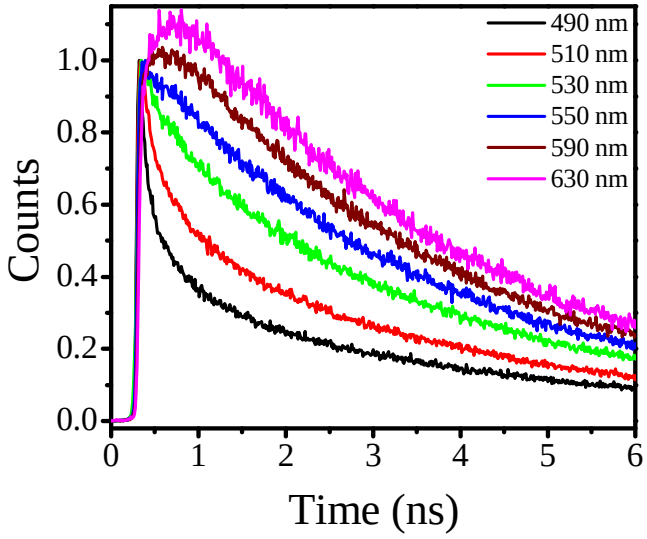

Figure 3 - Representative normalized wavelength-resolved fluorescence decay traces of C153 at six different wavelengths in HEATN at 55°C.

the spectrum are characterized by a faster response, whereas those collected at longer wavelengths are accompanied by a rise time that was due to the population flux from the initially excited state to the relaxed state. This trend of wavelength dependent decays is a signature of local solvation dynamics. Time-resolved emission spectra at 50 ps and 7.05 ns of C153 in HEATN are presented in Figure 4 at two representative temperatures. The corresponding "steady-state" and "zero-time" spectra are also included. Note that unlike the spectrum at 55°C, the 7.05 ns spectrum crosses the steady-state spectrum at 25°C, indicating that this spectrum cannot be interpreted to convey adequately the completed solvation of C153, as would usually be expected for highly viscous solvents.[11,65,66] The spectrum recorded at 7.05 ns is red-shifted by ~270 cm^{-1} relative to the steady-state spectrum, demonstrating that solvation is slightly slower than the population decay of the S_1 state of C153. This phenomenon has been previously observed in the case of the slowly relaxing

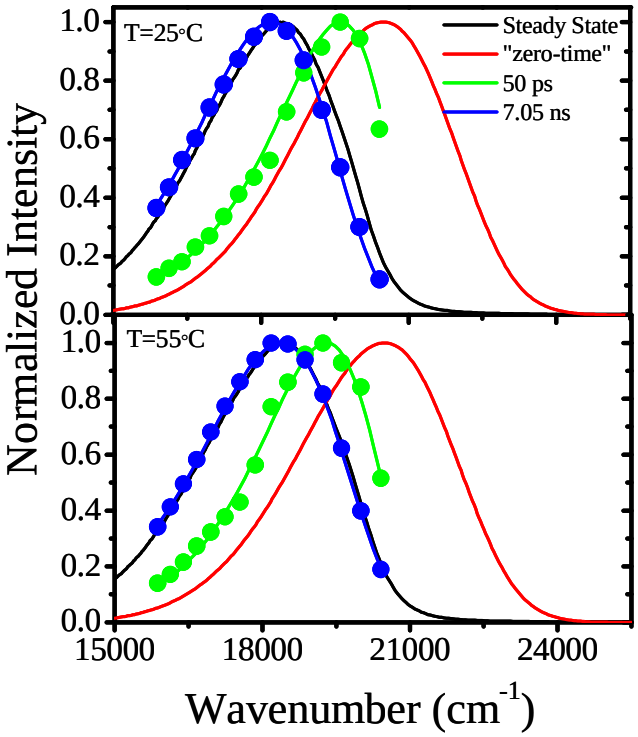

Figure 4 - Time-resolved fluorescence emission spectra (TRES) of C153 in HEATN at 25°C (top panel) and 55°C (bottom panel) at 50 ps and 7.05 ns. Corresponding "steady-state" and "time-zero" spectra are also included. The error for the steady-state and time-zero spectra is ~ ± 100 cm^{-1}, while for the other timed points it was ~ ± 200 cm^{-1}.

phosphonium ionic liquids. In previous studies,[11] it was found that the amount of rapid solvation and the average solvation time decrease and increase, respectively, as the time-window of the experiment is increased. The occurrence of solvation that is slower than the population decay of the S_1 state has also been noticed elsewhere for related systems.[65,66] In order to compare the solvation in the ionic liquid media, an attempt was made to study the parent compound (Figure 1b) which is the neutral 4-amino-1,2,4-triazole (melting point ~ 85 °C). A solvent induced spectral shift was not observed in the molten state at 85 °C using the time resolution afforded by our TCSPC apparatus, suggesting a very fast response for the triazole, which is consistent with the low viscosity (~ 6.2 cP) of the triazole at the melting temperature.

The spectral shift dynamics are represented by the decay of the solvation correlation function $C(t)$ in Figure 5. The $C(t)$s are constructed at five temperatures (25, 35, 45, 55 and 65°C) and the solvation parameters can be seen in Table 4. At all temperatures, the solvation dynamics are well described by biphasic decays, with an initial faster component preceded

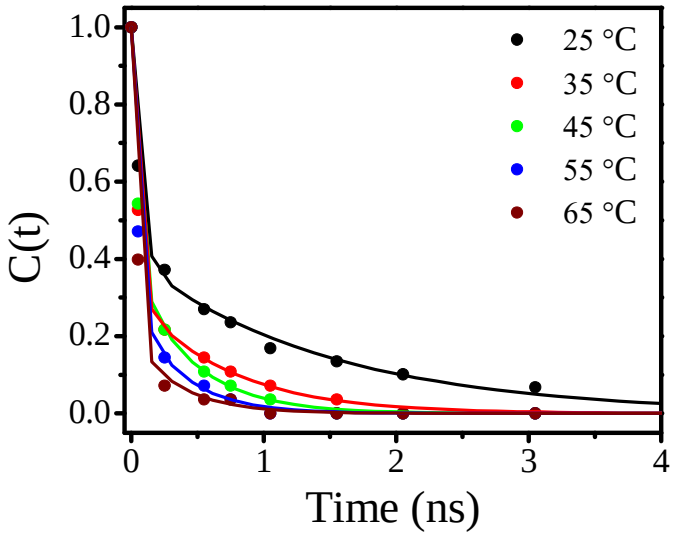

Figure 5 - Solvation correlation function ($C(t)$) decay curves of C153 in HEATN plotted as a function of temperature. The decays were fit with two exponentials and the average solvation time as well as the fractional solvation values can be found in Table 4. The typical error for each data point is < 0.05. Water content was determined to be < 0.3 wt. %.

by a slower response. At 25°C, ~ >30% of the solvation is completed within the instrumental time resolution (~50ps). The fractional solvation, f_{50ps} listed in Table 4 is the solvent response that is missed due to the finite time-resolution of the TCSPC apparatus. The missing Stokes-shift was accounted for by using the "zero-time" spectra estimated by the method of Fee and Maroncelli.[64] Recently Kerr-gated emission (KGE)[72,73] and fluorescence upconversion techniques[74,75] were used to measure spectral dynamics in ionic liquids with much shorter time-resolution ranging from 200 fs - 500 fs. Both the Maroncelli and Vauthey groups have reported a small but significant amount of a subpicosecond component in the case of solvation in ionic liquids. Maroncelli and coworkers have used a combination of KGE and TCSPC data to resolve complete solvation response in ionic liquids using 4-dimethylamino-4`-cyanostilbene (DCS) as a probe.[72,73] The observed response functions were well described by biphasic decays, consisting of both a sub-picosecond component of ~10-20% amplitude and a dominant slower component relaxing over a few picoseconds up to several nanoseconds. The faster component was associated with the inertial characteristics of the constituent ions, and the slower component to solvent viscosity. The missing portion of the initial relaxation contains both subpicosecond inertial contributions as well as components relaxing on the 1-10 ps time scale[73] and this interpretation was also corroborated by simulations performed by Kobrak.[76]

Table 4. Solvation and anisotropy parameters in different ionic liquids.

Ionic Liquid	T (K)	η[a] (cP)	R_+[b] (Å)	R_-[c] (Å)	Anisotropy[d] r_0	Anisotropy[d] $\langle\tau_{rot}\rangle$ (ns)	Anisotropy[d] C_{rot}[e]	Solvation f_{obs}[f]	Solvation $\langle\tau_{solv}\rangle$[g] (ns)	Solvation t_+[h] (ns)	Solvation t_-[h] (ns)
HEATN	298	427	2.90	2.09	0.35 ±0.03	21.1 ±0.6	0.48	0.36	0.62	4.7	1.3
	308	272			0.36 ±0.10	11.3 ±0.5	0.42	0.47	0.22	2.9	0.70
	318	133			0.32 ±0.02	5.7 ±0.4	0.45	0.45	0.16	1.4	0.30
	328	69			0.38 ±0.02	4.3 ±0.7	0.67	0.53	0.10	0.7	0.18
	338	40			0.36 ±0.01	2.6 ±0.1	0.72	0.60	0.07	0.4	0.10
BMIM Cl[i]	343	334	3.29	2.09				0.21	0.59		
BIM NTf_2[i]	293	90	3.16	3.39				0.65	0.20		
MIM NTf_2[i]	293	77	2.69	3.39				0.64	0.42		
CVIM NTf_2[j]	342	38	4.05	3.39				0.62	0.28		
$P(C_4)_3C_{16}$ Br[k]	339	268	4.96	2.26				0.29	5.3		
$P(C_6)_3C_{14}$ Cl[k]	331	80	5.18	2.09				0.33	3.9		

[a] Error bars for viscosity measurements are within ±1-2%.

[b] van der Waals volume of the cations (V_w) are calculated from the Edward's atomic increments[78], and the radius of (R_+) are obtained using the relation $R_+ = (3V_w / 4\pi)^{1/3}$

[c] Radius of anions (R_-) are obtained from Bondi[79] and Jin et al.[77]

[d] The error bars in the anisotropy experiments are obtained from triplicate measurements.

[e] Rotational decoupling constant (C_{rot}) is calculated using equation 4.

[f] Fractional solvation, f_{obs} are calculated at 50 ps for HEATN samples and 100 ps for other ionic liquids.

[g] Average solvation times, $\langle\tau_{solv}\rangle$ are obtained by the fitting $C(t)$ curves with two exponentials.

[h] The cation (t_+) and anion(t_-) diffusion times are calculated using the equation $t_\pm = \eta R_\pm^3 / f_\pm k_B T$, where the parameters are defined in the text.

i From reference[60]

j From reference[61]

[k] From reference[11]

As expected, the solvation times decreased with increasing temperature. This was most likely because of the decrease in the viscosity of the ionic liquid, which allowed the neighboring solvent molecules to reorganize faster around the excited state dipole of C153. Figure 6a shows the dependence of solvation time on viscosity in different types of ionic liquids namely those based on imidazolium, phosphonium and triazolium cations. The solvation times of C153 in HEATN show a reasonable correlation with viscosity, whereas in imidazolium based ionic liquids the correlation is not as good. Marked deviations are observed for the case of phosphonium ionic liquids. This observation is consistent with those reported by Maroncelli and coworkers,[66,77] who attributed the deviations in phosphonium ionic liquids to the enormous size of the cation moiety. Solvation in phosphonium ionic liquids is much slower than that of the imidazolium and HEATN systems. For example, although $(C_6)_3C_{14}P^+$ Br^- [77] is isoviscous (~270 cP) with HEATN (at 35°C), the solvation is 5 times slower in the phosphonium liquid. This observation can be interpreted in terms of the van der Waals volumes of the constituent ions. The radii of the cations and anions listed in Table 4 were estimated using Edward's[78] and Bondi's[79] van der Waals increment methods. The radii decrease in the order of phosphonium (~5.3Å) > imidazolium (~3.4Å) > triazolium (~2.9Å). This probably also explains the 2-fold faster average solvation times in HEATN compared to the isoviscous imidazolium based ionic liquids. It is noteworthy in this context that in all of the imidazolium based ionic liquids studied so far, the completely relaxed state or equilibrium condition is represented adequately by the steady-state spectrum of the probe, however this was not the case in HEATN under ambient temperature.

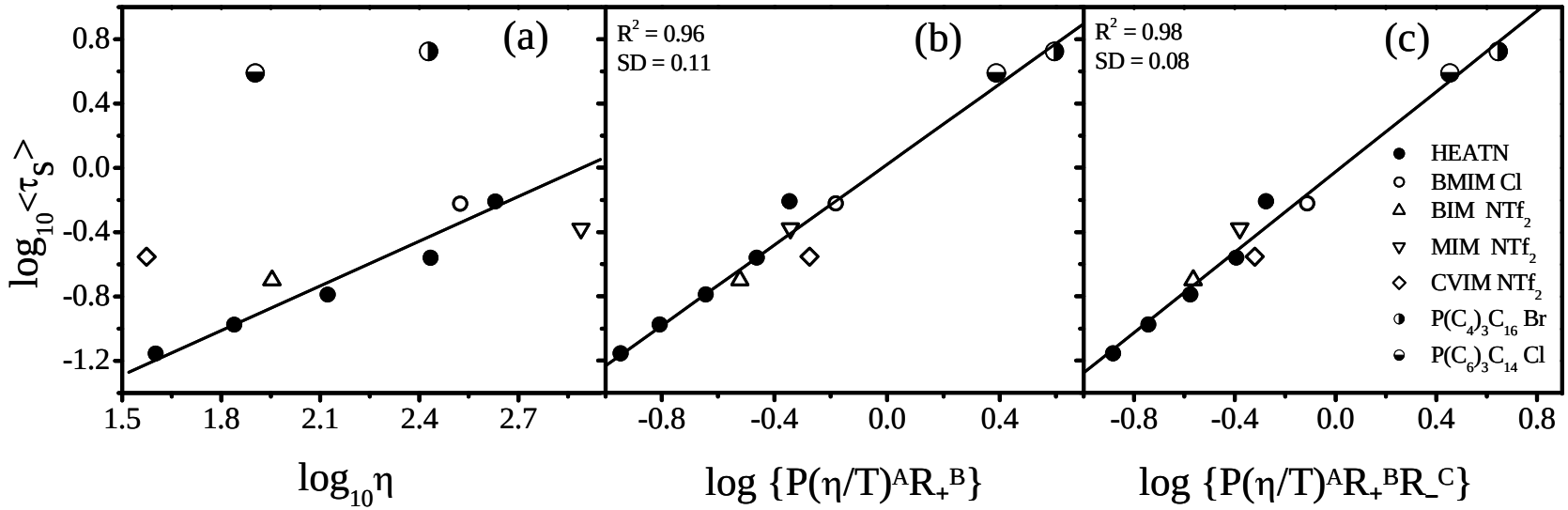

Figure 6 - (a) The average solvation time (<τ_S>) of C153 is plotted as a function of viscosity (η) in different ionic liquids based on imidazolium, phosphonium and triazolium cations. The solvation times of C153 in HEATN show a reasonable correlation with viscosity, whereas in imidazolium and phosphonium ionic liquids studied previously poor agreement is seen. The straight line is drawn to help guide the eye. (b) Correlation of <τ_S> in the ionic liquids with η/T and cation radius (R_+). The proportionality of <τ_S> varies as $(\eta / T)^A R_+^B$, where R_+ is the radius of the cation, and A and B are constants determined to be 0.5 and 4.5 by multiple regression analysis. This correlation is slightly improved when the anion size $(R_-)^{-0.5}$ is incorporated (c). The R^2 and standard deviation (SD) are obtained from the fit represented by the straight line in 'b' and 'c.'

As discussed above, besides viscosity (η), the size of the individual ions strongly influences the solvent response. In order to elucidate how the ion size might affect the observed solvation times, different analyses were performed motivated by the methods of Maroncelli and coworkers.[77] The ion sizes were correlated to the logarithm of the solvation times (τ_S) and to various measured and calculated properties. A plot of log $<\tau_S>$ versus η/T did not provide substantial improvement compared to a plot of log $<\tau_S>$ against η only. Consistent with the reports of Jin et al.,[77] a much better correlation was found, as shown in Figure 6b, in which the solvation time varies as $(\eta/T)^A R_+^B$, where R_+ is the radius of the cation, and A and B are constants determined to be 0.5 and 4.5 by multiple regression analysis. This correlation was slightly improved when the anion size (R_-) is incorporated as shown in Figure 6c. Thus, the dependence of solvation time could be best described as follows:

$$< \tau_S > \propto \sqrt{\frac{\eta/T}{R_-}} R_+^{4.5} \qquad (2)$$

The diffusion times of the cation and anion of HEATN, which is the amount of time needed to move a root mean square distance equal to the radius of the liquid, were calculated using the relation $t_\pm = \eta R_\pm^3 / f_\pm k_B T$, where k_B is the Boltzman constant and f is an empirical correction factor,[80,81] 0.53 and 0.74[82] for '+' and '–' which refer to the cation and anion respectively. The calculated diffusion times are presented in Table 4. The correlation of solvation time with the diffusion time of the cation and anion, as shown in **Figure 7,** indicates that the contribution of the reorientational motion of ions to the overall relaxation process cannot be neglected.

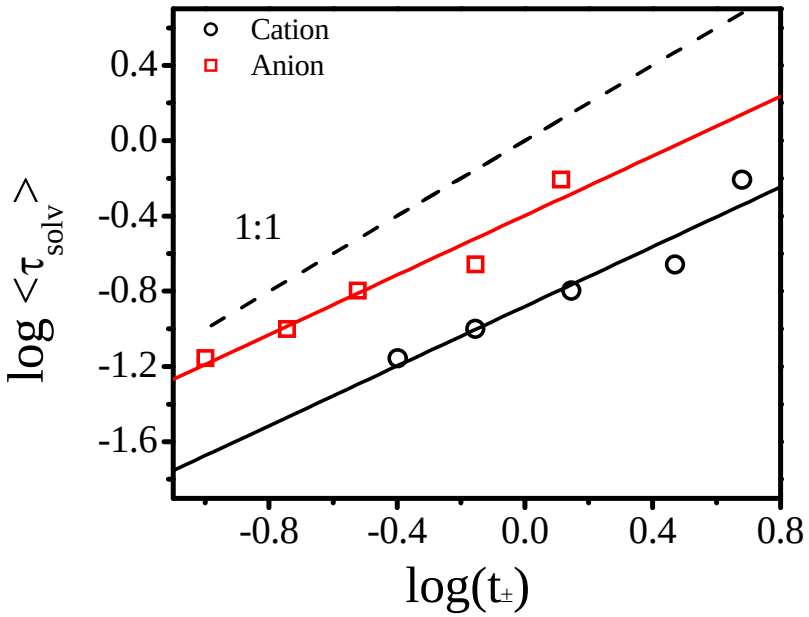

Figure 9 - Solvation times of C153 in HEATN at five different temperatures versus estimates of the cation and anion diffusion time determined using the equation $t_{\pm} = \eta R_{\pm}^3 / f_{\pm} k_B T$, where the parameters are defined in the text. The linear fits are shown as solid straight lines, whereas the dashed line represents the 1:1 correlation.

Rotational Dynamics of C153 in HEATN

The fluorescence anisotropy of C153 in HEATN was measured at five different temperatures and was found to decrease with temperature. The anisotropy decay was non-exponential at all temperatures investigated, unlike in normal polar solvents. The limiting anisotropy (r_0) and rotational times are presented in Table 4. Figure 8 gives the variation of rotational time (τ_{rot}) of C153 in HEATN as a function of viscosity and temperature in the form of η/T. This plot shows a good correlation in the form $< \tau_{rot} > \propto A(\eta / T)^{0.8}$, where *A* is a constant determined from the linear fit to be 1.1. Ionic

liquids have been reported to show similar correlation as established by normal polar solvents.[77]

The experimentally measured anisotropy decay times of C153 in HEATN have been analyzed within the framework of Stokes–Einstein–Debye (SED) hydrodynamic theory. According to this theory, the rotational diffusion of a medium sized solute molecule in a solvent continuum is assumed to occur by small step diffusion and the reorientation time of the solute and is related to the macroscopic viscosity of the solvent by the following relation[83,84]

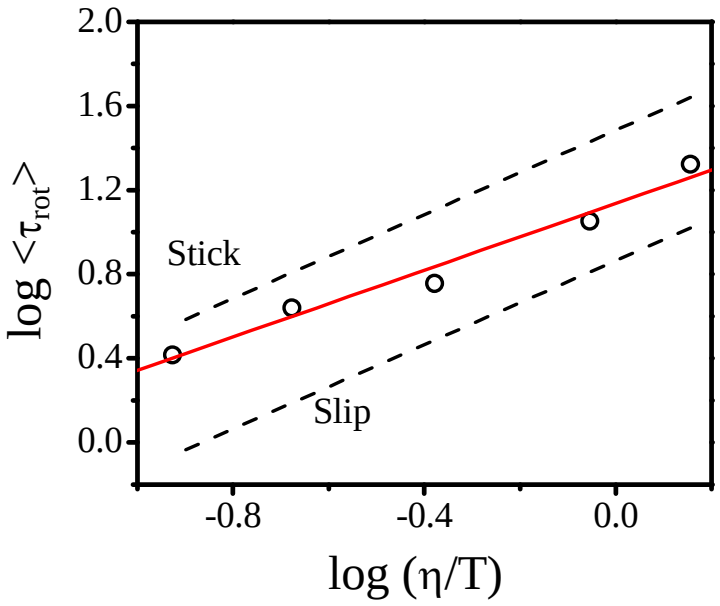

Figure 10 - Correlation of the average rotational time ($<\tau_{rot}>$) of C153 in HEATN with viscosity (η/cP) and temperature (T/K). The solid line (red) shows the best fit of the data to the proportionality $<\tau_{rot}> = 1.13\text{x}10^{-9}$ (sKcP^{-1}) (η/T).$^{0.8}$ The dashed lines are the average rotational times predicted from hydrodynamic models assuming an ellipsoidal shape of C153[85] using "stick" and "slip" boundary conditions. The experimentally observed rotational times fall within the boundaries of hydrodynamic predictions and the deviations can be estimated by the rotational coupling factor (C_{rot}) as described in the text.

$$\tau_{hyd} = \frac{V\eta}{k_B T} fC \qquad (3)$$

The dashed lines in Figure 8 are the predictions of hydrodynamic models, made by assuming C153 has- ellipsoidal shape with semi-axis dimensions of 2.0, 4.8, and 6.1 Å[85]. In Eq. (3) V is the van der Waals volume (246 Å^3) of the solute, f is a shape factor (1.71),

and C is a "rotational coupling factor" which measures the extent of coupling between the solute and the solvent. For stick boundary conditions C =1, and for slip boundary conditions C=0.24.[85] All of the rotation times in HEATN measured at different temperatures fall between these two limiting predictions. Deviations from the hydrodynamic predictions can be estimated from the value of the rotational coupling factor (C_{rot}) using the relation

$$C_{rot} = \frac{k_B T}{V \eta f} = \frac{< \tau_{rot} >}{\tau_{stick}}, \qquad (4)$$

where τ_{stick} is the stick hydrodynamic prediction. The values of C_{rot} are listed in Table 4. The average value in HEATN is 0.55, whereas those in conventional polar solvents were reported to be 0.57±0.09.[77] Thus the coupling of solute and solvent between C153 and HEATN is reasonably comparable to conventional polar solvents. These results are consistent with those of Maroncelli and coworkers who reported that all ionic liquids, besides bulky ones based on phosphonium, fall within the scatter of the polar solvents.[77] Cadena et al. [86] shown via molecular dynamics studies that the rotational time correlation of triazolium systems show a strong temperature dependence. As the temperature rises the rotational motion increases; this is consistent with the data presented here. Castner and coworkers[87] have recently studied solvation and rotational dynamics using C153 over a range of temperatures from 5 to 80°C, in ionic liquids based on ammonium and pyrrolidinium cations. They reported small amplitudes of very long orientation relaxation time constants on the order of 100 ns, which were missing in the experiments reported on herein. All of the C153 rotational time constants in HEATN ranged from 2 – 20 ns and are in agreement with the reports by Maroncelli and coworkers.[77] The dynamics reported

in the time-scale of 100 ns may be unreliable where the lifetime of C153 is ~3-5 ns owing to the lack of sufficient photons at long times.

Conclusions

The structure and dynamics of the high-energy ionic liquid system, 1-hydroxyethyl-4-amino-1,2,4-triazolium nitrate (HEATN), were investigated. This system maintains a significant charge separation as demonstrated by the electrostatic potential derived charges. There were no instances in which proton transfer was found to occur without an energy barrier, in contrast to other reports on triazolium ionic liquids.[18] The MP2 level optimizations find six dimer and five tetramer structures and show a significant, highly hydrogen bonded network within HEATN. The FMO method adequately treats this ionic liquid system, as evidenced by the small relative errors in the relative energies. Further calculations using the FMO method on the HEATN ionic liquid system are expected to give similar accuracy while using less computer resources and avoiding the prohibitive scaling of traditional full *ab initio* methods.

Besides the structural characterization, thorough temperature dependent studies of the solvation and rotational dynamics in HEATN using C153 as a probe were undertaken and compared with the results previously obtained from earlier studies on imidazolium and phosphonium ionic liquids. The solvation time in HEATN is faster than the isoviscous imidazolium and phosphonium ionic liquids, probably due to the smaller size of the cationic moiety. The solvation times in HEATN show an excellent correlation with viscosity, and the ionic radii. The fluorescence depolarization studies showed that the rotational time of C153 in HEATN at different temperatures lies within the limits of

hydrodynamic predictions. The presence of the amino and hydroxyethyl groups allows HEATN to participate in significant hydrogen bonding interactions. Surprisingly, these interactions do not seem to produce a substantial difference in the dynamics of the HEATN system with respect to imidazolium systems. An exception is given in Figure 6a, where HEATN shows a linear correlation with a significant difference in slope compared to the imidazolium and phosphonium systems. Despite the inherent difference of having the additional nitrogen atom in the ring, no significant changes in the dynamics of this system were observed. Finally, to the authors' knowledge this is the first experimental study of solvation dynamics in a triazolium based ionic liquid.

Acknowledgements

The authors acknowledge Dr. Gregory Drake, Mr. Michael Tinnirello, Ms. Leslie Hudgens, and Mr. Spencer Pruitt for many helpful discussion and guidance. This work was supported by a grant from the Air Force Office of Scientific Research. S. B. was supported by the U.S. Department of Energy, Office of Basic Energy Sciences, Division of Chemical Sciences, Geosciences, and Bioscience through the Ames Laboratory (S.B.). The Ames Laboratory is operated for the U.S. Department of Energy by Iowa State University under Contract No. DE-AC02-07CH11358.

References

(1) Deetlefs, M.; Hakala, U.; Seddon, K. R.; Wahala, K. “Ionic Liquids IV: Not just solvents anymore”; ACS 2007, Washigton, D.C.

(2) Earle, M. J.; Seddon, K. R. *Pure Appl. Chem.* **2000**, *72*, 1391.

(3) Brennecke, J. F.; Maginn, E. J. *AIChe* **2001**, *47*, 2384.

(4) Forsyth, S. A.; Pringle, J. M.; MacFarlane, D. R. *Aust. J. Chem.* **2004**, *57*, 113.

(5) Krossing, I.; Slattery, J. M.; Daguenet, C.; Dyson, P. J.; Oleinikova, A.; Weingartner, H. *J. Am. Chem. Soc.* **2006**, *128*, 13427.

(6) Seddon, K. R. *Nature (Materials)* **2003**, *2*, 363.

(7) Anderson, J. L.; Ding, J.; Welton, T.; Armstrong, D. W. *J. Am. Chem. Soc* **2002**, *124*, 14247.

(8) Welton, T. *Chem. Rev.* **1999**, *99*, 2071.

(9) Chowdhury, P. K.; Halder, M.; Sanders, L.; Calhoun, T.; Anderson, J. L.; Armstrong, D. W.; Song, X.; Petrich, J. W. *J. Phys. Chem. B* **2004**, *108*, 10245.

(10) Adhikary, R.; Bose, S.; Mukherjee, P.; Thite, A.; Kraus, G. A.; Wijeratne, A. B.; Sharma, P.; Armstrong, D. W.; Petrich, J. W. *J. Phys. Chem. B* **2008**, *112*, 7555.

(11) Mukherjee, P.; Crank, J. A.; Sharma, P. S.; Wijeratne, A. B.; Adhikary, R.; Bose, S.; Armstrong, D. W.; Petrich, J. W. *J. Phys. Chem. B* **2008**, *112*, 3390.

(12) Bose, S.; Wijeratne, A. B.; Thite, A.; Kraus, G. A.; Armstrong, D. W.; Petrich, J. W. *J. Phys. Chem. B* **2009**, *113*, 10825.

(13) Hu, Z.; Margulis, C. J. *Acc. Chem. Res.* **2007**, *40*, 1097.

(14) Rogers, R. D.; Voth, G. A. *Acc. Chem. Res.* **2007**, *40*, 1077.

(15) Bose, S.; Armstrong, D. W.; Petrich, J. W. *J. Phys. Chem. B* **2010**, *114*, 8221.

(16) Bose, S.; Barnes, C. A.; Petrich, J. W. *Biotechnol. Bioeng.* **2011**, DOI: 10.1002/bit.23352.

(17) Fischer, G.; Holl, G.; Klapötke, T. M.; Weigand, J. J. *Thermochim. Acta* **2005**, *437*, 168.

(18) Schmidt, M. W.; Gordon, M. S.; Boatz, J. A. *J. Phys. Chem. A* **2005**, *109*, 7285.

(19) Zorn, D. D.; Boatz, J. A.; Gordon, M. S. *J. Phys. Chem. B* **2006**, *110*, 11110.

(20) Pimienta, I. S. O.; Elzey, S.; Boatz, J. A.; Gordon, M. S. *J. Phys. Chem. A* **2007**, *111*, 691.

(21) Singh, R. P.; Verma, R. D.; Meshri, D. T.; Shreeve, J. M. *Angew. Chem.* **2006**, *45*, 3584.

(22) Drake, G.; Hawkins, T.; Brand, A.; Hall, L.; Mckay, M.; Vij, A.; Ismail, I. *Propellants, Explos., Pyrotech.* **2003**, *28*, 174.

(23) Drake, G.; Hawkins, T.; Tollison, K.; Hall, L.; Vij, A.; Sobaski, S. "(1R)-4-Amino-1,2,4-triazolium Salts: New Families of Ionic Liquids"; ACS Symp. Ser. 902, 2005, Washington D.C.

(24) Jiang, W.; Yan, T.; Wang, Y.; Voth, G. A. *J. Phys. Chem. B* **2008**, *112*, 3121.

(25) Wasserscheid, P.; Keim, W. *Angew. Chem., Int. Ed.* **2000**, *39*, 3772.

(26) Drake, G.; Hawkins, T.; Hall, L.; Boatz, J. A.; Brand, A. *Propellants, Explos., Pyrotech.* **2005**, *30*, 329.

(27) Gordon, M. S.; Mullin, J. M.; Pruitt, S. R.; Roskop, L. B.; Slipchenko, L. V.; Boatz, J. A. *J. Phys. Chem. B* **2009**, *113*, 9646.

(28) Fedorov, D. G.; Kitaura, K. *J. Phys. Chem. A* **2007**, *111*, 6904.

(29) Fedorov, D. G.; Kitaura, K. Theoretical Background of the Fragment Molecular Orbital Method. In *The Fragment Molecular Orbital Method - Practical Applications to Large Molecular Systems (FMO) Method and Its Implementation in GAMESS*; Fedorov, D. G., Kitaura, K., Eds.; CRC Press, , 2009: Boca Raton, FL, 2009; pp 5.

(30) Fedorov, D. G.; Kitaura, K. Theoretical Development of the Fragment Molecular Orbital (FMO) Method In *Modern Methods for Theoretical Physical Chemistry of Biopolymers*; Starikov, E. B., Lewis, J. P., Tanaka, S., Eds.; Elsevier: Amsterdam, 2006; pp 3.

(31) Kitaura, K.; Ikeo, E.; Asada, T.; Nakano, T.; Uebayasi, M. *Chem. Phys. Chem. Lett.* **1999**, *313*, 701.

(32) Nakano, T.; Kaminuma, T.; Sato, T.; Fukuzawa, K.; Akiyama, Y.; Uebayasi, M.; Kitaura, K. *Chem. Phys. Lett.* **2002**, *351*, 475.

(33) Fedorov, D. G.; Ishida, T.; Uebayasi, M.; Kitaura, K. *J. Phys. Chem. A* **2007**, *111*, 2722.

(34) Ishikawa, T.; Mochizuki, Y.; Nakano, T.; Amari, S.; Mori, H.; Honda, H.; Fujita, T.; Tokiwa, H.; Tanaka, S.; Komeiji, Y. *Chem. Phys. Lett.* **2006**, *427*, 159.

(35) Fletcher, G. D.; Pruitt, S. R.; Gordon, M. S.; Fedorov, D. G. *J. Chem. Theory. Comp.* **2011**.

(36) Pruitt, S. R.; Gordon, M. S., In preparation.

(37) Maroncelli, M.; Fleming, G. R. *J. Chem. Phys.* **1987**, *86*, 6221.

(38) Horng, M. L.; Gardecki, J. A.; Papazyan, A.; Maroncelli, M. *J. Phys. Chem.* **1995**, *99*, 17311.

(39) Lewis, J. E.; Maroncelli, M. *Chem. Phys. Lett.* **1998**, *282*, 197.

(40) Changenet-Barret, P.; Choma, C. T.; Gooding, E. F.; DeGrado, W. F.; Hochstrasser, R. M. *J. Phys. Chem. B* **2000**, *104*, 9322.

(41) Jiang, Y.; McCarthy, P. K.; Blanchard, D. J. *Chem. Phys.* **1994**, *183*, 249.

(42) Palmer, P. M.; Chen, Y.; Topp, M. R. *Chem. Phys. Lett.* **2000**, *318*, 440.

(43) Chen, Y.; Palmer, P. M.; Topp, M. R. *Int. J. Mass Spectrom* **2002**, *220*, 231.

(44) Agmon, N. *J. Phys. Chem.* **1990**, *94*, 2959.

(45) Chakrabarty, D.; Hazra, P.; Chakraborty, A.; Seth, D.; Sarkar, N. *Chem. Phys. Lett.* **2003**, *381*, 697.

(46) Halder, M.; Mukherjee, P.; Bose, S.; Hargrove, M. S.; Song, X.; Petrich, J. W. *J. Chem. Phys.* **2007**, *127*, 055101/1.

(47) Bose, S.; Adhikary, R.; Mukherjee, P.; Song, X.; Petrich, J. W. *J. Phys. Chem. B* **2009**, *113*, 11061.

(48) Bose, S.; Adhikary, R.; Barnes, C. A.; Fulton, D. B.; Hargrove, M. S.; Song, X.; Petrich, J. W. *J. Phys. Chem. A* **2011**, *115*, 3630.

(49) Samanta, A. *J. Phys. Chem. Lett.* **2010**, *1*, 1557.

(50) Wishart, J. *J. Phys. Chem. Lett.* **2010**, *1*, 1629.

(51) Møller, C.; Plesset, M. S. *Phys. Rev.* **1934**, *46*, 618.

(52) Hehre, W. J.; Ditchfield, R.; Pople, J. A. *J. Chem. Phys.* **1972**, *56*, 2257.

(53) Clark, T.; Chandrasekhar, J.; Spitznagel, G. W.; Schleyer, P. v. R. *J. Comput. Chem.* **1983**, *4*, 294.

(54) Fedorov, D. G.; Olson, R. M.; Kitaura, K.; Gordon, M. S.; Koseki, S. *J. Comput. Chem.* **2004**, *25*, 872.

(55) Schmidt, M. W.; Baldridge, K. K.; Boatz, J. A.; Elbert, S. T.; Gordon, M. S.; Jensen, J. H.; Koseki, S.; Matsunaga, N.; Nguyen, K. A.; Su, S.; Windus, T. L.; Dupuis, M.; Montgomery, J. A., Jr. *J. Comp. Chem.* **1993**, *14*, 1347.

(56) Gordon, M. S.; Schmidt, M. W. Advances in electronic structure theory: GAMESS a decade later. In *Theory and Applications of Computational Chmistry: The First Forty Years* Dykstra, C. E., Frenking, G., Kim, K. S., Scuseria, G. E., Eds.; Elsevier Science: Amsterdam, 2005; pp 1167.

(57) Bode, B. M.; Gordon, M. S. *J. Mol. Graphics Model.* **1998**, *16*, 133.

(58) Astleford, B. A.; Goe, G. L.; Keay, J. G.; Scriven, E. F. V. *J. Org. Chem.* **1989**, *54*, 731.

(59) Drake, G.; Hawkins, T.; Tollison, K. Energetic Ionic Salts USA, 2010; Vol. US 7745635

(60) Headley, L. S.; Mukherjee, P.; Anderson, J. L.; Ding, R.; Halder, M.; Armstrong, D. W.; Song, X.; Petrich, J. W. *J. Phys. Chem. A* **2006**, *110*, 9549.

(61) Mukherjee, P.; Crank, J. A.; Halder, M.; Armstrong, D. W.; Petrich, J. W. *J. Phys. Chem. A* **2006**, *110*, 10725.

(62) Earle, M. J.; Gordon, C. M.; Plechkova, N. V.; Seddon, K. R.; Welton, T. *Anal. Chem.* **2007**, *79*, 758.

(63) Cross, A. J.; Fleming, G. R. *Biophys. J.* **1984**, *46*, 45.

(64) Fee, R. S.; Maroncelli, M. *Chem. Phys.* **1994**, *183*, 235.

(65) Arzhantsev, S.; Ito, N.; Heitz, M.; Maroncelli, M. *Chem. Phys. Lett.* **2003**, *381*, 278.

(66) Ito, N.; Arzhantsev, S.; Heitz, M.; Maroncelli, M. *J. Phys. Chem. B* **2004**, *108*, 5771.

(67) Klapötke, T. M. *High Energy Density Materials*; Springer, 2007; Vol. 125.

(68) Adhikari, A.; Sahu, K.; Dey, S.; Ghosh, S.; Mandal, U.; Bhattacharyya, K. *J. Phys. Chem. B* **2007**, *111*, 12809.

(69) Mandal, P. K.; Paul, A.; Samanta, A. *J. Photochem. and Photobiol. A* **2006**, *182* 113.

(70) Khurmi, C.; Berg, M. A. *J. Phys. Chem. Lett.* **2010**, *1*, 161.

(71) Triolo, A.; Russina, O.; Bleif, H.-J.; Cola, E. D. *J. Phys. Chem. B* **2007**, *111*, 4641.

(72) Arzhantsev, S.; Hui, J.; Naoki, I.; Maroncelli, M. *Chem. Phys. Lett.* **2006**, *417*, 524.

(73) Arzhantsev, S.; Jin, H.; Baker, G. A.; Maroncelli, M. *J. Phys. Chem. B* **2007**, *111*, 4978.

(74) Lang, B.; Angulo, G.; Vauthey, E. *J. Phys. Chem. A* **2006**, *110*, 7028.

(75) Halder, M.; Headley, L. S.; Mukherjee, P.; Song, X.; Petrich, J. W. *J. Phys. Chem. A* **2006**, *110*, 8623.

(76) Kobrak, M. N. *J. Chem. Phys.* **2006**, *125*, 064502/1.

(77) Jin, H.; Baker, G. A.; Arzhantsev, S.; Dong, J.; Maroncelli, M. *J. Phys. Chem. B* **2007**, *111*, 7291.

(78) Edwards, J. T. *J. Chem. Educ.* **1970**, *47*, 261.

(79) Bondi, A. *J. Phys. Chem.* **1964**, *68*, 441.

(80) Tokuda, H.; Hayamizu, K.; Ishii, K.; Susan, M. A. B. H.; Watanabe, M. *J. Phys. Chem. B FIELD Full Journal Title:Journal of Physical Chemistry B* **2004**, *108*, 16593.

(81) Tokuda, H.; Hayamizu, K.; Ishii, K.; Susan, M. A. B. H.; Watanabe, M. *J. Phys. Chem. B* **2005**, *109*, 6103.

(82) Arzhantsev, S.; Hui, J.; Baker, G. A.; Naoki, I.; Maroncelli, M. “Solvation dynamics in ionic liquids, results from ps and fs emission spectroscopy.” Femtochemistry VII, 2006.

(83) Dutt, G. B.; Ghanty, T. K. *Journal of Chemical Physics* **2002**, *116*, 6687.

(84) Dutt, G. B. *J. Phys. Chem. B* **2010**, *114*, 8971.

(85) Horng, M.-L.; Gardecki, J. A.; Maroncelli, M. *J. Phys. Chem. A* **1997**, *101*, 1030.

(86) Cadena, C.; Maginn, E. J. *J. Phys. Chem. B* **2006**, *106*, 18026.

(87) Funston, A. M.; Fadeeva, T. A.; Wishart, J. F.; Castner, E. W., Jr. *J. Phys. Chem. B* **2007**, *111*, 4963.

CHAPTER VI: COMPUTATIONAL INVESTIGATION OF AMINE SYSTEMS WITH SIMILAR $\Delta pK_a^{(aq)}$ VALUES

To be submitted to the *Journal of Physical Chemistry B*

Philip J. Carlson,[a] Ekaterina I. Izgorodina,[b] Douglas R. MacFarlane,[b] and Mark S. Gordon[a]

[a] U.S. Department of Energy Ames Laboratory, and Department of Chemistry, Iowa State University, Ames, Iowa 50011

[b] School of Chemistry, Monash University, Wellington Rd, Clayton, 3800 VIC, Australia

Abstract

Primary, secondary, and tertiary amine systems with similar pK_a values were combined with acetic, and their ability to undergo proton transfer was studied. The calculated binding energies demonstrate that the relative stabilities of these systems are in the order: tertiary amine > secondary amine > primary amine. This trend does seem to follow the decrease of the hyperconjugation effect among the ammonium cations. An improved thermodynamic criterion that is based on the effective ΔpK_a was used to predict the extent of proton transfer and is proposed as a new measure of the extent of ionization among protic ionic liquids. The transition states for the acid-base proton transfer processes were used to estimate the crossover temperature that could be used to control

these processes. The crossover temperature is predicted to increase from the tertiary amine to the secondary amine.

Introduction

Ionic liquids (ILs) have been known for nearly a century but have only recently gained broad attention.[1] These organic/inorganic ionic salts have a number of attractive features that typical molecular liquids do not possess, making ionic liquids highly interesting for a number of applications. By definition these liquids are composed of ions and melt below the boiling point of water (≤100 °C). Due to the organic nature of ions many ILs are liquid at room temperature. Ionic liquids exhibit unique properties including easy synthesis, high chemical and thermal stability, low vapor pressure, high fluidity, high conductivity, and excellent solvating properties.[2-4] These properties can be customized to some extent by varying the cation or anion. Ionic liquids are often categorized into two groups, aprotic and protic. The proton transfer from a Brønsted acid to a Brønsted base forms a protic ionic liquid (PIL). Many early studies were focused on the aprotic salts and interest in PILs has slowly been increasing as many fascinating applications have been found.[5] Some of these include using PILs as electrolytes, explosives, anti-microbials, lubricants, propellants, in pharmaceuticals and in fuel cells.[6-11] PILs have highly tunable chemical properties and many unique properties compared to conventional aprotic ILs, including higher conductivities and fluidity, as well as lower melting points.[12,13]

Many of the properties of PILs depend to a large extent on their degree of ionization, that is, the extent of proton transfer from acid to base. It has been proposed

that less than 1% of the neutral species should be present for an ionic liquid to be considered "pure."[14] Angell and co-workers have suggested the use of a Walden plot (log equivalent conductivity versus log fluidity) to assess the degree of iconicity in PILs with some caveats.[15-19] The Walden plot estimates the degree of ion association/aggregation through the relationship between molar conductivity and fluidity, forming an ideal line for the fully dissociated electrolyte. The position of the ideal line depends on the size of the ions involved in the formation of the ionic liquids as described in the Nernst-Einstein equation.[20] The deviation from the ideal line flags reduction in conductivity due to the presence of non-conductive species such as ion pairs of ionic clusters. In the case of PILs the deviation from an ideal line might indicate either incomplete proton transfer between acid and base or the formation of neutral clusters consisting of ionized species. [8,21]

Yoshizawa *et al.* have proposed to use used aqueous pK_a values as an assessment of the extent of proton transfer in PILs.[15] The correlation between the excess boiling point, ΔT_b, that is, how much higher the boiling point of the PIL is than the average of the acid and base boiling points, and the $\Delta pK_a^{(aq)}$ value led to the conclusion that the aqueous pK_a values are useful for predicting the degree of proton transfer in PILs.[6] $\Delta pK_a^{(aq)}$ refers to the difference in the aqueous pK_a values of the acid and the base: $\Delta pK_a^{(aq)} = pK_a^{(aq)}(\text{base}) - pK_a^{(aq)}(\text{acid})$. This correlation led Yoshizawa *et al.* to the conclusion that a $\Delta pK_a^{(aq)} > 10$ was required for the full proton transfer to occur among the PILs studied.[15] MacFarlane and co-workers explored the idea of using the $\Delta pK_a^{(aq)}$ value as a predictor of the degree of ionization (with some doubt) among PILs and by plotting the degree of ionization as a function of $\Delta pK_a^{(aq)}$ these authors showed that a $\Delta pK_a^{(aq)} = 4$ should mathematically be sufficient for 99% ionization.[22] Further, in the field of active

pharmaceutical ingredients (APIs) a $\Delta pK_a^{(aq)} > 3$ (the "rule of three") is considered to be sufficient to form a crystalline salt.[23] Yet, Stoimenovski *et al.,* demonstrated that some PILs based on APIs exhibit a "low degree of ionisation" even with a $\Delta pK_a^{(aq)}$ value of 7.52.[8] Similarly, Rogers and co-workers have reported APIs with a $\Delta pK_a^{(aq)} \approx 3$ that exhibited no salt formation.[24] The complex energetics of these systems is explored in some detail by MacFarlane and co-workers, indicating that the enviornment plays a significant role in the extent of proton transfer.[7]

Stoimenovski *et al.* discussed the relationship between $\Delta pK_a^{(aq)}$ and extent of proton transfer in primary, secondary and tertiary amine systems.[21] The amine bases with similar $pK_a^{(aq)}$ vaues were combined with a common acid (acetic acid) to measure the extent of proton transfer. They observed restricted proton transfer among the tertiary amine base systems for which a $\Delta pK_a^{(aq)} >> 6$ was necessary to provoke strong proton transfer. This is consistent with the conclusions of Yoshizawa *et al.*[15] regarding experiments on tertiary amines. When primary amine systems were used, a $\Delta pK_a^{(aq)} > 2$ was already enough to result in 90% proton transfer (with a $\Delta pK_a^{(aq)} \geq 4$ required for >99% ionization). Their investigation of secondary amines showed that they lie somewhere between those extremes. The differences among the $\Delta pK_a^{(aq)}$ values and the degree of proton transfer was attributed to the superior hydrogen bonding ability of primary amines over secondary and tertiary ones.[21]

The degree of ionization among PILs depends largely on their enviornment. It is necessary to understand the proton transfer in PILs in more detail to determine how this behavior may be controled. The present work uses *ab initio*-based computational methods to provide additional details about the energetics of the proton transfer process. The

investigation was carried out using a primary amine, secondary amine, and tertiary amine (see **Figure 1**) in conjunction with acetic acid and a solvent model to study the proton transfer reaction between each base molecule and acetic acid. The complexes between the acid and three bases as well as their ionized counterparts (*i.e.* protonated bases and deprotonated acid) were investigated with the goal of predicting the thermodynamic stabilities of the ionized complexes with respect to the neutral ones. The transition state energies facilitated the estimation of a crossover temperature at which overbarrier and quantum mechanical tunnelling transitions are equally possible. At temperatures above that of the crossover the classical motion of the proton "climbing" over the barrier dominates, allowing the proton to reside at the energetically preferable position and move along the potential energy surface within the limits of the kinetic energy. The knowledge of the crossover temperature would allow for a greater control of the proton transfer process in a wider range of temperatures, especially temperatures below RT. Based on the binding energies of the ionized complexes "effective" ΔpK_a value of these amine systems were determined and compared with experimental data. This study further sheds light on the proton transfer process among similar $\Delta pK_a^{(aq)}$ protic ionic liquid systems.

Theoretical Methods

All calculations were performed using the General Atomic and Molecular Electronic Structure System (GAMESS)[25,26] and the 6-311++G(d,p) split-valence triple-zeta Pople type basis set.[27,28] Second order Møller-Plesset perturbation theory (MP2)[29] was used for all calculations, in some cases in conjunction with the conductor-like polarizable continuum model (CPCM)[30] to model solvent effects. All structures were

verified to be minima or saddle points by computing and diagonalizing the hessian matrix (the energy second derivatives). The binding energies ($E_{Binding}$) were calculated using the following equation:

$$E_{Binding} = E_{AB} - E_A - E_B$$

where E_{AB} is the total energy of the AB complex, whereas E_A and E_B are the energies of the components, A and B, respectively, evaluated at their minimum energy geometries. All the energies used in this equation were corrected for the zero-point vibrational energies and were determined using the same solvent model. All calculations were visualized when possible using MacMolPlt[31]

Results and Discussion

Each amine system was investigated using the MP2 method with the CPCM solvent chosen to be ethanol. The choice of ethanol was rationalized by comparing dielectric constants of routinely used ionic liquids with those of molecular solvents. The majority of ILs have modest dielectric constants, close to those of medium-chained alcohols.[32] The energies of the neutral base-acid complex, transition state of the proton transfer process, and the ionized base-acid complex were computed for three amine bases: 1) the primary amine, *n*-propylamine (see **Figure 2**), 2) the secondary amine, eiethylamine (see **Figure 3**) and 3) the tertiary amine, methylpyrrolidine (see **Figure 4**).

Energetics of ionized vs. neutral acid-base complexes

As seen from **Table 1**, out of the three amines, *n*-propylamine favors the formation of the neutral complex with the acetic acid. For the tertiary amine the situation reverses, with the ionized complex becoming more stable by about 0.5 kcal/mol. The secondary amine

represents an interesting case as both neutral and ionized complexes are thermodynamically equal.

From the experimental point of view, the $\Delta pK_a^{(aq)}$ values for all three systems given in **Table 2** are positive and > 5, indicating that the proton tratsfer should be present. Interestingly, the calculated results show that only the tertiary amine system (**Figure 4**) is thermodynamically preferred to undergo the proton transfer, thus forming a protic ionic liquid. This outcome contradicts the previously observed experimental results that indicated that the mixture of methylpyrrolidine and acetic acid did not form a protic ionic liquid, whereas the primary and secondary amines of similar $pK_a^{(aq)}$ values existed in a highly ionized state. [21,33] The calculated binding energies increase in the series: tertiary amine > secondary amine > primary amine. The trend is not reflected in the experimental $\Delta pK_a^{(aq)}$ values that remain almost constant in the same series. The found theoretical trend is not erroneous, as it accounts for decreased hyperconjugation in the corresponding ammonium-based cations. It was already pointed out before[21] that the $pK_a^{(aq)}$ values could be “insensitive” to the environment and potentially to some electronic effects such as hyperconjugation.

The unusual result for the tertiary amine could be explained by the lack of the basis set superposition error (BSSE) correction that is expected to be larger for the ioninized compelxes than in the neutral ones. The BSSE phenomenon is usually important in non-covalently bound complexes due to incompleteness of basis sets used. The BSSE calcualtions to correct for deficiency of the basis set are currently underway. To counteract the BSSE issue a larger basis set is needed and the optimization of the neutral and ionized species are currently performed with the 6-311+G(3df,2p) basis set.

Another explanation for the thermodynamic preference for the neutral complexes in the case of the primary and secondary amine bases could be the fact that the envornment was fully not taken into account. For example, in the case of the primary amine the presence of two hydrogens on the nitrogen centre might allow for the formation of a hydrogen-bonded network, thus resuling in stabilising cooperativity effects and encouraging the proton transfer. Currently, studies of clusters containing two acids and two bases are underway to investigate whether additonal hydrogen bonding does indeed enhance the proton transfer, thus making ionized clusters more thermodynamically stable.

Effective ΔpK_a values

To understand the effect of alkylation in the amine bases on the proton transfer, "effective" ΔpK_a values were calucalted based on the binding energies of the ionized complex:

$$A\text{-}H + B = B\text{-}H^{+}\ldots A^{-}$$

$$\Delta_r G = -RT\ln\left(K_{eq}\right) = -RT\ln\left(\frac{[BH^{+}\cdots A^{-}]}{[AH][B]}\right)$$

There are two asusmptions used here: 1) $\log(K_{eq})$ represents the effective ΔpK_a and 2) The entropy during the proton transfer does not change for the three amines studied and therefore, the Gibbs free energy can be approximated by $\Delta_r H$, *i.e.* the binding energy. The resulting effective ΔpK_a can be expressed as follows:

$$\Delta pK_a(eff) = -\frac{E_{binding}}{2.303\cdot RT}.$$

The first assumption would not be valid in aqueous solutions as the ionized species are expected to be strongly solvated by the surrounding water molecules. Neat protic ionic

liquids that are fully ionized usually have high melting points and deviate from the ideal line on the Walden plot due to ion association.[7] It is expected that after the proton transfer the protonated base and the dissociated acid would be engaged in ion pairing as was shown in the *ab initio* (DFT) MD simulations of methylammonium nitrate.[34]

The calculated effective ΔpK_a are presented in **Table 2**. As one can see, these numbers increase from the primary amine to the tertiary amine by 2.6 pK units, which is quite significant. Based on the Yoshizawa criterion that ΔpK_a should be > 10 for a full proton transfer, the effective value for methylpyrrolidine would still not allow for the full proton transfer. The proposed ΔpK_a(eff) could be an improved thermodynamic criterion to predict the extent of proton transfer. Currently, a systematic study that incorporates a number of amine bases and carboxylic acids is underway.

Transition states and crossover temperatures

It is usually assumed that the proton transfer is a barrier-less process in the acid-base system. It was indeed shown that in the case of the triazolium-based ionic liquid coupled with the nitric acid the proton transfer was found to be instantaneous.[35] For each of the amine systems studied here the proton transfer between the acetic acid and the base occurs through a transition state and not spontaneously. The optimized structures and the corresponding reaction barriers are given in **Figures 2-4**. Although the barriers are relatively low ranging from 0.8 to 1 kca/mol they are not negligible.

In the theory of thermally activated tunnelling process[36] it is believed that the proton transfer is a pure quantum tunneling effect at temperatures below the crossover temeprature (T_C), whereas the classic behaviour of the proton “climbing” over the

reaction barrier dominates at temperatures above T_C. As a result, the proton must be very mobile at temperatures above T_C and is usually found in the area between the two spceis undergoing the proton transfer as was shown by Wilson through the extensive X-Ray and neturon difraction data in the case of carboxylic acid dimers. [37,38] Once the temperature cools down below T_C the quantum tunnelling starts to dominate, resulting in the proton equally residing on both species.[37,38] For protic ionic liquids the knowledge of the crossover temeprature would enable a greater control of the proton transfer process itself as well as transport properties, especially conductivity. This could also open up a new avenue for using protic ionic liquids as conducting materials at lower temperatures.

The crossover temperature can be estimated based on the imganery frequency of the transtiton state as was demonstrated by Richardson and Althorpe[39,40] using the following equation:

$$T_C = \frac{\hbar\omega_b}{2\pi k}$$

where k is the Boltzmann constant, and ω_b is the imaginary frequency of the transition state.

The calculated crossover temperatures are given in **Table 2**. Analysis of these data reveals that T_C increases in the series: tertiary amine > secondary amine > primary amine from 109 to 155 K, indicating that quantum tunneling becomes less important at low temperatures in the case of tertiary amines and could well be present for primary amines at temperatures not far from RT.

Conclusions

The degree of proton transfer among similar pK_a amine systems was studied. Primary, secondary, and tertiary amine systems combined with acetic acid provided an excellent case study given their similar pK_a values. The calculated binding energies increase in the series: tertiary amine > secondary amine > primary amine. While this result is not directly supported with experiment, the trend does seem to follow the decrease of the hyperconjugation effect among the ammonium cations. This trend may also be found to vary based on the BSSE, which may be a factor here. It is expected that explicit modeling of the environment may affect the thermodynamic preference for the neutral complexes in the case of the primary and secondary amine bases. An improved thermodynamic criterion based on the effective ΔpK_a was used to predict the extent of proton transfer has been proposed as a new measure of the extent of ionization. Lastly, it has been shown that there exists a transition state between the acid and bases studied in this report. These transition state barriers were used to estimate the crossover temperature that could be used to control the proton transfer process among these systems. The crossover temperature was found to increase from the tertiary amine to the secondary amine.

Acknowledgements. This work was supported in part by a grant from the Air Force Office of Scientific Research.

Figures

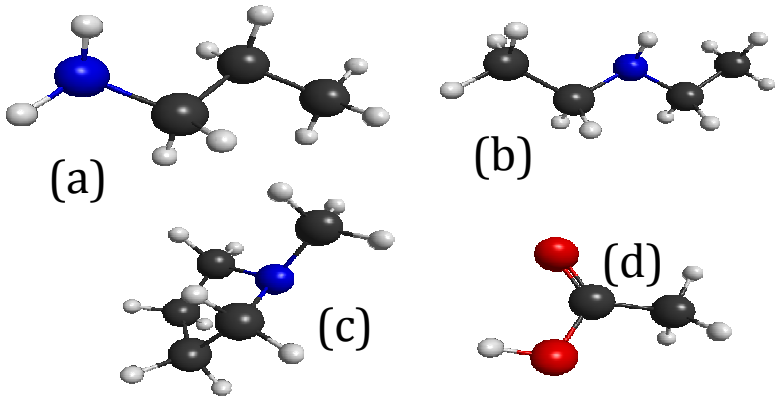

Figure 1. Optimized structures of (a) a primary amine – npropylamine (b) a secondary amine – diethylamine (c) a tertiary amine – methylpyrrolidine and (d) acetic acid.

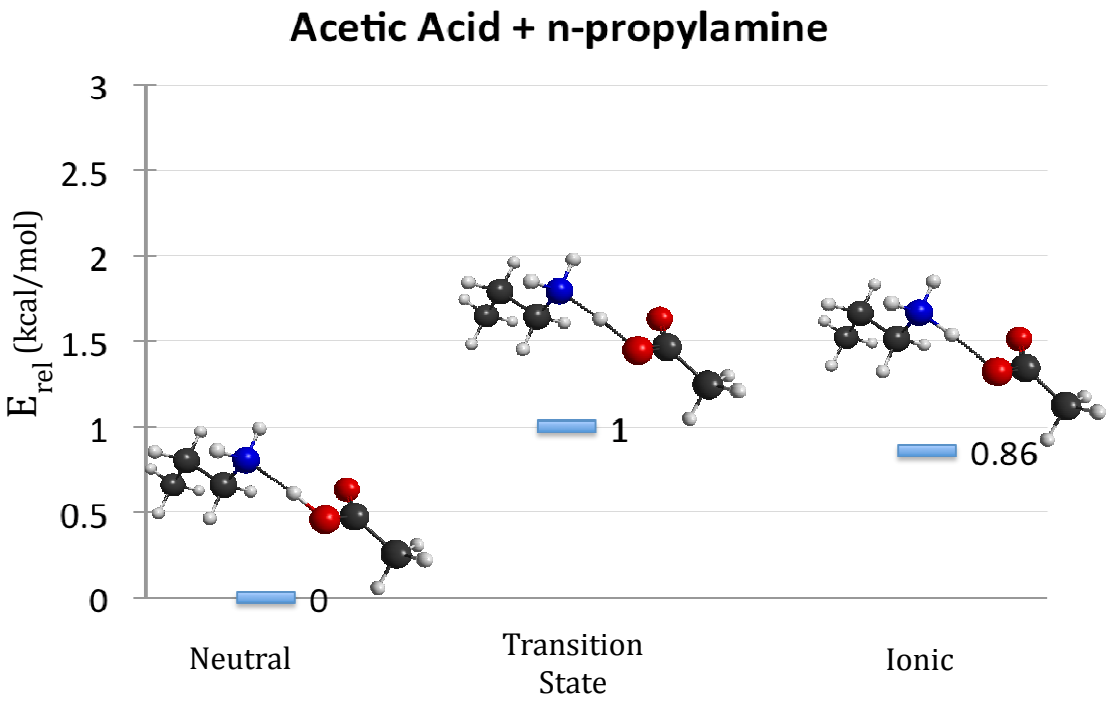

Figure 2. Schematic diagram of the optimized neutral complex, transition state and ionized complex between acetic acid, and n-propylamine and corresponding relative energies (E_{rel}, kcal/mol)

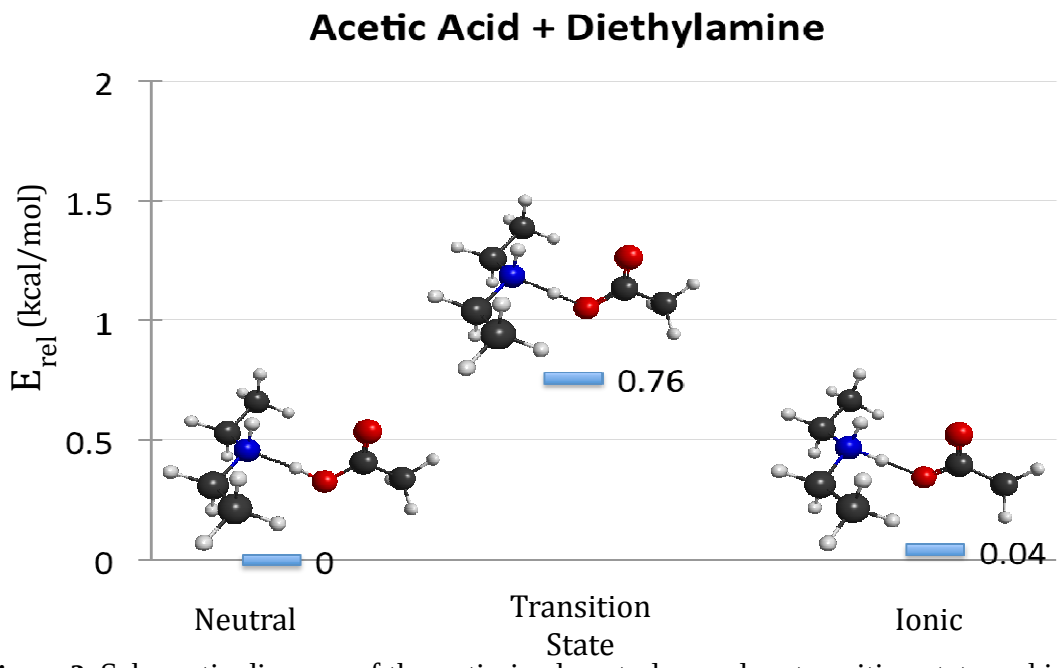

Figure 3. Schematic diagram of the optimized neutral complex, transition state and ionized complex between acetic acid and diethylamine and corresponding relative energies (E_{rel}, kcal/mol)

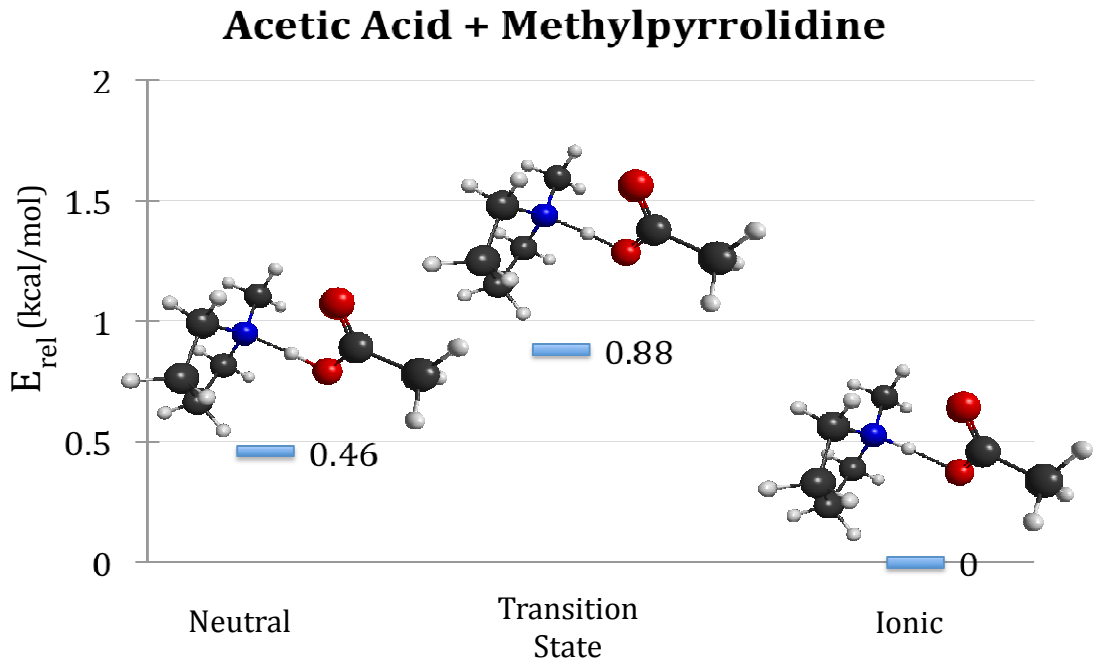

Figure 4. Schematic diagram of the optimized neutral complex, transition state and ionized complex between acetic acid and methylpyrrolidine and corresponding relative energies (E_{rel}, in kcal/mol)

Table 1. Binding energies of neutral and ionized complexes and lengths of the N-H and O-H bonds.

	Neutral		Ionized	
	$E_{binding}$ (kcal/mol)	O-H (Å)	$E_{binding}$ (kcal/mol)	N-H (Å)
Acetic Acid + n-propylamine	-9.20	1.04	-8.34	1.10
Acetic Acid + diethylamine	-10.40	1.06	-10.36	1.09
Acetic Acid + methylpyrrolidine	-11.37	1.08	-11.83	1.09

Table 2. Effective ΔpK_a values, $\Delta pK_a^{(eff)}$ and crossover temperatures (in K).

	T_C (K)	$\Delta pK_a^{(aq)}$ Exp.	ΔpK_a(eff) Calc.
Acetic Acid + *n*-Propylamine		5.78	6.1
Acetic Acid + Diethylamine	154.8	6.08	7.6
Acetic Acid + Methylpyrrolidine	108.8	5.70	8.7

References

(1) Walden, P. *Bull. Acad. Imper. Sci. St. Petersberg* **1914**, *8*, 405–422.

(2) Welton, T. *Chem. Rev.* **1999**, *99*, 2071–2083.

(3) Rogers, R. D. *Science* **2003**, *302*, 792–793.

(4) Earle, M. J.; Esperança, J. M. S. S.; Gilea, M. A.; Canongia Lopes, J. N.; Rebelo, L. P. N.; Magee, J. W.; Seddon, K. R.; Widegren, J. A. *Nature* **2006**, *439*, 831–834.

(5) Angell, C. A.; Byrne, N.; Belieres, J. P. *Chem Commun* **2007**, *40*, 1228–1236.

(6) And, T. L. G.; Drummond, C. J. *Chem. Rev.* **2008**, *108*, 206–237.

(7) Stoimenovski, J.; Dean, P. M.; Izgorodina, E. I.; MacFarlane, D. R. *Faraday Discuss.* **2011**, *154*, 335–352.

(8) Stoimenovski, J.; MacFarlane, D. R.; Bica, K.; Rogers, R. D. *Pharm Res* **2010**, *27*, 521–526.

(9) Susan, M.; Noda, A.; Mitsushima, S.; Watanabe, M. *Chem Commun* **2003**, 938–939.

(10) Pernak, J.; Goc, I.; Mirska, I. *Green Chem.* **2004**, *6*, 323–329.

(11) Luo, H.; Baker, G. A.; Lee, J. S.; Pagni, R. M.; Dai, S. *J Phys Chem B* **2009**, *113*, 4181–4183.

(12) Greaves, T. L.; Weerawardena, A.; Fong, C.; Krodkiewska, I.; Drummond, C. J. *J Phys Chem B* **2006**, *110*, 22479–22487.

(13) Bautista-Martinez, J. A.; Tang, L.; Belieres, J. P.; Zeller, R.; Angell, C. A.; Friesen, C. *J Phys Chem C* **2009**, *113*, 12586–12593.

(14) MacFarlane, D. R.; Seddon, K. R. *Aust. J. Chem.* **2007**, *60*, 3–5.

(15) Yoshizawa, M.; Xu, W.; Angell, C. *J Am Chem Soc* **2003**, *125*, 15411–15419.

(16) Xu, W.; Cooper, E.; Angell, C. *J Phys Chem B* **2003**, *107*, 6170–6178.

(17) Angell, C. A.; Byrne, N.; Belieres, J.-P. *Acc Chem Res* **2007**, *40*, 1228–1236.

(18) Xu, W.; Angell, C. *Science* **2003**, *302*, 422–425.

(19) Belieres, J.-P.; Angell, C. A. *J Phys Chem B* **2007**, *111*, 4926–4937.

(20) MacFarlane, D. R.; Forsyth, M.; Izgorodina, E. I.; Abbott, A. P.; Annat, G.; Fraser, K. *Phys Chem Chem Phys* **2009**, *11*, 4962–4967.

(21) Stoimenovski, J.; Izgorodina, E. I.; MacFarlane, D. R. *Phys Chem Chem Phys* **2010**, *12*, 10341–10347.

(22) MacFarlane, D. R.; Pringle, J. M.; Johansson, K. M.; Forsyth, S. A.; Forsyth, M. *Chem Commun* **2006**, 1905–1917.

(23) Banerjee, R.; Bhatt, P.; Ravindra, N.; Desiraju, G. *Cryst Growth Des* **2005**, *5*, 2299–2309.

(24) Bica, K.; Shamshina, J.; Hough, W. L.; MacFarlane, D. R.; Rogers, R. D. *Chem Commun* **2011**, *47*, 2267–2269.

(25) Schmidt, M. W.; Baldridge, K. K.; Boatz, J. A.; Elbert, S. T.; Gordon, M. S.; Jensen, J. H.; Koseki, S.; Matsunaga, N.; Nguyen, K. A.; Su, S.; Windus, T. L.; Dupuis, M.; Montgomery, J. A. *J Comput Chem* **1993**, *14*, 1347–1363.

(26) Gordon, M. S.; Schmidt, M. In *Theory and Applications of Computational Chemistry: the First Forty Years*; Dykstra, C. E.; Frenking, G.; Kim, K. S.; Scuseria, G. E., Eds. Elsevier: Amsterdam, 2005; pp. 1167–1189.

(27) Frisch, M. J.; Pople, J. A.; Binkley, J. S. *J Chem Phys* **1984**, *80*, 3265.

(28) Krishnan, R.; Binkley, J. S.; Seeger, R.; Pople, J. A. *J Chem Phys* **1980**, *72*, 650–

654.

(29) Møller, C.; Plesset, M. S. *Phys. Rev.* **1934**, *46*, 618–622.

(30) And, Y. T.; Houk, K. N. *J Chem Theory Comput* **2005**, *1*, 70–77.

(31) Bode, B. M.; Gordon, M. S. *Journal of Molecular Graphics and Modelling* **1998**, *16*, 133–138.

(32) Izgorodina, E. I.; Forsyth, M.; MacFarlane, D. R. *Phys Chem Chem Phys* **2009**, *11*, 2452–2458.

(33) Johansson, K. M.; Izgorodina, E. I.; Forsyth, M.; MacFarlane, D. R.; Seddon, K. R. *Phys Chem Chem Phys* **2008**, *10*, 2972–2978.

(34) Zahn, S.; Thar, J.; Kirchner, B. *J Chem Phys* **2010**, *132*, 124506–124506–13.

(35) Schmidt, M.; Gordon, M.; Boatz, J. *J Phys Chem A* **2005**, *109*, 7285–7295.

(36) Christov, S. G. *Molecular Engineering* **1997**, *7*, 109–147.

(37) Thomas, L. H.; Blagden, N.; Gutmann, M. J.; Kallay, A. A.; Parkin, A.; Seaton, C. C.; Wilson, C. C. *Cryst Growth Des* **2010**, *10*, 2770–2774.

(38) Wilson, C. C. *New J. Chem.* **2002**, *26*, 1733–1739.

(39) Richardson, J. O.; Althorpe, S. C. *J Chem Phys* **2009**, *131*, 214106–214106–12.

(40) Richardson, J. O.; Althorpe, S. C. *J Chem Phys* **2011**, *134*, 054109–054109–11.

CHAPTER VIII: GENERAL CONCLUSIONS

Chapter 3 presented unambiguous results to demonstrate that excited-state intramolecular hydrogen atom transfer (ESIHT) is a major photophysical process of curcumin in the TX-100, DTAB and SDS micelles. The fluorescence upconversion transient of curcumin in each micelle shows a biexponential decay, with time constants of 3 – 8 ps (fast) and 50 – 80 ps (slow). The slow component exhibits a pronounced isotope effect, producing a decay time constant of 80 – 130 ps in the micelles, which is assigned to ESIHT. The ESIHT rate of curcumin in the TX-100 micelle is lower than those in the other two micellar system. The hydrogen bonding between curcumin and the TX-100 surfactant may contribute to this effect. The fast decay component, unlike the ESIHT process, is insensitive to deuteration of curcumin and has been attributed to solvation dynamics using results from multiwavelength fluorescence upconversion studies. The water molecules in the micellar structure give rise to solvation dynamics of curcumin. The solvation dynamics observed in the micelles are slower than that in bulk water, which are attributed to water molecules at the micelle interface that are labile or bulklike and those that are bound to the surface of the micelles.

Chapter 4 demonstrated with fluorescence upconversion that curcumin undergoes ESIHT and ESIHT plays a major role in the photophysics of curcumin. Photoexcitation of curcumin in methanol and ethylene glycol produces a fluorescence signal that decays with a bi-exponential fashion on the order of 12–20 ps and 70–105 ps. The long-lived signal, which exhibits a prominent isotope effect in deuterated solvents, is attributed to ESIHT. It was also shown that curcumin exhibits a long solvation component of ~12 ps

in methanol and ~30 ps in ethylene glycol. In addition to alcohols, ESIHT is also a major photophysical process of curcumin in the TX-100, DTAB, and SDS micelles. The fluorescence upconversion transient shows a bi-exponential decay, with time constants of 3–8 ps (fast) and 50–80 ps (slow). Similar to the cases of curcumin in alcohols, the slow component exhibits a pronounced isotope effect, producing a decay time constant of 80–130 ps, which is assigned to ESIHT. The ESIHT rate of curcumin in the TX-100 micelle is lower than those in the other two micellar system systems, possibly because the hydrogen bonding between curcumin and the TX-100 surfactant may contribute to this effect. The fast decay component, however, is insensitive to deuteration of curcumin and has been attributed to solvation dynamics. The water molecules at the micelle interface, which are labile or bulk-like, and those that are bound to the surface of the micelle give rise to solvation dynamics of curcumin. Our work in this area forms a part of the continuing efforts to elucidate the photodynamic therapy properties of curcumin.

Chapter 5 discusses the structure and dynamics of the high-energy ionic liquid system, 1-hydroxyethyl-4-amino-1,2,4-triazolium nitrate (HEATN). This system maintains a significant charge separation as demonstrated by the electrostatic potential derived charges. There were no instances in which proton transfer was found to occur without an energy barrier, in contrast to other reports on triazolium ionic liquids.[18] The MP2 level optimizations find six dimer and five tetramer structures and show a significant, highly hydrogen bonded network within HEATN. The FMO method adequately treats this ionic liquid system, as evidenced by the small relative errors in the relative energies. Further calculations using the FMO method on the HEATN ionic liquid

system are expected to give similar accuracy while using less computer resources and avoiding the prohibitive scaling of traditional full *ab initio* methods.

Besides the structural characterization, thorough temperature dependent studies of the solvation and rotational dynamics in HEATN using C153 as a probe were undertaken and compared with the results previously obtained from earlier studies on imidazolium and phosphonium ionic liquids. The solvation time in HEATN is faster than the isoviscous imidazolium and phosphonium ionic liquids, probably due to the smaller size of the cationic moiety. The solvation times in HEATN show an excellent correlation with viscosity, and the ionic radii. The fluorescence depolarization studies showed that the rotational time of C153 in HEATN at different temperatures lies within the limits of hydrodynamic predictions. The presence of the amino and hydroxyethyl groups allows HEATN to participate in significant hydrogen bonding interactions. Surprisingly, these interactions do not seem to produce a substantial difference in the dynamics of the HEATN system with respect to imidazolium systems. An exception is given in Chapter 5 - Figure 6a, where HEATN shows a linear correlation with a significant difference in slope compared to the imidazolium and phosphonium systems. Despite the inherent difference of having the additional nitrogen atom in the ring, no significant changes in the dynamics of this system were observed. Finally, to the authors' knowledge this is the first experimental study of solvation dynamics in a triazolium based ionic liquid.

In chapter 6 the degree of proton transfer among similar pK_a amine systems was studied. Primary, secondary, and tertiary amine systems combined with acetic acid provided an excellent case study given their similar pK_a values. The calculated binding energies increase in the series: tertiary amine > secondary amine > primary amine. While

this result is not directly supported by experiment, the trend does seem to follow the decrease of the hyperconjugation effect among the ammonium cations. This trend may also be found to vary based on the BSSE, which may be a factor here. It is expected that explicit modeling of the environment may affect the thermodynamic preference for the neutral complexes in the case of the primary and secondary amine bases. An improved thermodynamic criterion based on the effective ΔpK_a was used to predict the extent of proton transfer has been proposed as a new measure of the extent of ionization. Lastly, it has been shown that there exists a transition state between the acid and bases studied in this report. These transition state barriers were used to estimate the crossover temperature that could be used to control the proton transfer process among these systems. The crossover temperature was found to increase from the tertiary amine to the secondary amine.